

# **DESIGNER QUANTUM MATERIALS**

by

**Vanita Srinivasa**

B.S., University of Pittsburgh, 2006

M.S., University of Pittsburgh, 2007

Submitted to the Graduate Faculty of  
the Kenneth P. Dietrich School of Arts and Sciences in partial  
fulfillment

of the requirements for the degree of

**Doctor of Philosophy**

University of Pittsburgh

2012

UNIVERSITY OF PITTSBURGH  
KENNETH P. DIETRICH SCHOOL OF ARTS AND SCIENCES

This dissertation was presented

by

Vanita Srinivasa

It was defended on

February 3, 2012

and approved by

Jeremy Levy, Professor, Department of Physics and Astronomy

David H. Waldeck, Professor and Chair, Department of Chemistry

Robert B. Griffiths, Otto Stern University Professor of Physics, Carnegie Mellon University

M. V. Gurudev Dutt, Assistant Professor, Department of Physics and Astronomy

Eric S. Swanson, Associate Professor, Department of Physics and Astronomy

Dissertation Director: Jeremy Levy, Professor, Department of Physics and Astronomy

Copyright © by Vanita Srinivasa  
2012

# DESIGNER QUANTUM MATERIALS

Vanita Srinivasa, PhD

University of Pittsburgh, 2012

Spin-based quantum information processing relies on the ability to identify and coherently manipulate quantum bits (qubits) existing in nature in the form of spin- $\frac{1}{2}$  particles such as electrons. The work described in this thesis is based on an alternative perspective: that these spin- $\frac{1}{2}$  objects, together with their interactions, can be regarded as building blocks of a variety of “designer quantum materials” with features not present for isolated single spins. Theoretical proposals are presented for two classes of spin-based designer quantum materials relevant for quantum information transport and manipulation.

The first class of materials involves spin- $\frac{1}{2}$  networks coupled by spatially-varying exchange interactions, in which moving domain walls can produce topologically-stable “flying spin qubits,” and pairs of domain walls can be used to generate and transport Einstein-Podolsky-Rosen pairs of entangled qubits. The effective exchange between two domain-wall qubits can be tuned by adjusting the positions of the domain walls and can be ferromagnetic even when all spin-spin couplings are antiferromagnetic.

The second class of designer quantum materials consists of electron spins in quantum wires with spatially-varying spin-orbit coupling. The presence of the spin-orbit interaction introduces pseudo-Zeeman couplings of the electron spins to effective magnetic fields and further enhances the building-block toolset: by periodically modulating this spin-orbit coupling in space, it is possible to create the spatial analogue of spin resonance, without the need for any real magnetic fields. The mapping of time-dependent operations onto a spatial axis suggests a new mode for quantum information processing in which gate operations are encoded into the band structure of the material.

## TABLE OF CONTENTS

<b>PREFACE</b> . . . . .	ix
<b>1.0 INTRODUCTION</b> . . . . .	1
1.1 SPIN QUANTUM MECHANICS . . . . .	1
1.1.1 Single-spin systems . . . . .	1
1.1.2 Multi-spin systems . . . . .	4
1.2 EXCHANGE INTERACTION . . . . .	6
1.3 SPIN-ORBIT INTERACTION . . . . .	11
1.4 SPIN-BASED QUANTUM INFORMATION PROCESSING . . . . .	15
1.4.1 Physical implementation of quantum information processing . . . . .	15
1.4.2 Single-spin qubits and exchange interactions . . . . .	20
1.4.3 Multi-spin qubits and exchange interactions . . . . .	23
1.4.4 Single-spin qubits and spin-orbit interaction . . . . .	33
<b>2.0 FLYING SPIN QUBITS</b> . . . . .	36
2.1 INTRODUCTION . . . . .	36
2.2 DIMERIZED SPIN CHAINS . . . . .	39
2.3 ANALYTICAL MODEL . . . . .	43
2.4 EINSTEIN-PODOLSKY-ROSEN PAIR GENERATION . . . . .	47
2.5 PHYSICAL REALIZATION . . . . .	48
2.6 CONCLUSION . . . . .	50
<b>3.0 TAILORING EFFECTIVE EXCHANGE INTERACTIONS VIA DOMAIN WALLS IN COUPLED HEISENBERG RINGS</b> . . . . .	52
3.1 INTRODUCTION . . . . .	52

3.2	ANTIFERROMAGNETIC HEISENBERG SPIN RINGS	55
3.3	ANALYTICAL MODEL FOR EFFECTIVE EXCHANGE	58
3.4	NUMERICAL STUDIES OF EFFECTIVE EXCHANGE	62
3.5	CONSTRUCTION OF QUANTUM SPIN SYSTEMS BY TAILORING OF THE EFFECTIVE EXCHANGE	67
3.5.1	FM triangle of qubits	67
3.5.2	Dimerized Heisenberg triangle ring with domain wall	69
3.5.3	Effective spin-1 chain	71
3.6	PHYSICAL IMPLEMENTATION	74
3.7	CONCLUSION	77
<b>4.0</b>	<b>RASHBA SPIN-ORBIT INTERACTION IN QUANTUM WIRES</b>	<b>78</b>
4.1	CONTINUUM MODEL	78
4.2	INTERPLAY OF SPIN-ORBIT AND ZEEMAN INTERACTIONS	80
4.3	SPATIALLY-VARYING SPIN-ORBIT INTERACTION AND TIGHT-BINDING MODEL	87
<b>5.0</b>	<b>SPATIAL ANALOGUE OF QUANTUM SPIN DYNAMICS VIA SPIN-ORBIT INTERACTION</b>	<b>93</b>
5.1	INTRODUCTION	93
5.2	SPIN-ORBIT SUPERLATTICE QUANTUM WIRES	95
5.3	SPIN SPATIAL RESONANCE	99
5.4	SPATIALLY-ENCODED SINGLE-QUBIT GATE SEQUENCE	104
5.5	CONCLUSION	105
<b>6.0</b>	<b>SUMMARY AND FUTURE PROSPECTS</b>	<b>108</b>
	<b>APPENDIX A. QUANTUM SPIN DYNAMICS</b>	<b>111</b>
A.1	UNITARY TIME EVOLUTION OPERATOR	111
A.2	FLOQUET STATES FOR THREE-SPIN RING	113
A.3	SPATIAL FORMULATION OF SPIN RESONANCE	117
	<b>APPENDIX B. SPIN-ORBIT SUPERLATTICE QUANTUM WIRE HAMILTONIAN</b>	<b>120</b>
	<b>BIBLIOGRAPHY</b>	<b>125</b>

## LIST OF FIGURES

1.1	Spectrum of the Heisenberg exchange Hamiltonian . . . . .	9
1.2	Spin-orbit interaction for a one-dimensional electron system . . . . .	13
1.3	Bloch sphere representation of a single qubit state. . . . .	21
1.4	Spectra of uniform antiferromagnetic Heisenberg spin- $\frac{1}{2}$ chains . . . . .	29
1.5	Spin density for $n_c = 9$ spin cluster qubit . . . . .	31
2.1	Dimerized Heisenberg spin- $\frac{1}{2}$ chains . . . . .	41
2.2	Interconversion between stationary and flying spin qubits . . . . .	42
2.3	Generation of a flying spin qubit . . . . .	44
2.4	Analytical model for flying spin qubits . . . . .	46
2.5	Generation of EPR pairs . . . . .	49
2.6	Experimental realization for flying spin qubits . . . . .	51
3.1	Three-spin ring pseudospin space spectrum . . . . .	57
3.2	Coupled pairs of spin triangles and effective exchange . . . . .	59
3.3	Tuning of effective exchange via domain wall position for two coupled spin triangles . . . . .	63
3.4	Effective exchange vs. domain wall position for two coupled five-spin rings . . . . .	65
3.5	Quasi-continuous effective exchange variation for coupled five-spin rings . . . . .	68
3.6	Triangle of qubits coupled by uniform FM effective exchange . . . . .	70
3.7	Effective AFM Heisenberg rings of nine spin-triangle qubits . . . . .	72
3.8	Effective spin-1 chain constructed from spin triangles with domain walls . . . . .	73
3.9	Possible physical realization of effective spin-1 chain . . . . .	76
3.10	Ge/Si quantum dot arrays . . . . .	76
4.1	Electronic energy subbands for quantum wire . . . . .	81

4.2 Spin-orbit gap for quantum wire with spin-orbit and Zeeman interactions . . . . .	85
4.3 Spectrum of tight-binding model for uniform spin-orbit coupling . . . . .	92
5.1 Spin-orbit superlattice quantum wire . . . . .	97
5.2 Spin spatial resonance . . . . .	101
5.3 Spin spatial resonance for ground-state superposition . . . . .	102
5.4 Spin spatial resonance for $N = 40$ sites . . . . .	103
5.5 Spatial mapping of a spin echo pulse sequence . . . . .	106

## PREFACE

The work presented in this thesis was achieved through the dedicated support of many people, to whom I am greatly indebted. It is with sincere pleasure that I convey my thanks to them.

First and foremost, I would like to express my deepest gratitude to my advisor, Jeremy Levy, for allowing me the honor of working with him these past few years, for providing me with a strong foundation for my scientific career, and for making the journey from my undergraduate research days all the way through my Ph.D. work as exciting, enjoyable, and fulfilling as it has been through his expert guidance, endless enthusiasm, and constant encouragement. I would also like to convey my heartfelt thanks to Chandralekha Singh for inspiring me to begin this journey in the first place, for giving me the foundation to pursue this work as well as whatever I may encounter in the future, and for the countless ways she has supported both my undergraduate and graduate education all along. The opportunity to realize my aspirations under the careful direction of these extraordinary role models has truly been the greatest and most valuable experience I have ever had.

I also wish to thank the members of my thesis committee, David Waldeck, Robert Griffiths, Gurudev Dutt, and Eric Swanson, not only for all of their valuable guidance and support during my research work, but also for being inspiring teachers who have cultivated my interest in and understanding of both physics and chemistry, even as an undergraduate.

In the course of this work, I have been very fortunate to have had the opportunity to interact with several prominent scientists outside the University of Pittsburgh who have been both very inspiring and very helpful. I am very grateful to C. Stephen Hellberg for the many fruitful collaborations and interesting discussions, starting with my undergraduate research, as well as for providing the LMSCS code used to carry out the numerical Lanczos diagonalization. I also thank Jacob Taylor, Florian Meier, Yaakov Weinstein, Sergey Smirnov, Yuriy Pershin, Guido Burkard, and many others for insightful comments and helpful discussions that have greatly clarified my

understanding of and perspectives on the work presented in this thesis.

I would also like to thank the current and past members of Jeremy's research group for bearing with my long, involved explanations of theoretical calculations amidst discussions of their exciting experiments, and for keeping me connected to the real world. Patrick Irvin was always there to help with my random questions and problems, patiently explained his own work so that a theory student could at least attempt to do an experiment, and helped me figure out how to use  $\LaTeX$  and  $\text{LyX}$  (the software that has made writing this thesis far more pleasant than it might have been). I thank Patrick, Cen Cheng, Guanglei Cheng, Hongzhou Ma, and Peti Fodor for making my first experience in a research environment as an undergraduate so inviting that I was glad to continue in the group for my doctoral work. Yanjun Ma also helped me keep working efficiently by solving the little glitches that seemed to come out of nowhere and that I had no clue how to get rid of, and assisted me in learning to use  $\LaTeX$  and  $\text{LyX}$  as well. Other group members have graciously provided help and support on several occasions. I am also grateful to friends outside the research group who have helped make my graduate student experience a very enjoyable one, as well as to the departmental office staff for taking care to see that things ran smoothly.

Many thanks go to my AP Physics teacher, Mr. Caine, and AP Calculus teacher, Mr. Collins, at Huron High School in Ann Arbor, Michigan, who aroused my initial interest in physics and higher mathematics and helped me see the inseparability of the two subjects. I would not be where I am now without the strong foundation they laid during the early stages of my education.

Finally, this work is dedicated to my parents, Ramanujan and Sobhana Srinivasa, for the infinite love, support, guidance, and inspiration they have given me throughout my entire life. I present it to them on the occasion of their 31st wedding anniversary as a tribute to the high standards they have set for me by their own example. I also thank my sister, Savita, for asking relevant questions that improved my ability to explain concepts clearly, making tea to keep me refreshed during the long hours of writing this thesis, and reminding me to laugh and stay light-hearted throughout the last few years. Many other family members, teachers, and friends have provided valuable inspiration and support at various stages, and although I cannot name everyone here, I express thanks to all of them.

Financial support from NDSEG, the University of Pittsburgh through the Andrew Mellon and Mary E. Warga Predoctoral Fellowships, the National Science Foundation (DMR-0704022 and

DMR-0602846), ARO MURI (W911NF-08-1-0317), the Department of Energy, Basic Energy Sciences (DE-FG02-07ER46421), and the DARPA QuIST program (DAAD-19-01-0650) is gratefully acknowledged.

## 1.0 INTRODUCTION

The unifying theme for the work presented in this thesis is “designer quantum materials,” which refers to the idea that spin- $\frac{1}{2}$  objects and their interactions can be regarded as naturally-existing building blocks of a quantum “toolkit” with which one can *construct* the phenomena of quantum mechanics. This thesis attempts to demonstrate that the concept of designer quantum materials is fruitful in terms of both the fundamental physics that emerges in the constructed systems and the new resources and capabilities existing for these materials in the context of quantum information processing in solid-state systems. In the spirit of such a “bottom-up” approach to quantum mechanics, this introductory chapter presents fundamental aspects of a specific set of building blocks for quantum materials: the formal descriptions of single-spin and multi-spin systems are reviewed, and basic principles underlying the exchange and spin-orbit interactions are outlined. The final section of the chapter describes quantum information processing and the requirements for its physical implementation, as well as the realization of quantum bits (qubits) via both single-spin and multi-spin systems and their interactions, in order to provide the perspectives and motivation guiding the theoretical design of the quantum materials that are the focus of this work.

### 1.1 SPIN QUANTUM MECHANICS

#### 1.1.1 Single-spin systems

The elementary physical unit of the designer quantum materials considered in this thesis is a spin- $\frac{1}{2}$  object. Spin is an angular momentum intrinsic to the most fundamental constituents of matter that was first proposed for electrons by Uhlenbeck and Goudsmit [1] and exists only in a quantum-

mechanical description of nature; i.e., it has no analogue in classical physics. Using spin as a building block therefore naturally leads to *quantum* materials - those that exemplify the very essence of quantum mechanics. The particular case of a spin- $\frac{1}{2}$  object is characterized by a spin quantum number  $s = \frac{1}{2}$  associated with the eigenvalue of an operator  $S^2 = \mathbf{S} \cdot \mathbf{S}$ , where  $\mathbf{S}$  denotes the operator used to represent spin in quantum theory. For concreteness, the discussion in this thesis is written with the specific example of an electron spin in mind, but many of the ideas and mechanisms that are presented apply more generally to any spin- $\frac{1}{2}$  object.

The mathematical description of a spin- $\frac{1}{2}$  system is based on a two-dimensional Hilbert space. Basis states spanning this complex vector space can be expressed using quantum numbers derived from the eigenvalues of mutually commuting operators which act in the space. The spin vector operator is defined in terms of three components as  $\mathbf{S} = (S_x, S_y, S_z)$ , where the axes  $\tau = x, y, z$  correspond to a mapping of the complex two-dimensional spin space onto an equivalent three-dimensional real-space representation. In the language of group theory, the SU(2) and SO(3) group representations associated with rotations in these spaces are homomorphic [2], such that every real-space matrix in the group SO(3) can be associated with two spin matrices in the group SU(2). The real-space representation is also the basis of the Bloch sphere, which provides a geometric description for the state of a single qubit and will be discussed in more detail in Sec. 1.4.2.

Because  $\mathbf{S}$  is an angular momentum operator, its components satisfy the characteristic commutation relation  $[S_i, S_j] \equiv S_i S_j - S_j S_i = i\hbar \epsilon_{ijk} S_k$ . Here,  $\hbar = h/2\pi$ , where  $h$  is Planck's constant. Since this relation indicates that the spin component operators do not commute among themselves, all three components of spin  $(S_x, S_y, S_z)$  do not have a common set of eigenstates and cannot be simultaneously well-defined. On the other hand, the commutator between the operator  $S^2$  and any single component  $S_\tau$  does vanish:  $[S^2, S_\tau] = 0$ . The basis states can therefore be written as  $|s, m_s\rangle$ , where the notation corresponds to the eigenvalue equations

$$S^2 |s, m_s\rangle = s(s+1)\hbar^2 |s, m_s\rangle \quad (1.1)$$

and

$$S_\tau |s, m_s\rangle = m_s \hbar |s, m_s\rangle. \quad (1.2)$$

Through the action of the spin raising and lowering operators  $S_\pm \equiv S_x \pm iS_y$  on  $|s, m_s\rangle$ , it can be

shown that the allowed values of the spin magnetic quantum number  $m_s$  range from  $-s$  to  $s$  in steps of 1. For  $s = \frac{1}{2}$ ,  $m_s = \pm\frac{1}{2}$  so that the two possible states are  $|\frac{1}{2}, \frac{1}{2}\rangle$  and  $|\frac{1}{2}, -\frac{1}{2}\rangle$ . Often, the choice  $\tau = z$  is made in Eq. (1.2). The spin basis in this case is typically expressed in terms of the “spin-up” state  $|\uparrow\rangle \equiv |\frac{1}{2}, \frac{1}{2}\rangle$  and the “spin-down” state  $|\downarrow\rangle \equiv |\frac{1}{2}, -\frac{1}{2}\rangle$ . The most general spin state in the space can be written as a linear superposition of these two basis states in the form

$$|\psi\rangle = \alpha|\uparrow\rangle + \beta|\downarrow\rangle, \quad (1.3)$$

where  $\alpha$  and  $\beta$  are complex numbers satisfying the normalization condition  $|\alpha|^2 + |\beta|^2 = 1$ , which is obtained by requiring that  $\langle\psi|\psi\rangle = 1$ .

Quantum mechanics can be formulated within the two-dimensional spin Hilbert space for  $s = \frac{1}{2}$  using the language of linear algebra, which involves representing states by vectors and operators by matrices. The  $\tau = z$  spin basis states are typically represented by

$$|\uparrow\rangle \rightarrow \begin{pmatrix} 1 \\ 0 \end{pmatrix}, \quad |\downarrow\rangle \rightarrow \begin{pmatrix} 0 \\ 1 \end{pmatrix}. \quad (1.4)$$

A general state in the space can then be written as

$$|\psi\rangle \rightarrow \alpha \begin{pmatrix} 1 \\ 0 \end{pmatrix} + \beta \begin{pmatrix} 0 \\ 1 \end{pmatrix} = \begin{pmatrix} \alpha \\ \beta \end{pmatrix}. \quad (1.5)$$

The spin operator can be written in the form  $\mathbf{S} = \frac{\hbar}{2}\boldsymbol{\sigma}$ , where  $\boldsymbol{\sigma} = (\sigma_x, \sigma_y, \sigma_z)$  is the vector of Pauli spin operators. Their matrix representations according to Eq. (1.4) are given by

$$\sigma_x = \begin{pmatrix} 0 & 1 \\ 1 & 0 \end{pmatrix}, \quad \sigma_y = \begin{pmatrix} 0 & -i \\ i & 0 \end{pmatrix}, \quad \sigma_z = \begin{pmatrix} 1 & 0 \\ 0 & -1 \end{pmatrix}. \quad (1.6)$$

The Pauli matrices satisfy  $[\sigma_i, \sigma_j] = 2i\epsilon_{ijk}\sigma_k$ , which is consistent with the commutation relation for the spin component operators given above. In the remainder of this thesis, reference to a single “spin” is assumed to mean a spin- $\frac{1}{2}$  object (i.e., one for which  $s = \frac{1}{2}$ ) and the convention  $\hbar = 1$  is chosen unless otherwise specified.

### 1.1.2 Multi-spin systems

In the previous section, states and operators in the Hilbert space for a single spin were defined. The concept of a tensor product allows these states and operators to be extended into a space, known as a product space, that describes systems having two or more spins [3]. The product space concept is therefore central to the mathematical description of designer quantum materials constructed from multiple spins.

In general, given  $n$  vector spaces  $\mathcal{H}_1, \mathcal{H}_2, \dots, \mathcal{H}_n$ , the product space  $\mathcal{H}_p$  is obtained by taking the tensor product of the individual vector spaces:

$$\mathcal{H}_p = \mathcal{H}_1 \otimes \mathcal{H}_2 \otimes \dots \otimes \mathcal{H}_n.$$

The dimension of  $\mathcal{H}_p$  is the product of the dimensions of  $\mathcal{H}_1, \mathcal{H}_2, \dots, \mathcal{H}_n$ . An  $n$ -spin space is therefore  $2^n$ -dimensional. A state vector in  $\mathcal{H}_p$  is obtained by taking the tensor product of the state vectors defined in the individual vector spaces  $\mathcal{H}_1, \mathcal{H}_2, \dots, \mathcal{H}_n$ :

$$|\Psi\rangle = |\psi_1\rangle \otimes |\psi_2\rangle \otimes \dots \otimes |\psi_n\rangle \equiv |\psi_1, \psi_2, \dots, \psi_n\rangle$$

In particular, a basis for a product space can be found by taking the tensor products of basis vectors in the individual spaces. Similarly, the matrix representation of an operator in the product space is given by the tensor product of the matrix representations of the operators in the individual vector spaces. If an operator  $A_i$  acts in only one of the vector spaces (denoted by  $i$ ), the identity operator is used for the remaining spaces in the tensor product,

$$A_i^{\text{ext}} = \mathbf{1}_1 \otimes \mathbf{1}_2 \otimes \dots \otimes A_i \otimes \dots \otimes \mathbf{1}_n,$$

and the resulting product operator  $A_i^{\text{ext}}$  is known as the extension of  $A_i$  into the product space.

As a concrete example, consider two  $s = \frac{1}{2}$  spins represented by the operators  $\mathbf{S}_1$  and  $\mathbf{S}_2$ . In this case, the product spin space has dimension  $d = 2^2 = 4$ . One possible basis for the two-spin system consists of the four possible product states formed by taking the tensor products of the single-spin states  $|\uparrow\rangle$  and  $|\downarrow\rangle$ :

$$\{|\uparrow\uparrow\rangle, |\uparrow\downarrow\rangle, |\downarrow\uparrow\rangle, |\downarrow\downarrow\rangle\} \quad (1.7)$$

An alternative basis which spans the product space for two spins can be defined in terms of the spin quantum numbers  $S$  and  $S_Z$  associated with the eigenvalues of the total-spin operators  $S^2 = (\mathbf{S}_1 + \mathbf{S}_2)^2$  and  $S_Z = S_{1z} + S_{2z}$ , respectively, via two-spin analogues of Eqs. (1.1) and (1.2). In this case,  $S^2$ ,  $S_Z$ ,  $S_1^2$ , and  $S_2^2$  form a complete set of commuting observables. According to the theory of angular momentum addition, the possible values for the total spin are  $S = 0, 1$ . Each value of  $S$  is associated with a subspace of dimension  $2S + 1$ . Since  $s_1 = s_2 = \frac{1}{2}$  for all states, the eigenstates can be denoted by  $|S, S_Z\rangle$ , where  $S_Z$  is the quantum number for the  $z$  component of total spin. Using this notation, the singlet state with  $S = 0$  is given by

$$|0, 0\rangle = \frac{1}{\sqrt{2}}(|\uparrow\downarrow\rangle - |\downarrow\uparrow\rangle). \quad (1.8)$$

The remaining three states have  $S = 1$  and are the triplet states,

$$\begin{aligned} |1, 1\rangle &= |\uparrow\uparrow\rangle, \\ |1, 0\rangle &= \frac{1}{\sqrt{2}}(|\uparrow\downarrow\rangle + |\downarrow\uparrow\rangle), \\ |1, -1\rangle &= |\downarrow\downarrow\rangle, \end{aligned} \quad (1.9)$$

The states  $(|\uparrow\downarrow\rangle \pm |\downarrow\uparrow\rangle)/\sqrt{2}$  are examples of Einstein-Podolsky-Rosen (EPR) pairs, which are *entangled* states of two spins [4, 5]. In general, an entangled state is defined in a product space and is a superposition of product states that cannot be written as a single product of states of the individual systems in any basis [6].

The product space concept can be extended to the case of an  $n$ -spin system, allowing the calculation of spin operators such as the square of the total spin angular momentum  $S^2 = (\sum_{k=1}^n \mathbf{S}_k)^2$  and the total  $z$  component of spin  $S_Z = \sum_{k=1}^n S_{kz}$  which act in the  $n$ -spin product space. Once representations of states and operators for single-spin and multi-spin systems have been determined, they can be used to write expressions for Hamiltonians that yield the spin-dependent spectral properties of these systems. The Hamiltonians relevant for the construction of the designer quantum materials discussed in the present work are those describing the exchange and spin-orbit interactions. These interactions are therefore the focus of the next two sections.

## 1.2 EXCHANGE INTERACTION

The exchange interaction is an *effective* coupling between electron spins that emerges from the combined effects of Coulomb (electrostatic) interactions, the symmetrization postulate for the wavefunction of a multi-fermion system, and the Pauli exclusion principle. An illustration of how these factors effectively give rise to exchange interactions between spins is provided by a system with just two electrons. The repulsive interaction between the electrons prevents a separation of the Hamiltonian into terms describing individual electrons and therefore does not allow for an exact solution of the Schrödinger equation. Approximate analytical approaches such as the Heitler-London method [7] have therefore been used to study two-electron systems such as the hydrogen molecule  $\text{H}_2$ . The Heitler-London approach is mentioned here since it provides one way to understand how the Heisenberg exchange interaction between spins arises.

In order to describe the  $\text{H}_2$  system in the presence of Coulomb interactions, the Heitler-London approximation employs two-electron orbital states of the form

$$\Phi_{\pm} = N_{\pm} [\phi_a(\mathbf{r}_1)\phi_b(\mathbf{r}_2) \pm \phi_b(\mathbf{r}_1)\phi_a(\mathbf{r}_2)], \quad (1.10)$$

where  $\phi_a$  and  $\phi_b$  are single-electron orbital eigenfunctions of the Hamiltonian for each hydrogen (H) atom,  $\mathbf{r}_1$  and  $\mathbf{r}_2$  are the positions of the electrons, and  $N_{\pm}$  are normalization constants. The states  $\Phi_{\pm}$  are linear superpositions of products of orbital wavefunctions that are related by an *exchange* of the electronic coordinates  $\mathbf{r}_1$  and  $\mathbf{r}_2$ . Note that under this exchange,  $\Phi_{\pm} \rightarrow \pm\Phi_{\pm}$ ; i.e.,  $\Phi_+$  is a symmetric function, while  $\Phi_-$  is an antisymmetric function. It can be shown [8, 9] that the Coulomb interactions give rise to an energy splitting  $E_- - E_+$ , called the *exchange splitting*, for the orbital states  $\Phi_{\pm}$ . In order to construct the total two-electron wavefunctions, the spin states of the electrons must also be specified. The possible two-electron spin states are the singlet [Eq. (1.8)] and triplet [Eq. (1.9)] states resulting from the addition of two spins described in Sec. 1.1.2. While the singlet state is antisymmetric with respect to exchange of the spin states of the electrons, all three of the triplet states are symmetric.

Taken together, the symmetries of the orbital and spin states under exchange determine the overall symmetry of the full two-electron state. Because electrons have half-integral spin ( $s = \frac{1}{2}$ ),

they are fermions. The symmetrization postulate therefore requires that the total state of a multi-electron system be antisymmetric with respect to the simultaneous exchange of both the spatial and spin coordinates of the electrons. In terms of the two-electron orbital states in Eq. (1.10) and spin states in Eqs. (1.8) and (1.9), the antisymmetry of the total state can be achieved in two ways: either the symmetric orbital state  $\Phi_+$  can be combined with the antisymmetric singlet state [Eq. (1.8)], or the antisymmetric orbital state  $\Phi_-$  can be combined with any of the symmetric triplet states [Eq. (1.9)]. In other words, two electrons in a symmetric spatial state must have total spin  $S = 0$ , and two electrons in an antisymmetric spatial state must have  $S = 1$ . The antisymmetry of the total electronic wavefunction is also an expression of the Pauli exclusion principle, which states that two electrons cannot exist in completely identical orbital and spin states simultaneously. This can be seen, for example, from the two-electron antisymmetrized state

$$|\Phi_-\rangle |\uparrow\uparrow\rangle = N_- (|\phi_a, \phi_b\rangle - |\phi_b, \phi_a\rangle) |\uparrow\uparrow\rangle, \quad (1.11)$$

where  $\langle \mathbf{r}_1, \mathbf{r}_2 | \phi_a, \phi_b \rangle \equiv \phi_a(\mathbf{r}_1) \phi_b(\mathbf{r}_2)$  and  $\langle \mathbf{r}_1, \mathbf{r}_2 | \phi_b, \phi_a \rangle \equiv \phi_b(\mathbf{r}_1) \phi_a(\mathbf{r}_2)$ . Eq. (1.11) describes two electrons in identical spin states. If both electrons are also in the same orbital state, so that  $\phi_a = \phi_b$ , then Eq. (1.11) vanishes. Therefore, two electrons cannot have identical total wavefunctions. This implies that two electrons in the same orbital state must have opposite spin states, while two electrons which have the same spin state must be in different orbitals. Thus, even though spin is not explicitly included in the Hamiltonian for the two-electron system, the symmetrization postulate and the Pauli exclusion principle introduce a correlation between the spatial and spin states of the two electrons.

To understand how this correlation leads to an effective spin-spin interaction, consider the energy splitting  $E_- - E_+$ . Because  $E_+$  and  $E_-$  are the energies of the states  $\Phi_+$  and  $\Phi_-$ , and because these states are in turn correlated with the singlet [Eq. (1.8)] and triplet [(1.9)] spin states, respectively, the splitting  $E_- - E_+$  is also equal to the singlet-triplet energy gap  $\Delta E_{st}$  between the  $S = 0$  and  $S = 1$  states. For the hydrogen molecule  $\text{H}_2$ ,  $\Delta E_{st} = E_- - E_+ > 0$  [8], so that the singlet state is energetically favored.

Werner Heisenberg [10] realized that the two-electron spectrum characterized by the singlet-triplet energy splitting  $\Delta E_{st}$  can also be obtained from a *spin* Hamiltonian of the form

$$H_{\text{exch}} = J \mathbf{S}_1 \cdot \mathbf{S}_2 = J (S_{1x} S_{2x} + S_{1y} S_{2y} + S_{1z} S_{2z}) \quad (1.12)$$

where  $J = \Delta E_{st}$  is known as the exchange constant and is a real number that represents the strength of the interaction between the spins. Eq. (1.12) is the Hamiltonian representing the Heisenberg exchange interaction. Semiclassically, the dot product of two spin operators,  $\mathbf{S}_1 \cdot \mathbf{S}_2$ , expresses the energy of the two-electron system in terms of the relative orientations of the two spins. The spectrum of the Heisenberg Hamiltonian can be found by rewriting Eq. (1.12) using  $S^2 = S_1^2 + S_2^2 + 2\mathbf{S}_1 \cdot \mathbf{S}_2$ , which gives

$$H_{\text{exch}} = \frac{J}{2} (S^2 - S_1^2 - S_2^2). \quad (1.13)$$

Since  $[H_{\text{exch}}, S^2] = [H_{\text{exch}}, S_Z] = 0$ , the eigenstates are the two-spin states  $\{|S, S_Z\rangle\}$  discussed in Sec. 1.1.2. Applying Eq. (1.13) to these states gives the eigenvalues  $E_s = -3J/4$  and  $E_t = J/4$  for the singlet ( $S = 0$ ) and triplet ( $S = 1$ ) states, respectively. A matrix representation of Eq. (1.12) in the two-spin product-state basis  $\{|\uparrow\uparrow\rangle, |\uparrow\downarrow\rangle, |\downarrow\uparrow\rangle, |\downarrow\downarrow\rangle\}$  can be determined by writing Eq. (1.12) in the alternate form

$$H_{\text{exch}} = J \left[ S_{1z}S_{2z} + \frac{1}{2} (S_{1+}S_{2-} + S_{1-}S_{2+}) \right] \quad (1.14)$$

and calculating the action of these operators on the basis states or by applying the product space formalism for two spins described in Sec. 1.1.2 to Eq. (1.12) directly. Either method leads to the Hamiltonian matrix

$$H_{\text{exch}} \rightarrow J \begin{pmatrix} \frac{1}{4} & 0 & 0 & 0 \\ 0 & -\frac{1}{4} & \frac{1}{2} & 0 \\ 0 & \frac{1}{2} & -\frac{1}{4} & 0 \\ 0 & 0 & 0 & \frac{1}{4} \end{pmatrix}. \quad (1.15)$$

Diagonalization of this matrix confirms that the eigenstates of the Heisenberg Hamiltonian are precisely the singlet and triplet states in Eqs. (1.8) and (1.9). Since these states include EPR pairs, we see that the Heisenberg exchange interaction can produce entanglement between two spins.

The spectrum of  $H_{\text{exch}}$  is illustrated in Fig. 1.1. The size of the splitting is  $\Delta E_{st} = E_t - E_s = J$ . According to the sign convention adopted in writing Eq. (1.12),  $J > 0$  (Fig. 1.1) implies that the singlet state is the ground state and represents an *antiferromagnetic* (AFM) exchange interaction, while  $J < 0$  implies that the triplet states are lower in energy and corresponds to *ferromagnetic*

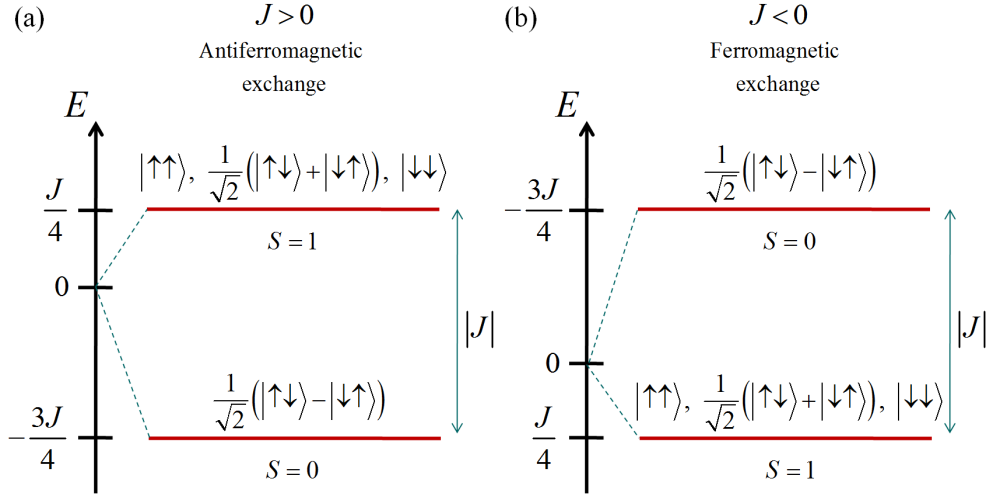


Figure 1.1: Spectrum of the Heisenberg exchange Hamiltonian for two spins [Eq. (1.12)]. (a) Antiferromagnetic (AFM) exchange coupling ( $J > 0$ ). (b) Ferromagnetic (FM) exchange coupling ( $J < 0$ ).

(FM) exchange. The singlet ground state of the  $H_2$  molecule therefore indicates that the two electron spins are coupled by AFM exchange. The energy splitting  $J = \Delta E_{st}$  can be identified with the exchange splitting  $E_- - E_+$  from the Heitler-London calculation. In this way, the Heisenberg Hamiltonian, which contains only spin, is able to capture the essential features of the spectrum for a two-electron Hamiltonian with only electrostatic (charge) interactions and no explicit spin-dependent term.

This effective Hamiltonian approach is also useful in describing the spin-dependent spectrum for multi-electron systems, since the calculation of the spectrum does not require dealing directly with the multiple pairwise electron-electron interactions that complicate the original Hamiltonian. Because *atomic* orbitals are used to construct the Heitler-London orbital states [Eq. (1.10)] associated with the exchange splitting, the Heisenberg model describing this splitting is a reasonable approximation only for well-localized electrons. By generalizing the Heisenberg model and assuming that the electrons are localized at the sites of a lattice, multi-electron systems can be described as systems of exchange-coupled spins. In this thesis, only nearest-neighbor exchange interactions

(i.e., those between spins located at adjacent sites) are considered. Summing all distinct pairwise interactions of the form given in Eq. (1.12) for a one-dimensional system of  $n$  spins coupled via nearest-neighbor Heisenberg exchange yields the Hamiltonian

$$H = \sum_{k=1}^N J_k (\mathbf{S}_k \cdot \mathbf{S}_{k+1}) = \sum_k J_k (S_{kx}S_{k+1,x} + S_{ky}S_{k+1,y} + S_{kz}S_{k+1,z}), \quad (1.16)$$

where  $N = n - 1$  for open boundary conditions, or  $N = n$  with  $k \pm n \equiv k$  for periodic boundary conditions. The symmetries of  $H_{\text{exch}}$  for two spins [Eq. (1.12)] also extend to the  $n$ -spin case:  $H$  commutes with both  $S^2 = (\sum_{k=1}^n \mathbf{S}_k)^2$  and  $S_Z = \sum_{k=1}^n S_{kz}$ , and eigenstates can be defined in terms of the quantum numbers  $S$  and  $S_Z$  associated with these operators. For an arbitrary spin basis, block diagonalization of  $H$  can be carried out such that calculations can be restricted to a subspace of definite  $S$  and/or  $S_Z$ . These symmetries exist for any set of exchange constants  $\{J_k\}$  in Eq. (1.16), and we therefore use the quantum numbers  $S$  and  $S_Z$  to describe the Heisenberg spin systems with spatially-modulated exchange that we discuss in this thesis.

As in the two-spin case, the sign convention used in writing Eq. (1.16) implies that an exchange interaction  $J_k$  between spins  $k$  and  $k + 1$  is AFM for  $J_k > 0$  and FM for  $J_k < 0$ . An AFM spin chain is described by  $H$  in Eq. (1.16) with  $J_k > 0$  for all  $k$ , while a FM spin chain is described by  $H$  with  $J_k < 0$  for all  $k$ . According to the Lieb-Mattis theorem, the ground states of AFM spin chains have minimum total spin  $S$  [11], while those of FM spin chains have maximum  $S$  [12]. The simplest manifestation of this theorem is found in the two-spin case (see Fig. 1.1). This ordering of energy levels can be understood semiclassically as arising from the tendency for AFM (FM) interactions to favor antiparallel (parallel) alignment of neighboring spins. In addition, Haldane's conjecture [13, 14] predicts that the spectrum of AFM chains of spin- $s$  objects contains a finite gap above the ground state for integer values of  $s$  and zero gap for half-integer values of  $s$ .

The Heisenberg Hamiltonian in Eq. (1.16) describes a one-dimensional chain of spins coupled by *isotropic* exchange, since the terms involving the interactions between the  $x$ ,  $y$ , and  $z$  components of spins  $k$  and  $k + 1$  all have the same exchange interaction strength  $J_k$ . The case of a uniform spin chain, which is defined by  $J_k = J$  for all  $k$ , can be solved exactly via the Bethe ansatz [15]. In this thesis, *spatially-varying* isotropic exchange plays a key role in the construction of designer

quantum materials based on exchange-coupled spins. Anisotropic exchange interactions can be described by generalizing Eq. (1.16) to

$$H = \sum_k (J_{kx} S_{kx} S_{k+1,x} + J_{ky} S_{ky} S_{k+1,y} + J_{kz} S_{kz} S_{k+1,z}). \quad (1.17)$$

Special cases of this Hamiltonian include Ising interactions, for which only one of the three exchange constants  $J_{kx}$ ,  $J_{ky}$ ,  $J_{kz}$  is nonzero, XY exchange, for which  $J_{kz} = 0$ ,  $J_{kx} \neq 0$ , and  $J_{ky} \neq 0$  for all  $k$ , and XXZ exchange, for which  $J_{kx} = J_{ky} \neq J_{kz}$  for all  $k$ . Although this thesis focuses on isotropic (Heisenberg) exchange interactions, anisotropic exchange interactions are relevant for certain physical systems. For example, the presence of spin-orbit coupling (which is the topic of the next section) leads to anisotropic exchange terms such as the Dzyaloshinskii-Moriya interaction [16, 17]. Both isotropic and anisotropic exchange Hamiltonians can be generalized in order to describe interacting spins in two and three dimensions and can also be mapped to systems of spinless noninteracting fermions via the Jordan-Wigner transformation [18, 19, 20].

Finally, we note that the Heisenberg Hamiltonian can also be obtained by taking the “strong coupling” limit of the one-dimensional single-band Hubbard model at “half-filling,” i.e., with one electron per site [21]. This model involves the interplay of kinetic energy represented by a hopping amplitude  $t$  that is associated with the movement of electrons between sites, and an “on-site” energy  $U$  describing Coulomb repulsion between electrons on the same site. The kinetic energy term of this Hamiltonian corresponds to the single-band tight-binding Hamiltonian in one dimension that is described in Chs. 4 and 5. The “strong coupling” limit is defined as  $U \gg t$  and yields an intermediate expression known as the  $t - J$  model, which for half-filling reduces to the Heisenberg model with the exchange coupling given by  $J = 4t^2/U$ .

### 1.3 SPIN-ORBIT INTERACTION

So far, the discussion in this thesis has regarded the spatial and spin degrees of freedom of electrons separately. The connection between the orbital states in the presence of electrostatic interactions

[Eq. (1.10)] and the spin eigenstates of the Heisenberg Hamiltonian [Eqs. (1.8)-(1.9)] exists because of an equivalence of the spectral splitting between the states and the symmetrization requirement for the total electronic wavefunction. This correlation does not imply that a direct coupling between the spin and orbital (or spatial) degrees of freedom is present, as illustrated by the fact that the eigenstates can still be expressed in the form of product states such as Eq. (1.11).

It can be shown [22] that the Hamiltonian of a single electron in a solid in general contains, in addition to terms such as the kinetic energy associated with its motion and the periodic potential describing the lattice [23], a term which describes a coupling of the electron spin to its spatial motion. In order to understand the physical consequences of this spin-orbit coupling term, it is useful to consider the analogous coupling of spin to external magnetic fields. This is based on the association of a magnetic dipole moment  $\boldsymbol{\mu}$  with an electron spin  $\mathbf{S}$  via the relation  $\boldsymbol{\mu} = -g\mu_B\mathbf{S}/\hbar$ , where  $g$  is the electron g-factor<sup>1</sup> and  $\mu_B = e\hbar/2m_e$  is the Bohr magneton, with  $e$  the magnitude of the electronic charge and  $m_e$  the free electron mass. By analogy with classical physics, the energy of a magnetic dipole moment in an external magnetic field  $\mathbf{B}$  is given by  $-\boldsymbol{\mu} \cdot \mathbf{B}$ , which leads to the spin Hamiltonian for the Zeeman interaction:

$$H_Z = -\frac{g\mu_B}{\hbar}\mathbf{B} \cdot \mathbf{S} = -\frac{g\mu_B}{2}\mathbf{B} \cdot \boldsymbol{\sigma}. \quad (1.18)$$

Note that in  $H_Z$ , the external magnetic field  $\mathbf{B}$  is treated as a classical quantity rather than as an operator.

The spin-orbit interaction in solids has the general form [22, 24]

$$H_{\text{so}} = \frac{\hbar^2}{4m^{*2}c^2}(\nabla V \times \mathbf{k}) \cdot \boldsymbol{\sigma}, \quad (1.19)$$

where  $\nabla V$  denotes the gradient of the potential  $V$  experienced by the electron,  $\hbar\mathbf{k}$  is the electronic momentum,  $m^*$  is the electron effective mass, and  $c$  is the speed of light. By comparing Eqs. (1.19) and (1.18), it can be seen that the spin-orbit interaction has the form of a coupling of the electron spin to a momentum-dependent *effective* magnetic field  $\mathbf{B}_{\text{eff}} = (-\hbar^2/2g\mu_B m^{*2}c^2)(\nabla V \times \mathbf{k})$  (Fig. 1.2). The origin of this effective magnetic field can be understood intuitively using concepts from relativity theory. Because an electron has a negative charge and exists in an environment of charged entities in a solid, an electric field is present in the system. The spatial motion of the electron in this

---

<sup>1</sup>In general, the value of  $g$  for a material is direction dependent, and  $g$  is therefore a tensor.

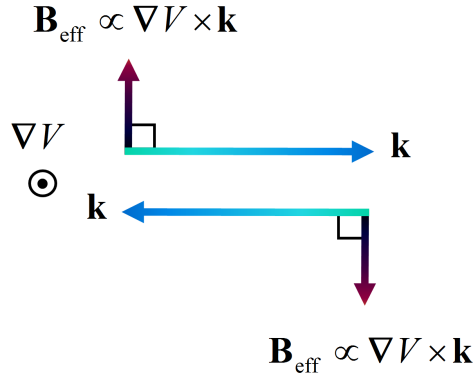


Figure 1.2: Effective magnetic field due to spin-orbit interaction in a one-dimensional electron system with a perpendicular potential gradient.

electric field can be viewed as a motion of the surrounding charge in the rest frame of the electron, and this charge current gives rise to an effective magnetic field that couples to the electron spin in a manner analogous to Eq. (1.18). The Zeeman-like coupling term obtained in this way must be multiplied by a factor of 1/2, which accounts for the fact that an electric field perpendicular to the velocity of the electron causes the electron to move in a circular trajectory. This motion corresponds to a rotation of the electron's rest frame, and the associated acceleration results in an additional precession of the electron spin known as Thomas precession [25]. With this correction, the Hamiltonian (1.19) describing the spin-orbit interaction can be obtained. This term can also be derived by taking a nonrelativistic limit of the Dirac equation [24], which is the counterpart of the Schrödinger equation in relativistic quantum mechanics.

The analogy between (1.18) and (1.19) implies that the spin-orbit interaction can be used to manipulate spins in a manner analogous to the Zeeman interaction. The important distinction is that the effective magnetic field due to spin-orbit coupling can be controlled by an electric field  $\mathbf{E}$ , via its dependence on the potential gradient  $\nabla V = e\mathbf{E}$ , as well as through the momentum  $\mathbf{k}$  of the electron. These additional mechanisms for producing and controlling magnetic fields via spin-orbit coupling therefore provide new resources that enhance the toolkit for constructing spin-based designer quantum materials.

Although the spin-orbit interaction gives rise to an effective magnetic field  $\mathbf{B}_{\text{eff}}$ , this field is fundamentally different from an external magnetic field  $\mathbf{B}$ . The distinction lies in the Hamiltonians  $H_{\text{so}}$  [Eq. (1.19)] and  $H_Z$  [Eq. (1.18)] associated with these fields: while  $H_Z$  breaks time-reversal symmetry,  $H_{\text{so}}$  preserves it. This can be seen by recalling the effect of the antiunitary time reversal operator  $K$  on the operators involved in these Hamiltonians [26]. Because the magnetic field  $\mathbf{B}$  is treated as a classical quantity rather than as a quantum-mechanical operator, it is not affected by  $K$ . Since the potential  $V$  is a function of the position operator  $\mathbf{r}$ ,  $\nabla V = \nabla V(\mathbf{r})$ . Using  $K^\dagger \mathbf{r} K = \mathbf{r}$ ,  $K^\dagger \mathbf{k} K = -\mathbf{k}$ , and  $K^\dagger \boldsymbol{\sigma} K = -\boldsymbol{\sigma}$  leads to  $K^\dagger H_Z K = -H_Z$  and  $K^\dagger H_{\text{so}} K = H_{\text{so}}$ . Rewriting these relations gives  $[H_Z, K] \neq 0$  and  $[H_{\text{so}}, K] = 0$ . Thus,  $H_Z$  does not preserve time-reversal symmetry, whereas  $H_{\text{so}}$  is invariant under time reversal. Note also that the internal field  $\mathbf{B}_{\text{eff}}$  is a quantum-mechanical operator, whereas the external field  $\mathbf{B}$  is treated classically.

Spin-orbit coupling exists in those physical systems for which the potential experienced by electrons in a solid is asymmetric under spatial inversion (corresponding to the transformations  $\mathbf{r} \rightarrow -\mathbf{r}$ ,  $\mathbf{k} \rightarrow -\mathbf{k}$ , and  $\boldsymbol{\sigma} \rightarrow \boldsymbol{\sigma}$ ). This inversion asymmetry can arise from either the crystal structure of the bulk solid (“bulk inversion asymmetry”), which gives rise to Dresselhaus spin-orbit coupling [27], or from an externally-imposed confinement potential (“structural inversion asymmetry”), which produces Rashba spin-orbit coupling [28, 29]. A heterostructure formed from two different materials provides a typical example of a system in which both types of spin-orbit interaction may exist [24]. Electrons confined by the potential formed at the interface between the materials move in an effectively two-dimensional region (see Ch. 4). If the confinement potential is asymmetric with respect to inversion, a net electric field  $\mathbf{E} = \nabla V/e$  is present in the direction parallel to the confinement. Assuming the confinement to be along the  $z$  direction, the two-dimensional motion of electrons in this electric field gives rise to a Rashba spin-orbit interaction that can be written as

$$H_R = \alpha(k_x \sigma_y - k_y \sigma_x), \quad (1.20)$$

where the strength  $\alpha$  of the coupling depends on the magnitude of the electric field. The tuning of  $\alpha$  in heterostructures using electric fields produced by gate voltages has been experimentally demonstrated [30]. This tunability suggests that the Rashba form of the spin-orbit interaction is

naturally suited to the construction of designer quantum materials with tailored spin-orbit interactions. In this thesis, we focus on spin-orbit coupling in quantum wires, which confine the motion of electrons to one spatial dimension. General features of Rashba spin-orbit coupling in these systems are accordingly discussed in Ch. 4. We note here that some of the features we describe are more general and also apply to the form of the Dresselhaus spin-orbit interaction that depends linearly on momentum,

$$H_D = \beta(k_x\sigma_x - k_y\sigma_y), \quad (1.21)$$

where  $\beta$  is the strength of the interaction. While the spin is always perpendicular to the momentum in  $H_R$ , the spin and momentum are parallel for the form of  $H_D$  given in Eq. (1.21). An effective magnetic field along a particular direction can be produced by either type of spin-orbit interaction, as long as the momentum is in the direction required to produce that field via the form of spin-orbit coupling existing in the system.

## 1.4 SPIN-BASED QUANTUM INFORMATION PROCESSING

### 1.4.1 Physical implementation of quantum information processing

While the term “information” might suggest an abstract concept, the idea of quantum information processing is rooted in the recognition that information ultimately always exists in the form of some concrete physical system [31]. At a fundamental level, physical systems are described by quantum theory. It therefore follows naturally that elementary units of quantum information can be defined using two distinct quantum states of elementary physical units such as electrons and atoms [6]. Unlike the bits encoded via voltages in conventional computers (i.e., processors of classical information) that can take only one of two discrete values “0” and “1” (corresponding to “low” and “high” voltages, respectively), the states  $|0\rangle$  and  $|1\rangle$  representing the logical basis of the *quantum* bit (qubit) define a continuous two-dimensional space of possible superposition states of the form

$$|\psi\rangle = \alpha|0\rangle + \beta|1\rangle, \quad (1.22)$$

where  $\alpha$  and  $\beta$  are any two complex numbers satisfying the normalization condition  $|\alpha|^2 + |\beta|^2 = 1$ . The fact that the fundamental unit of quantum information can effectively exist in more than one logical state at a time already indicates one way in which the processing of information governed by the laws of quantum mechanics would be far more powerful than its classical counterpart: because superpositions of states are possible, logical gate operations can be carried out simultaneously on the states  $|0\rangle$  and  $|1\rangle$  of every qubit [32], enabling computations to occur in parallel with one another in an inherently quantum-mechanical way. Such new capabilities in computational power promised by quantum information processing, particularly in the context of simulating quantum systems, also inspired the fundamental work of Feynman in this field [33, 34].

In order to build a quantum information processor, it is necessary to find physical systems in which qubits can be stored, manipulated, measured, and transported from one location to another with a high degree of control while minimizing errors. DiVincenzo specifies the requirements to be satisfied by quantum information processing implementations via a set of seven criteria [35]:

1. A scalable physical system with well-characterized qubits
2. The ability to initialize the qubits to a reference state such as  $|000\dots\rangle$
3. Long relevant decoherence times that are much longer than gate operation times
4. A “universal” set of quantum gates
5. The ability to measure specific qubits
6. Interconversion between stationary and “flying” qubits
7. Faithful transmission of flying qubits

Requirements 1-5 relate to quantum computation, while requirements 6 and 7 are concerned with the transport of quantum information. According to these guidelines, the first step in constructing a quantum computer is to identify qubits within a suitable physical system that can also be scaled up to incorporate many qubits (requirement 1). The qubit must be well-defined, in the sense that (1) the logical basis states  $|0\rangle$  and  $|1\rangle$  used to define the qubit are distinguishable by some quantum number associated with a physical observable present in the Hamiltonian of the system, and (2) the Hamiltonians describing the interactions of an individual qubit with other qubits, external fields, and other degrees of freedom are known. Replacing the states  $|0\rangle$  and  $|1\rangle$  in the definition of a general qubit state  $|\psi\rangle$  with the basis states  $|\uparrow\rangle$  and  $|\downarrow\rangle$  representing the eigenstates of  $S_z$  for a

single spin given in Sec. 1.1.1 reveals that the definitions of a qubit and a single spin- $\frac{1}{2}$  object are equivalent. In addition, the Hamiltonians describing a single spin, the exchange interactions between spins (Sec. 1.2), and the coupling of spins to external magnetic fields and orbital degrees of freedom (Sec. 1.3) are known. A spin- $\frac{1}{2}$  object is therefore a well-defined qubit, and conversely, any qubit can be mapped onto a spin- $\frac{1}{2}$  system.

Once a suitable qubit encoding has been identified, it must be possible to initialize the qubits into a specific starting state (requirement 2). Methods that can be used to reach a desired initial state include cooling a system to the ground state of an appropriately-chosen Hamiltonian via dissipation of energy and performing measurements which project the system into the desired state. These initialization processes are irreversible and therefore cannot be represented by unitary transformations, for which inverses always exist. On the other hand, the quantum gates (requirement 4) that are used to manipulate the states of qubits in order to achieve a desired computational result *are* unitary transformations that are generated by the physical Hamiltonians describing the qubit and its interactions. An interaction between two qubits such as the exchange coupling between spins produces entanglement, which is a resource required for harnessing the true power of quantum information processing. For a given physical implementation, the set of possible quantum gates must be “universal” in the sense that any operation can be decomposed into a sequence of gates in the set. It has been shown that such a set can be composed only of gates acting on one and two qubits [36, 37].

The quantum gate operations must also be carried out rapidly compared to the characteristic timescales for the decay of the information encoded in the qubits (requirement 3). These *decoherence times* describe the dynamics of qubits interacting with their environment and depend on the particular physical implementation [38]. Due to this interaction, loss of the coherence represented by the definite relative phase between the states  $|0\rangle$  and  $|1\rangle$  that determines the specific qubit superposition state occurs. As a result, quantum gates effectively act on the wrong initial states. The decoherence times relevant for the specific physical system used to encode the qubit must therefore be much longer than the gate operation times. Finally, a method must exist by which the results of quantum computations can be read out (requirement 5). The read-out process involves a quantum measurement that projects the state of the qubits onto the space of eigenstates of some observable. In order to be able to measure specific qubits, the measurement of one qubit should not affect the

state of the remaining qubits in the quantum computer.

Several different physical systems have been proposed as realizations of qubits, including trapped ions [39, 40], neutral atoms [41, 42], ensembles of nuclear spins in molecules manipulated via nuclear magnetic resonance (NMR) [43, 44], photons [45, 46], spin [47] or charge [48] states of electrons confined to solid-state quantum dots, electronic and nuclear spins of impurities in solids [49, 50, 51], and superconducting systems [52, 53, 54]. Each of these systems possesses characteristic advantages and disadvantages that depend on the internal Hamiltonian, the nature of interactions with the environment, and practical considerations involved in the construction of a quantum information processor. The existence of well-developed spin resonance techniques provides a straightforward method for carrying out quantum gate operations in NMR-based systems, but scaling up these systems to large numbers of qubits is difficult [6]. Implementations based on trapped ions and neutral atoms are promising because these systems are well isolated from their environment, resulting in relatively slow decoherence. Recently, trapped calcium ions have been used to produce a “quantum register” consisting of 14 qubits in an entangled state [55], which represents the largest collection of qubits with controlled entanglement that has been realized to date.

We note here that the discussion so far has assumed a particular model of quantum computation, known as the circuit model, in which the quantum gates are unitary transformations. A different scenario is provided by “one-way” quantum computing [56, 57, 58]. This scheme allows for the manipulation of quantum information via nonunitary transformations by applying specific sequences of measurements to a network of qubits initially prepared in a highly-entangled “cluster state.” The emerging field of topological quantum computation proposes an alternative to quantum information processing schemes based on two-state *local* encodings of qubits: the quantum information is instead encoded in the collective degenerate ground states of multiple quasiparticles known as non-Abelian anyons [59]. Such an encoding is *nonlocal* and therefore protects the qubit from local perturbations, building fault tolerance into the physical “hardware” of a quantum information processor. Quantum gate operations are performed via “braiding” of the quasiparticles, which involves moving them around one another in  $2+1$  spacetime dimensions such that nontrivial unitary transformations of the qubit states are generated.

The work described in this thesis focuses on spin, which represents a strong candidate for

storing qubits in systems ranging from the hyperfine states of trapped ions [40] to the electronic and nuclear spins [47, 60, 49, 50, 51] in solid-state systems. While the weak coupling of spins to their environment poses challenges in the measurement of spin qubits, this isolation also enables spin-based qubits to have long decoherence times relative to, e.g., qubits encoded in charge (orbital) degrees of freedom that are sensitive to fluctuations of the electrostatic potential caused by the environment. Compared to physical realizations of quantum information processing involving ions and atoms, solid-state implementations are more readily scalable [6]. These advantages of using single spins in solid-state systems as qubits have inspired several proposals for spin-based implementations of quantum information processors [47, 60, 49, 61, 62, 63, 64, 50, 51]. The electron/nuclear spin systems associated with nitrogen-vacancy (N-V) centers present in diamond have especially long decoherence times and can be controlled even at room temperature [65]. For single electron spins in quantum dots, read-out of the states can be accomplished via electrical methods that typically involve spin-to-charge conversion via spin-dependent tunneling, or by optical methods in which the spin information is transferred to, e.g., the polarization of emitted light [66, 67]. Experimental research in the Levy research group centers on a proposed implementation based on Ge/Si quantum dots [63].

In addition to local quantum computation, quantum information processing tasks such as quantum teleportation [68] and long-range gating [69] require “flying qubits” (requirements 6 and 7). Meeting these criteria involves the identification of methods for efficiently interconverting the quantum information between stationary and flying qubits, as well as for faithfully transporting flying qubits from one location to another, without a significant loss of quantum information. In many proposals, flying qubits take the form of photons which can carry qubits in, e.g., their polarization or number state. Photons are well-suited to long-range quantum information transport because they can be carried over large distances using optical fibers [70]. However, since qubits are often stored locally in a form other than photons, the use of photons as flying qubits involves the typically inefficient process of transferring the quantum information between two *different* physical systems and the possibility of losing the quantum information during the transfer.

A promising alternative for solid-state implementations of quantum information processing is to use networks of exchange-coupled spins [71]. This method is particularly advantageous because it allows both local quantum computation and transport of quantum information to be carried out

within the *same* solid-state system. In Ch. 2, we describe existing proposals for using spin systems to transport qubits and present a qualitatively distinct mechanism for producing “flying spin qubits” in Heisenberg spin chains with dimerized exchange coupling via the motion of domain walls in the dimerization. The basic elements from which these systems are constructed - individual spins coupled by exchange interactions - themselves provide resources useful for the implementation of quantum computation, as we discuss in the next section.

### 1.4.2 Single-spin qubits and exchange interactions

While there are several promising realizations of qubits, encoding a qubit in a single spin has the advantage that there are no extra states into which the quantum information can “leak” since the qubit and spin- $\frac{1}{2}$  spaces are formally identical [72]. Because of the equivalence of these two descriptions, a spin acts as a natural qubit for quantum information processing. The connection between single spins and qubits is emphasized by the Bloch sphere picture [6], illustrated in Fig. 1.3, which is a geometrical representation of the state of a single qubit that is equivalent to the three-dimensional real-space representation of a single spin described in Sec. 1.1.1. The Bloch sphere essentially generalizes the two-dimensional unit circle used for a complex number of modulus unity to three dimensions. The spherical geometry arises from the fact that the most general state of either a spin [Eq. (1.3)] or a qubit [Eq. (1.22)] may also be written as

$$|\psi\rangle = e^{i\delta} \left[ \cos\left(\frac{\theta}{2}\right) |0\rangle + e^{i\phi} \sin\left(\frac{\theta}{2}\right) |1\rangle \right], \quad (1.23)$$

For a single qubit, the global phase factor  $e^{i\delta}$  is of no observable significance and can be set equal to unity. The angular spherical coordinates  $(\theta, \phi)$  parametrize the qubit state on the surface of a sphere of unit radius consisting of all points such that  $0 \leq \theta \leq \pi$  and  $0 \leq \phi \leq 2\pi$ . Pairs of points which are located directly opposite to each other on the Bloch sphere correspond to orthogonal states. In particular, the qubit basis states  $|0\rangle$  and  $|1\rangle$  are located at the poles of the sphere that lie along the  $z$  axis.

The connection between the Bloch sphere representation of the state of a single qubit and the three-dimensional real-space representation of a single spin can be seen by introducing a polarization vector  $\mathbf{P} = (P_x, P_y, P_z)$ , in which the components are real numbers [6]. On the surface of the

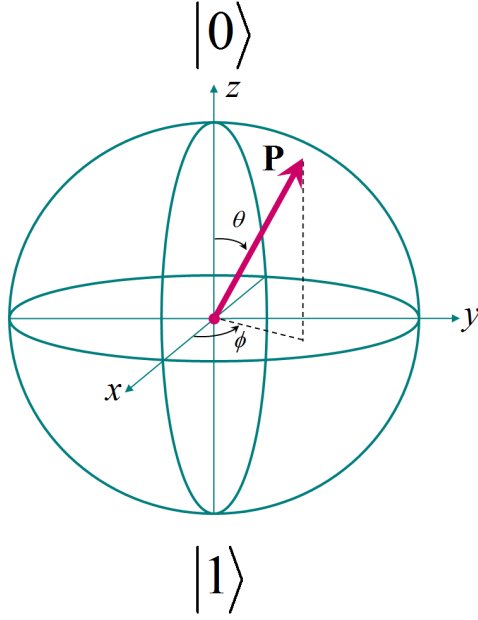


Figure 1.3: Bloch sphere representation of a single qubit state.

Bloch sphere,  $|\mathbf{P}| = 1$  and  $\mathbf{P}$  can be written as

$$\mathbf{P} = (\sin\theta \cos\phi, \sin\theta \sin\phi, \cos\theta). \quad (1.24)$$

The relation of  $\mathbf{P}$  to the spin vector  $\mathbf{S} = (\hbar/2) \boldsymbol{\sigma}$  can be obtained by calculating the expectation values  $\langle \sigma_\tau \rangle \equiv \langle \psi | \sigma_\tau | \psi \rangle$  (where  $\tau = x, y, z$ ) for the state given in Eq. (1.23). Comparing the results with the components of  $\mathbf{P}$  given in Eq. (1.24) yields  $\langle S_\tau \rangle = (\hbar/2) \langle \sigma_\tau \rangle = (\hbar/2) P_\tau$ . Thus, each component of the vector representing the qubit polarization in the Bloch sphere picture (Fig. 1.3) is directly proportional to the expectation value of the corresponding real-space spin component.

In solids, single-spin qubits can be realized by three-dimensional confinement of individual electrons to quantum dots [47, 66]. These potential wells for electrons can be regarded as “artificial atoms” with dimensions that are typically 10-100 nm and therefore comparable to the electron Fermi wavelength [73, 66]. Solid-state qubits also exist in the form of electronic and/or nuclear spins associated with impurities [49, 50, 51]. Spatially confining electrons to either quantum dots or impurities allows the electronic states to be well described by the spin degree of freedom. The

Zeeman interaction [Eq. (1.18)] enables single-spin rotations to be performed by applying local magnetic fields to the quantum dots or impurities. The Zeeman Hamiltonian generates a unitary transformation that describes a rotation of the spin about the axis along which the external magnetic field is applied [74]. For example, a rotation about the  $\tau$  axis (where  $\tau = x, y, z$ ) of the Bloch sphere (Fig. 1.3) is described by (see Appendix A)

$$U_\tau = \exp \left[ ig\mu_B S_\tau \int B_\tau(t) dt \right]. \quad (1.25)$$

If rotations of the spin about two orthogonal axes are possible, an arbitrary rotation to any point  $\mathbf{P}$  on the Bloch sphere can be achieved by a combination of these rotations via Euler’s rotation theorem [2]. Recent experiments have demonstrated the manipulation of single spins in solid-state systems with a high degree of control [66, 67], including the implementation of arbitrary rotations through techniques such as spin resonance. As described in Sec. 1.3, the spin-orbit interaction provides an alternative mechanism for controlling spins. The use of spin-orbit coupling to manipulate single-spin qubits is discussed in more detail in Sec. 1.4.4.

In addition to these one-qubit gates for single spins, quantum information processing based on single-spin qubits also requires interactions that can produce entanglement between two spins. Using a Heitler-London approach similar to that applied to the  $\text{H}_2$  molecule in Sec. 1.2 and improvements to this model, it has been shown that the Heisenberg exchange Hamiltonian [Eq. (1.12)] provides a reasonable approximation for the low-energy spectrum of a pair of electrons localized in neighboring quantum dots [72]. The Heisenberg exchange interaction between two single-spin qubits (whether in quantum dots or other systems such as coupled atoms or impurity spins) can be used to generate the SWAP gate  $U_{\text{sw}}$  that simply exchanges the states of the two spins, as well as two-qubit entangling operations that are essential elements of universal sets of quantum gates [36, 37]. For example, consider the two-qubit “controlled-NOT” gate  $U_{\text{cnot}}$ , which can be represented in the standard two-qubit product basis  $\{|00\rangle, |01\rangle, |10\rangle, |11\rangle\}$ , or equivalently in the basis (1.7) for two spins, by the matrix

$$U_{\text{cnot}} = \begin{pmatrix} 1 & 0 & 0 & 0 \\ 0 & 1 & 0 & 0 \\ 0 & 0 & 0 & 1 \\ 0 & 0 & 1 & 0 \end{pmatrix}. \quad (1.26)$$

This gate can be constructed from a sequence of single-qubit rotations and the “square-root-of-SWAP” gate  $U_{\text{sw}}^{1/2}$  [47]. Both  $U_{\text{sw}}$  and  $U_{\text{sw}}^{1/2}$  are unitary transformations generated by the Heisenberg exchange Hamiltonian:

$$U_{\text{exch}} = \exp \left[ -i \mathbf{S}_1 \cdot \mathbf{S}_2 \int J(t) dt \right]. \quad (1.27)$$

Turning on the exchange interaction for a time such that  $\int J(t) dt = \pi \pmod{2\pi}$  gives  $U_{\text{exch}} = U_{\text{sw}}$ , while  $\int J(t) dt = \pi/2 \pmod{2\pi}$  gives  $U_{\text{exch}} = U_{\text{sw}}^{1/2}$ . Additionally, the ground state of  $H_{\text{exch}}$  [Eq. (1.12)] for  $J > 0$  is itself the singlet state in which the states of the two spins are entangled.

For electrons in coupled quantum dots,  $J = J(B, E, a)$ , where  $B$  and  $E$  are magnetic and electric field strengths, respectively, and  $a$  is defined to be one-half the distance between the dots [72]. In other words, the exchange coupling can be controlled via external fields and/or through the quantum dot configuration. In Ref. 72, it was shown theoretically that the nature of the exchange interaction can be modified by a magnetic field: electrons are coupled by AFM exchange ( $J > 0$ ) for  $B = 0$  and FM exchange ( $J < 0$ ) if the magnetic field strength is increased beyond a critical value. Because the exchange interaction strength depends on the spatial overlap of the electronic wavefunctions, and because the wavefunctions correspond to a charge distribution that can couple to an electric field, the exchange interaction can also be controlled electrically. Due to the dependence of  $J$  on the wavefunction overlap, the exchange strength typically varies exponentially with the interdot distance. Applying a gate voltage between the dots can increase or decrease the tunneling barrier between them, which is physically equivalent to increasing or decreasing the distance between the dots, respectively. Rapid electrical control of exchange interactions between spins has been experimentally demonstrated [75].

### 1.4.3 Multi-spin qubits and exchange interactions

While a spin itself is a natural physical realization of a qubit as discussed in the previous section, systems containing multiple spins can also be used to encode single logical qubits. For  $n$  spins, this can be achieved by identifying a suitable two-dimensional subspace of states within the full  $2^n$ -dimensional Hilbert space. Encoding logical qubits within the expanded Hilbert space for  $n > 1$  spins has applications in quantum error correction [76], in which measurements performed on

additional or “ancillary” qubits rather than the encoded qubits allow nondestructive detection and correction of errors that occur due to imperfect quantum gate operations or unwanted interactions with the environment. Particular sets of states within the Hilbert space associated with multi-spin qubits can also be used to define decoherence-free subspaces (DFSs) [77, 78]. These subspaces take advantage of symmetries of the interaction between the spin qubits and the environment in order to protect the quantum information from decoherence that occurs in the same way for all spins (known as “collective decoherence”). Of particular significance in the context of the “flying spin qubits” and “domain-wall qubits” discussed in Chs. 2 and 3 is the encoding of qubits in the two-fold degenerate ground state of certain systems of spins coupled by two-body interactions for which there is an energy gap between the ground-state doublet and higher excited states [79, 80]. This encoding enables decoherence to be *energetically* suppressed, as the only relevant decoherence processes for these systems do not conserve energy. These “coherence-preserving qubits” are also intrinsically robust to decoherence that acts locally on individual spins.

In the spirit of designer quantum materials, new resources emerge in qubits constructed using multiple spins as building blocks, by virtue of the *internal* interactions present between spins in these “designer qubits” that do not exist for single-spin qubits. These new features have been demonstrated to exist even for the simplest nontrivial encoding of single logical qubits in  $n = 2$  spins [81, 75, 82, 83, 84, 85]. In this thesis, the notation  $|0\rangle \equiv |\uparrow\rangle$ ,  $|1\rangle \equiv |\downarrow\rangle$  is used to represent the basis states of single spins. Single logical qubits can be defined using the  $S_Z = 0$  subspace for two spins, which represents a DFS [77, 78, 86] and can be spanned by either the two-spin product states  $|01\rangle = |\uparrow\downarrow\rangle, |10\rangle = |\downarrow\uparrow\rangle$  or the entangled singlet and triplet states  $\frac{1}{\sqrt{2}}(|01\rangle \pm |10\rangle)$  discussed in Sec. 1.1.2.

If the logical qubit basis  $\{|01\rangle, |10\rangle\}$  is chosen [81] and the operators  $(X, Y, Z)$  are defined such that they have the same matrix representations as the Pauli matrices [Eq. (1.6)] in this basis, the exchange Hamiltonian [Eq. (1.12)] can be written as [see Eq. (1.15)]

$$\begin{aligned} H_{\text{exch}} &\rightarrow \frac{J}{2} \begin{pmatrix} 0 & 1 \\ 1 & 0 \end{pmatrix} - \frac{J}{4} \mathbf{1} \\ &= \frac{J}{2} X - \frac{J}{4} \mathbf{1}. \end{aligned} \tag{1.28}$$

Apart from a term proportional to the identity, which gives rise to trivial dynamics (as discussed in Appendix A),  $H_{\text{exch}}$  has a form analogous to the Zeeman Hamiltonian [Eq. (1.18)]. Here, the exchange interaction between the spins *within* the qubit plays the role of a magnetic field for the qubit and generates a rotation about the  $x$  axis of the Bloch sphere. For the alternate  $S_Z = 0$  basis choice  $\left\{ \frac{1}{\sqrt{2}}(|01\rangle - |10\rangle), \frac{1}{\sqrt{2}}(|01\rangle + |10\rangle) \right\}$  that defines the singlet-triplet qubit [75, 82],  $H_{\text{exch}}$  takes the form

$$\begin{aligned} H_{\text{exch}} &\rightarrow -\frac{J}{2} \begin{pmatrix} 1 & 0 \\ 0 & -1 \end{pmatrix} - \frac{J}{4} \mathbf{1} \\ &= -\frac{J}{2} Z' - \frac{J}{4} \mathbf{1}, \end{aligned} \quad (1.29)$$

where  $(X', Y', Z')$  are the Pauli matrices in the singlet-triplet basis. In this case, the exchange interaction acts as an effective magnetic field that generates a rotation about the  $z$  axis of the Bloch sphere for the singlet-triplet qubit. Thus, increasing the number of spins used to define the qubit even from one to two already provides a way to perform single-qubit rotations using the exchange interaction internal to the qubit rather than external magnetic fields. This capability does not exist for single spins.

To perform arbitrary rotations of a two-spin qubit, a rotation about a second orthogonal axis must also be possible (see Sec. 1.4.2). For the logical qubit represented by the basis  $\{|01\rangle, |10\rangle\}$ , this can be achieved by applying a static and spatially uniform magnetic field of strength  $B$  along the  $z$  axis in the presence of a difference  $\Delta g$  in the  $g$ -factors of the two spins that can arise if the spins have different local environments [81]. The resulting Zeeman interaction has the form  $H_Z = (-\Delta g \mu_B B / 2) Z$ . In the case of the singlet-triplet qubit, arbitrary rotations can be accomplished by combining exchange [Eq. (1.29)] with a static magnetic field gradient  $\Delta B$  along the  $z$  axis due to, e.g., the different hyperfine (electron-nuclear) interactions experienced by two electrons in neighboring quantum dots [84]. The Zeeman interaction is then given by  $H_Z = (-g \mu_B \Delta B / 2) X'$ . In either case, the combination of  $H_Z$  and the corresponding exchange interaction [Eq. (1.28) or Eq. (1.29)] allows arbitrary rotations of the qubit to be performed without applying time-dependent magnetic fields. Two-qubit gates, which involve two pairs of spins, can also be carried out using exchange interactions between spins belonging to different qubits.

Since the exchange interaction between spins can be controlled using gate voltages, as discussed in Sec. 1.4.2, this enables two-spin qubits to be manipulated electrically. The prospect of controlling spin qubits using electric fields is particularly advantageous in the context of meeting the challenging demands of building a quantum information processor [35]. As mentioned in Sec. 1.4.1, one of these requirements is that qubit manipulation must be completed rapidly compared to the timescale over which the coherence of the qubit is lost. Because the exchange between two spins is a relatively strong interaction and can be switched rapidly through voltages applied to gate electrodes, electric field control of the two-spin qubit is faster than using time-varying magnetic fields. For example, a square-root-of-swap operation between two exchange-coupled spins defining a single logical qubit with a dephasing time of 10 ns has been experimentally achieved in 180 ps [75]. Manipulation of two-spin qubits using electric fields is therefore favorable from the perspective of experimental realizations of quantum information processing.

Additional advantages for experimental implementations arise by adding one more spin, i.e., encoding single qubits in  $n = 3$  spins [87, 88, 89, 90]. As in the  $n = 2$  case, a three-spin system can be used to define DFSs [86]. Three-spin qubits are also the smallest systems for which the Heisenberg exchange interaction is *universal*, in the sense that exchange alone can generate both the single-qubit and the two-qubit elementary gates required for universal quantum computing [87]. The use of a single physical interaction for all gates is advantageous from the practical perspective of simplifying experimental implementations. Local magnetic fields are challenging to apply and typically give rise to slower single-qubit gates, making the spin more susceptible to decoherence. For localized single-spin qubits,  $H_{\text{exch}}$  cannot be universal because it commutes with both  $S^2$  and  $S_Z$ . Exchange alone therefore cannot change the quantum number  $S_Z$ , so that rotation between the basis states  $|0\rangle$  and  $|1\rangle$  is not possible without the addition of magnetic fields. As we show in the work presented in Ch. 5, real magnetic fields are not necessary for full three-dimensional manipulation of even single-electron spin qubits if the electrons are allowed to move spatially and the spin-orbit interaction is present. We will return to this point in the following section.

In the case of three-spin qubits, one way to achieve universality using the exchange interaction alone is to encode the qubit within a subspace of the full three-spin Hilbert space that is associated with a fixed set of quantum numbers  $(S, S_Z)$  [87, 88]. The only states which are coupled by Heisenberg exchange are those that lie within the same  $(S, S_Z)$  subspace. As an example, the log-

ical basis  $\left\{ \frac{1}{\sqrt{2}}(|010\rangle - |100\rangle), \frac{1}{\sqrt{6}}(2|001\rangle - |010\rangle - |100\rangle) \right\}$  can be used to represent the qubit within the  $(S, S_Z) = (\frac{1}{2}, \frac{1}{2})$  subspace [87]. Arbitrary rotations of this qubit are possible by sequentially turning on and off three or four exchange couplings between individual spins within the qubit in order to generate unitary transformations of the form in Eq. (1.27). Additionally, the entangling gate  $U_{\text{cnot}}$  between two three-spin qubits can be carried out within the  $(S, S_Z) = (1, 1)$  subspace using a sequence of 19 exchange interactions that couple pairs of spins both within the same qubit and those belonging to two different qubits. Together, these single-qubit and two-qubit operations constitute a universal set of quantum gates for which the only physical interaction required is Heisenberg exchange. For the particular case of a closed three-spin ring (or spin triangle) with uniform exchange couplings, adding a uniform magnetic field creates a gap between the ground state defining the logical qubit space and higher excited states that allows for energetic suppression of decoherence, producing a three-spin coherence-preserving qubit [88]. Recently, experimental control over both single [89] and coupled [90] three-spin qubits has been demonstrated. Thus, designer qubits constructed from multiple exchange-coupled spins provide entirely new classes of resources that are not available for single-spin qubits.

While exchange-coupled two-spin and three-spin qubits already have many useful properties, the schemes for the manipulation of these qubits discussed so far still require the application of local electric and magnetic fields in order to control individual spins. Practical difficulties therefore remain in the implementation of these methods. One way to address these challenges is to extend the spatial scale over which it is necessary to control the qubits. This is possible if qubits are defined using chains or clusters of an odd number of spins  $n_c$  coupled by nearest-neighbor AFM exchange interactions [91, 92], which are described by a Hamiltonian of the form

$$H = \sum_{k=1}^{n_c-1} f_k [J_{\perp} (S_{kx}S_{k+1,x} + S_{ky}S_{k+1,y}) + J_z S_{kz}S_{k+1,z}], \quad (1.30)$$

where  $J_{\perp} > 0$  and  $J_z > 0$ . Eq. (1.30) in general describes anisotropic exchange [Eq. (1.17)] for which  $J_x = J_y = J_{\perp}$  and is of the XXZ (XY) type for  $J_z \neq 0$  ( $J_z = 0$ ). Ising-type coupling is obtained in the limit  $J_z \gg J_{\perp}$ . Isotropic (Heisenberg) exchange is described by setting  $J_{\perp} = J_z$ , and spatially uniform exchange interactions are described by setting  $f_k = 1$  for all  $k$ .

In order to understand how a qubit can be defined based on Eq. (1.30), the specific case of a spin chain with uniform AFM Heisenberg exchange can be considered [91, 92]. In this case, Eq. (1.30) reduces to

$$H_{\text{unif}} = J \sum_{k=1}^{n_c-1} (\mathbf{S}_k \cdot \mathbf{S}_{k+1}), \quad (1.31)$$

which is the Heisenberg spin chain Hamiltonian [Eq. (1.16)] with  $n = n_c$  and  $J_k = J > 0$  for all  $k$ . As mentioned in Sec. 1.2, the Lieb-Mattis theorem [11] states that the minimum-energy states in the presence of AFM exchange are those having minimum total spin  $S$ . For odd  $n_c$ , the ground state of  $H_{\text{unif}}$  therefore has  $S = \frac{1}{2}$ . Since the corresponding possible values for the total  $z$  component of spin are  $S_Z = \pm \frac{1}{2}$ , this ground state is two-fold degenerate and can be used to define a qubit. This “spin-cluster qubit” is energetically stable due to the presence of an energy gap  $\Delta \propto J/n_c$  separating the ground state doublet from the first excited state [91, 92]. At sufficiently low temperatures, the gap protects the qubit from decoherence such as leakage of the quantum information to higher excited states.

As an illustration of the defining spectral features of spin cluster qubits, Fig. 1.4(a) shows the energy eigenvalues of Eq. (1.31) as a function of  $S_Z$  for the case  $n_c = 5$ . Since  $n_c$  is odd, there is a ground state doublet (indicated by a rectangle in the figure) that is separated from the first excited state by an energy gap. This ground-state doublet has  $S_z = \pm \frac{1}{2}$  and defines a spin cluster qubit. On the other hand, the ground state for an even number of spins such as  $n_c = 6$  [Fig. 1.4(b)] is a singlet. This non-degenerate ground state has  $S = 0$ ,  $S_Z = 0$  and cannot be used to define the effective two-dimensional Hilbert space required to represent a qubit. Note that the first excited state for the 6-spin chain consists of a triplet of states with  $S = 1$  and  $S_Z = -1, 0, 1$ . Thus, in the low-energy portion of the spectrum of Eq. (1.31), the odd- $n_c$  case is analogous to a single spin, while the even- $n_c$  case is analogous to two spins.

The basis states of a spin cluster qubit  $c$ , which we will denote as

$$\left\{ |\uparrow(c)\rangle \equiv \left| S = \frac{1}{2}, S_Z = \frac{1}{2} \right\rangle, |\downarrow(c)\rangle \equiv \left| S = \frac{1}{2}, S_Z = -\frac{1}{2} \right\rangle \right\} \quad (1.32)$$

in analogy with the notation used to represent the  $s = \frac{1}{2}$ ,  $m_s = \pm \frac{1}{2}$  states of a single spin (see Sec. 1.1.1), are in general superpositions of many product states of the individual spins [91, 92]. This

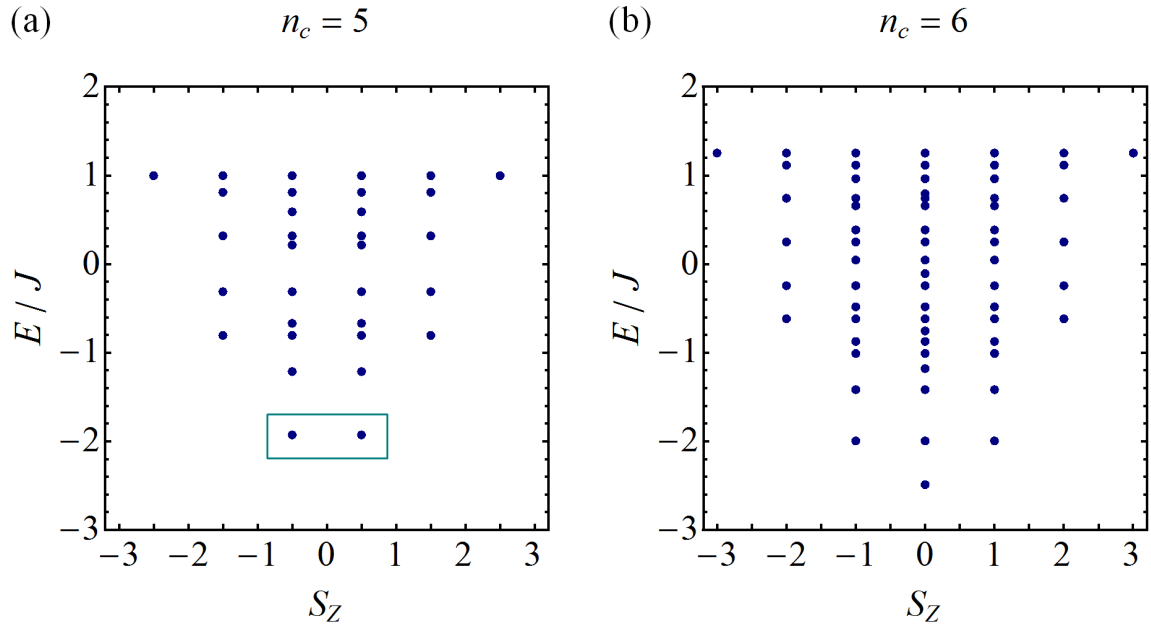


Figure 1.4: Spectrum of the  $s = \frac{1}{2}$  Heisenberg spin Hamiltonian with uniform AFM exchange [Eq. (1.31)] for (a)  $n_c = 5$  and (b)  $n_c = 6$ . The rectangle indicates the energy eigenstates that define a spin cluster qubit for the case  $n_c = 5$ . Energies are in units of the uniform exchange strength  $J$ .

follows from the fact that  $[S^2, S_{kz}] \neq 0$  for each  $k$ , similar to the two-spin case considered in Sec.

1.1.2. The well-known combination formula

$$\binom{n}{m} = \frac{n!}{m!(n-m)!} \quad (1.33)$$

gives the number of distinct arrangements of  $n$  objects, where  $m$  objects are of one type and the remaining  $n - m$  are of another type. By applying Eq. (1.33) to an odd number of spins  $n_c$ , for which each product state in the  $S = \frac{1}{2}$  subspace consists of  $(n_c + 1)/2$  spins in either the state  $|0\rangle$  or the state  $|1\rangle$  and  $(n_c - 1)/2$  spins in the opposite state, it is seen that the states  $\{|\uparrow(c)\rangle, |\downarrow(c)\rangle\}$  are each superpositions of  $n_c! / [(n_c + 1)/2]! [(n_c - 1)/2]!$  product states. Expressions for these basis states in terms of product states are therefore generally complicated. Alternatively, a useful visual representation of the basis states of a spin cluster qubit can be obtained by calculating the spin densities for these states, which are defined in this thesis as the sets of expectation values  $\langle \uparrow(c) | S_{kz} | \uparrow(c) \rangle$  and  $\langle \downarrow(c) | S_{kz} | \downarrow(c) \rangle$  at each site  $k$  in the spin chain. For illustration, the spin densities for the basis states of a  $n_c = 9$  spin cluster qubit described by Eq. (1.31) are shown in Fig. 1.5. For  $|\psi\rangle = |\uparrow(c)\rangle, |\downarrow(c)\rangle$ , the sum of the spin density values satisfies

$$\sum_{k=1}^{n_c} \langle \psi | S_{kz} | \psi \rangle = \langle \psi | \sum_{k=1}^{n_c} S_{kz} | \psi \rangle = \langle \psi | S_Z | \psi \rangle = S_Z, \quad (1.34)$$

so that  $\sum_{k=1}^{n_c} \langle \uparrow(c) | S_{kz} | \uparrow(c) \rangle = \frac{1}{2}$  and  $\sum_{k=1}^{n_c} \langle \downarrow(c) | S_{kz} | \downarrow(c) \rangle = -\frac{1}{2}$ . Thus, the spin- $\frac{1}{2}$  object that defines a spin cluster qubit is *distributed in space*, as is evident from the fully delocalized spin density for the basis states (Fig. 1.5). Eq. (1.34) also suggests that the state of the spin cluster qubit can be read out by measuring the  $z$  components of the individual spins and summing these values.

These spatially-extended qubits have the advantage that manipulation of the encoded quantum information does not require the application of local fields in order to control individual spins [91, 92]. Because the formal description of a spin cluster qubit in terms of the *total* spin operator  $S^2$  and *total*  $z$  component of spin  $S_Z$  is identical to that of a single spin, quantum gates for spin cluster qubits can in principle be carried out using the same mechanisms as those employed for implementing single-spin quantum gates. The application of a uniform magnetic field  $\mathbf{B}$  over the

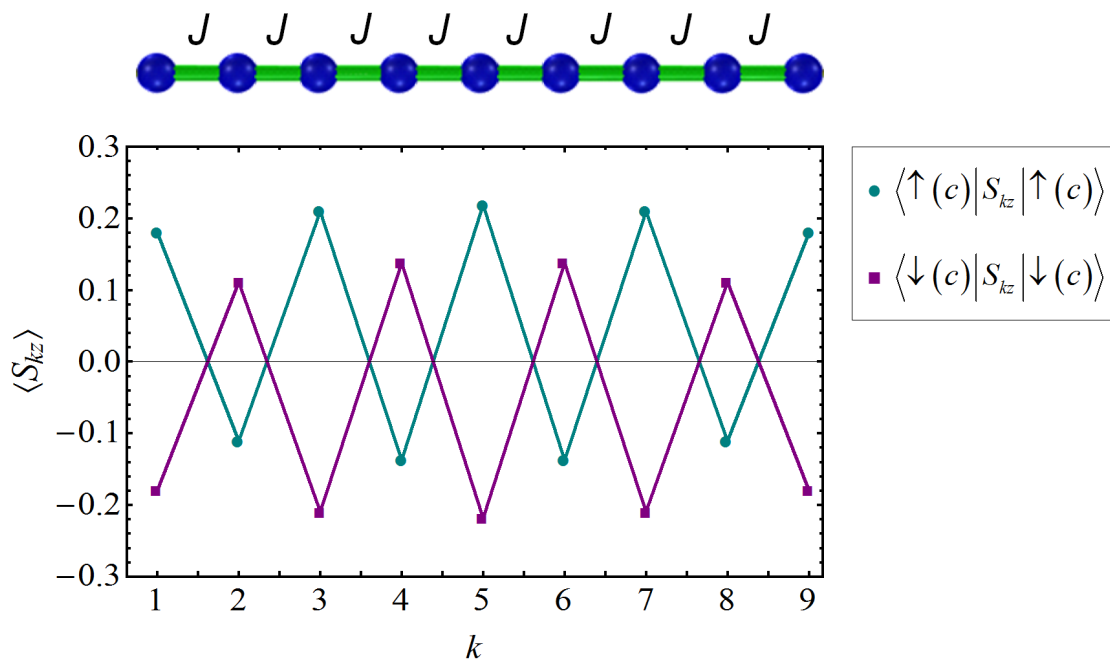


Figure 1.5: Spin density for the degenerate ground-state doublet of a uniform  $n_c = 9$  spin chain, consisting of the states with  $S = \frac{1}{2}$  and  $S_Z = \pm \frac{1}{2}$  that define a spin cluster qubit.

whole length of the spin chain is described by a sum of single-spin Zeeman Hamiltonians [Eq. (1.18)]:

$$\begin{aligned}
H_Z &= - \sum_{k=1}^{n_c} \frac{g\mu_B}{\hbar} \mathbf{B} \cdot \mathbf{S}_k \\
&= - \frac{g\mu_B}{\hbar} \mathbf{B} \cdot \sum_{k=1}^{n_c} \mathbf{S}_k \\
&= - \frac{g\mu_B}{\hbar} \mathbf{B} \cdot \mathbf{S},
\end{aligned} \tag{1.35}$$

where  $\mathbf{S}$  written without the subscript  $k$  labeling the spin site refers to the operator for the total spin. The identical forms of the Hamiltonians in Eq. (1.35) and Eq. (1.18) show that applying a spatially uniform magnetic field  $\mathbf{B}(t)$  generates rotations of the spin cluster qubit about the axes of the Bloch sphere, in full analogy with Eq. (1.25) for a single-spin qubit.

Two spin cluster qubits can be coupled by introducing additional exchange interactions between spins in different qubits, as in the case of the two-spin and three-spin qubits discussed above. For a pair of spin cluster qubits  $a$  and  $b$ , consider an AFM exchange interaction of the form  $H_* = J_* S_{n_c a} \cdot S_{1b}$  between spin  $n_c$  of cluster  $a$  and spin 1 of cluster  $b$ , where  $J_* > 0$ . If  $J_* \ll \Delta$ ,  $H_*$  can be treated as a perturbation relative to the Hamiltonian in Eq. (1.31) describing the isotropic exchange between spins *within* each spin cluster qubit. This leads to an effective Hamiltonian which acts in the space spanned by the two-qubit product-state basis

$$\{ |\uparrow(a)\rangle |\uparrow(b)\rangle, |\uparrow(a)\rangle |\downarrow(b)\rangle, |\downarrow(a)\rangle |\uparrow(b)\rangle, |\downarrow(a)\rangle |\downarrow(b)\rangle \} \tag{1.36}$$

that has the form [91, 92]:

$$H_* = J_{\text{eff}} S_a \cdot S_b + J_0 \mathbf{1}, \tag{1.37}$$

where the term proportional to the identity operator arises from the exchange within the spin cluster qubits, and the effective exchange strength  $J_{\text{eff}}$  is given by

$$J_{\text{eff}} = 4J_* \langle \uparrow(a) | S_{n_c a}^z | \uparrow(a) \rangle \langle \uparrow(b) | S_{1b}^z | \uparrow(b) \rangle. \tag{1.38}$$

From the form of Eq. (1.37), it is seen that an isotropic exchange interaction between two spins in different spin cluster qubits translates into an effective isotropic exchange interaction between the

qubits themselves. A time-dependent exchange constant  $J_{\text{eff}}(t)$  then generates a unitary transformation analogous to that for the single-spin case [Eq. (1.27)], which can be used to carry out useful two-qubit entangling operations such as  $U_{\text{sw}}^{1/2}$  and  $U_{\text{cnot}}$ . Since an effective Hamiltonian of the form in Eq. (1.37) is found even for multiple spin-spin couplings between the qubits [91, 92], control of the exchange is possible on the scale of  $n_c$  spins. In Refs. 91 and 92, these features of spin cluster qubits are shown to hold also more generally for nonuniform magnetic fields, anisotropic exchange interactions, and spatially-varying exchange interactions.

The justification for the expressions in Eqs. (1.37) and (1.38) is given in Ch. 3, where they are applied to a pair of antiferromagnetically-coupled Heisenberg spin rings with domain walls defined by a specific type of spatial variation in the exchange constants. The properties of individual rings with such exchange-based domain walls are described in Ch. 2 and represent designer quantum materials in which “flying spin qubits” may be produced. These systems are equivalent to the spin cluster qubits discussed above in the limit of a fixed number of spins coupled by spatially uniform exchange and have many of the same advantageous characteristics. In Chs. 2 and 3, we show that entirely new classes of features emerge for qubits defined by domain walls in exchange-coupled spin systems, several of which have relevance for quantum information processing.

#### 1.4.4 Single-spin qubits and spin-orbit interaction

In the previous section, we have explored some of the new resources provided by designer quantum materials constructed from *multiple* spins coupled by *spin-spin* exchange interactions. Additional mechanisms for *single*-spin manipulation arise when we consider the *spin-orbit* interaction. The new resources which emerge in spin systems with tailored spin-orbit coupling form the basis for the second class of designer quantum materials we describe in this thesis.

As discussed above, magnetic fields provide a natural means of manipulating single spins, such as those of electrons confined to quantum dots [47, 61, 63, 75, 66] or impurities [49, 50, 51], by means of the Zeeman interaction [Eq. (1.18)]. For example, perpendicular uniform and oscillating magnetic fields can be used for manipulation via electron spin resonance (ESR) [93, 94, 66, 67]. However, the magnetic fields must be applied locally, e.g., over lengthscales that correspond to the size of a single quantum dot or impurity, in order to selectively address individual spin qubits. Such

local magnetic fields are challenging to achieve experimentally. Alternative methods of controlling single spins using electric fields have therefore been widely investigated [95, 96, 97, 98, 99, 100, 101, 102], ranging from the modulation of the g-tensor using electric fields [96] to the use of the hyperfine interaction between electron and nuclear spins [101] and static magnetic field gradients [102]. In addition to enabling rapid control of the exchange coupling between spins [75], electric fields are well-suited to achieving local control of single-spin qubits. Local electric fields that oscillate in time can be generated by ac voltages applied to gate electrodes [96, 100].

New avenues for electrical spin manipulation emerge by virtue of the spin-orbit interaction and the spatial degree of freedom associated with the motion of electrons confined to a quantum wire. This has motivated many studies of the properties of quantum wires with both uniform [95, 103, 104, 105, 106, 107, 108, 109, 110, 111, 112, 113, 114] and spatially-varying [115, 116, 117, 118] spin-orbit coupling. As discussed in Sec. 1.3, the general form  $\mathbf{B}_{\text{eff}} \propto (\nabla V \times \mathbf{k})$  of the effective magnetic field due to the spin-orbit interaction [Eq. (1.19)] allows for the manipulation of spin qubits using electric fields in a manner analogous to the Zeeman interaction (Fig. 1.2). For example, the electrically-tunable Rashba interaction [30] provides one promising mechanism for controlling spins in one-dimensional systems. Basic features of Rashba spin-orbit coupling in quantum wires are described in Ch. 4.

The ability to manipulate spins electrically via spin-orbit coupling is the basis for the methods of electric dipole spin resonance (EDSR) [97, 98, 119, 120, 100] and ballistic spin resonance (BSR) [121]. In the EDSR approach, an oscillating electric field causes a time-periodic displacement of the electronic wavefunction (which also corresponds to the charge distribution), producing an oscillating effective magnetic field by means of a position-dependent spin-orbit interaction [100]. In contrast to the externally-driven dynamics in EDSR, BSR occurs via the oscillation of the electronic momentum in time that results when an electron moves by bouncing back and forth between the walls of a conducting channel. In both methods, a time-dependent oscillation of the effective magnetic field due to the spin-orbit interaction replaces the oscillating magnetic field required for ESR and enables the manipulation of spins using electric fields.

The effective magnetic field due to spin-orbit coupling is also the key ingredient in several proposals for single-qubit gates [122, 123, 124, 125, 126, 127]. One proposal for solid-state quantum computing that allows for the full control of single-spin qubits using electric fields alone combines

single-qubit gates based on the Rashba spin-orbit interaction with two-qubit gates based on the Heisenberg exchange interaction for two electrons moving in adjacent quantum wires [122]. A combination of Rashba and Dresselhaus interactions can also be used to implement single-qubit gates for such mobile qubits [125]. Universal quantum computation can also be achieved for electron spins localized in quantum dots by encoding each qubit in two spins and controlling the anisotropic exchange that exists between the spins due to spin-orbit coupling [123]. Adiabatically transporting a quantum dot containing an electron spin through a two-dimensional system in which spin-orbit coupling is present can be used to rotate the spin without applied magnetic fields [126]. Alternatively, the eigenstates of the spin-orbit interaction can themselves be used to encode single qubits [124, 127], for which quantum gates are also based on the spin-orbit interaction.

Spin-orbit coupling is sometimes regarded as undesirable for spin-based quantum computing because it can cause spin flips that result in spin relaxation [128, 129], a form of decoherence in which an excited state with definite spin decays via energy dissipation to a lower state that has the (usually undesired) opposite spin. Nevertheless, the promise of new capabilities such as electrically-driven ESR and quantum gates serves to show that the spin-orbit interaction is a valuable resource. In Ch. 5, we describe a mechanism by which we can map spin dynamics, such as ESR, from time to *space* within a quantum wire using the effective magnetic fields associated with uniform and spatially-varying spin-orbit coupling. This method of ESR does not require any “real” (i.e., external or classical) magnetic fields. Instead of being controlled by time-dependent external fields, spin manipulation is built into the spin-dependent band structure of the wire. Adding spin-orbit coupling to the quantum toolkit thus gives rise to an additional class of designer quantum materials useful for manipulating spins and performing quantum information processing in fundamentally new ways.

## 2.0 FLYING SPIN QUBITS

In this chapter, we present a method for encoding and transporting qubits within a dimerized Heisenberg spin- $\frac{1}{2}$  chain. Logical qubits are localized at the domain walls that separate the two possible dimerized states. The domain walls can be moved to produce “flying spin qubits.” The topological nature of these states makes them stable against local perturbations of the exchange profile. Pairs of domain walls can be used to generate Einstein-Podolsky-Rosen pairs of entangled qubits. We discuss speed limitations within an exactly solvable three-spin model and describe a possible physical realization using quantum dot arrays.<sup>1</sup>

### 2.1 INTRODUCTION

As discussed in Sec. 1.4, spin forms the basis for qubits in several quantum computing architectures [47, 49, 60, 61, 62, 63, 64, 50, 51]. In many proposals, logical quantum bits are formed from the  $2^n$ -dimensional Hilbert space corresponding to  $n$  spins [77, 78, 87, 81, 88, 75, 82, 83, 84, 85]. In Sec. 1.4.3, we have described how such encoding schemes are useful for the correction of [76] and protection against [77, 78, 86, 79, 80] errors, as well as for matching specific material systems to experimental capabilities by reducing the number of physical interactions required for universal quantum gating to, e.g., the Heisenberg exchange interaction alone in the case of  $n = 3$  spins [87, 88]. Furthermore, we have seen that exchange-coupled spin clusters having an odd number of spins can define energetically stable “spin cluster qubits” by virtue of the ground state doublet that is characteristic of the energy level spectrum for these systems [91, 92]. The Jordan-Wigner spin-particle mapping in one [18] or more [19, 20] dimensions suggests a wide range of candidate

---

<sup>1</sup>The material in this chapter is adapted from Ref. [130].

qubits one might construct from interacting spins.

The need for “flying qubits,” [35] i.e., a mechanism for rapidly transporting quantum information, has long been recognized as a weakness of spin-based quantum computing architectures. Several different methods have been proposed to implement long-range transport of quantum information. One method involves coupling spin qubits to an external “quantum bus,” e.g., an optical cavity mode [61]. Such an approach typically introduces an entirely new set of constraints, and engineering strong optical couplings can be challenging in practice. Alternatively, the quantum teleportation protocol [68] of Bennett *et al.* employs the generation and transport of EPR pairs to teleport qubits to their needed location.

As mentioned in Sec. 1.4.1, exchange-coupled spin networks enable both quantum computation and quantum information transfer to be carried out within the same solid-state system. One way to transfer quantum information within these systems is through multiple swap ( $U_{sw}$ ) operations between nearest-neighbor single spins, which are generated by Heisenberg exchange via Eq. (1.27) with  $\int J(t)dt = \pi \pmod{2\pi}$ . This method is not optimal for long-range transport in one-dimensional spin chains because of the large number of precise gate operations required and the relatively low error threshold ( $\sim 10^{-7}$ ) for quantum error correction [131, 132]. For example, if each swap operation has an error  $\delta$  such that  $\int J(t)dt = \pi \pm \delta$ , the state is not completely transferred from one spin to the next. If these errors accumulate at a rate greater than the threshold, the quantum information that is lost with each non-ideal swap operation cannot be recovered.

An alternative to the multiple-swap approach is to use the natural spin dynamics generated by the exchange coupling in spin chains to transport qubits. The initial proposal which makes use of this method involves a Heisenberg spin chain with FM exchange in a magnetic field [133]. Quantum state transfer is carried out by placing the spin at one end of the chain in a particular superposition of the two basis states for a single spin and allowing the state to evolve freely to the other end of the chain. In this scenario, external control is required only at the two ends where the spin state is prepared and measured. However, this scheme does not allow for optimal transport of the spin state, and the fidelity of the transport that describes how faithfully the state is reproduced at the receiving end of the chain (expressed as a value between zero and unity) decreases with increasing chain length. Various methods have been suggested in order to improve the fidelity [134, 135, 136, 137, 138]. In particular, perfect state transfer (corresponding to unit

fidelity) based on the dynamics of single exchange-coupled spin chains is possible in principle but typically requires specific types and/or values of exchange couplings. For example, spin chains with XY-type exchange couplings that are engineered to have values symmetric about the chain center can perfectly mirror the state of a spin qubit in order to transfer it from one end of the chain to the other. This mirroring occurs at specific times [134, 135, 138] which have also been shown to be optimal for free evolution [139]. An analogous mirroring is not possible for Heisenberg spin chains of more than two spins without the addition of local magnetic fields [140]. In addition, it has been shown [141, 142] that the fidelity of transmission depends critically on the values of the coupling strengths between the spins in the chain, making this approach susceptible to errors. One proposal to achieve robust quantum state transfer even in the presence of disorder in the exchange coupling strengths involves the adiabatic transport of spin states via a slowly-varying externally applied potential [143]. In addition, synchronized manipulation of the combined potential due to a static dot in a quantum wire defined at the interface of a heterostructure and a moving quantum dot carried through the wire by a surface acoustic wave can control the motion of a pair of electrons in order to efficiently convert between static and flying qubits as well as generate EPR pairs [144, 145, 146].

Here, we present a qualitatively different approach to the construction of flying qubits. The method relies on the design of a spin-based “designer quantum field,” constructed from a one-dimensional dimerized Heisenberg spin- $\frac{1}{2}$  chain. Logical qubits are localized at the domain walls that separate the two possible dimerized states. Unlike previous encoding schemes [77, 78, 87, 81, 88, 75, 82, 83, 84, 85], logical qubits are not associated with a definite number of spins; rather, these “defect” states exist even when the number of spins approaches infinity. Their topological nature [147, 148, 149] makes them stable with respect to local perturbations of the exchange profile. By moving the domain walls, it is possible to produce “flying spin qubits.” Below, we explore the properties of this class of systems both analytically for small chains (three spins) and numerically for larger chains (up to 30 spins). Numerical studies for the larger chains are carried out using the Lanczos method of diagonalization [150].

## 2.2 DIMERIZED SPIN CHAINS

A one-dimensional system of spin- $\frac{1}{2}$  objects interacting via nearest-neighbor Heisenberg exchange is described by the following effective Hamiltonian:

$$H = \sum_{k=1}^{n_c} J_k (\mathbf{S}_k \cdot \mathbf{S}_{k+1}) \equiv \sum J_k (\mathbf{S}_k \cdot \mathbf{S}_{k+1}) \quad (2.1)$$

where  $S_k = (S_{kx}, S_{ky}, S_{kz})$  are Pauli operators for the  $k$ th spin,  $\{J_k > 0\}$  quantify the strength of nearest-neighbor exchange interactions, and periodic boundary conditions apply if  $k \pm n_c \equiv k$ . In the absence of external magnetic fields, the total spin angular momentum operator  $S^2 = (\sum \mathbf{S}_k)^2$  as well as the total  $z$  component  $S_Z = \sum S_{kz}$  commute with  $H$ , so one may work within subspaces of definite  $S_Z$  and/or  $S^2$ .

To illustrate the properties of the dimerized Heisenberg spin systems investigated here, we initially consider an open, symmetric chain having an odd number of spins  $n_c$  and a single kink in the center [Fig. 2.1(a)]. The dimerization of the chain is described by a parameter  $a$ , such that  $\{J_{2d} = J_{n_c-2d} = aJ; J_{2d-1} = J_{n_c-2d+1} = J, d = 1, 2, \dots, (n_c - 1)/4\}$  and  $0 \leq a \leq 1$ . Because the system contains an odd number of spins, the minimum total spin angular momentum (corresponding to the ground state) is  $S = \frac{1}{2}$ ; here, we consider the  $S_Z = \frac{1}{2}$  “spin-up” subspace, but an identical analysis applies for the  $S_Z = -\frac{1}{2}$  “spin-down” subspace. The ground state is calculated by numerical diagonalization of the Hamiltonian in Eq. (2.1) as a function of  $a$ , and the spin density  $\langle S_{kz} \rangle$  can be computed [Fig. 2.1(b)]. The case  $a = 0$  corresponds to a single spin localized at the center of the chain, surrounded by uncoupled dimers on either side. The spin chain may be initialized in this configuration by cooling the system to the ground state. As  $a$  is increased, the spin density becomes more delocalized. The uniform open spin chain ( $a = 1$ ) has already been investigated within the context of quantum computation and forms a well-defined “spin cluster qubit” [91, 92]. Adiabatic variation of  $a$  between 0 and 1 (Fig. 2.2) provides an explicit mechanism for interconversion between a single isolated spin and a delocalized spin cluster state, allowing an initially stationary qubit to be transformed into a movable flying spin qubit. After transporting the qubit to another location, the transformation may be reversed to reproduce the localized spin state. This state may then be measured using techniques developed for single spins.

The Hamiltonian in Eq. (2.1) can be mapped onto a variety of quantum field theories [151] via the Jordan-Wigner mapping. The spectrum resembles that of a semiconductor with a soliton-like defect state which is closely related to those in conducting polymers, inheriting many of the same properties such as spin-charge separation and topological stability [149]. For example, polyacetylene [147, 148] can be regarded as a quasi-one-dimensional conductor with one electron per carbon atom in which bond dimerization occurs spontaneously (a phenomenon known as the Peierls transition [152]), doubling the spatial period relative to a one-dimensional lattice with equally-spaced points. A periodic potential with lattice constant  $a$  opens a gap at the edges  $\pm\pi/a$  of the Brillouin zone in reciprocal space [23], so that the doubling in periodicity due to dimerization changes the lattice constant to  $2a$  and consequently introduces gaps into the spectrum at wavevectors  $\pm\pi/2a$ . Two possible dimerized configurations exist, illustrated in terms of “strong” (=) and “weak” (–) bonds by the patterns  $= - = - \dots$  and  $- = - = \dots$ , which are degenerate in energy. In the language of quantum field theory, one can say that there is a two-fold degeneracy in the vacuum state of the system [149]. A topological excitation, known as a soliton, can therefore exist in the form of a defect or “domain wall” separating regions of different dimerized configurations and introduces a single electronic state with energy near the center of the gap produced by the dimerization. When occupied by a single electron, this state is associated with neutral charge and spin  $\frac{1}{2}$ . Identifying the bonds between atoms with the exchange couplings between spins reveals an analogy between the polyacetylene system and the spin systems considered here. Continuum field-theoretic descriptions [153] are also applicable to these dimerized spin systems, provided the defect extends over many spin lattice sites.

We now consider a specific parametrization  $J_k = J_0 \exp[(-1)^k \alpha(k)]$  of the Hamiltonian in Eq. (2.1), where  $\alpha$  is a staggered order parameter describing dimerization in the chain. Spatially localized qubits are produced at the zero crossings of  $\alpha$  and represent particle-like excitations of a designer quantum field. We illustrate the localization of these qubits by considering a closed chain with  $n_c = 29$  and  $J_0 = 1$  [Fig. 2.3(a)]. A single domain wall is centered at  $k_0$  with width  $w$  for

$$\alpha(k - k_0) = a_0 \sum_{r=-\infty}^{\infty} (-1)^r \tanh \left[ \frac{k - (k_0 + rn_c)}{w} \right], \quad (2.2)$$

where  $a_0 = 1$ ,  $k_0 = 15$ , and  $w = 2$ . The hyperbolic tangent function used to describe the domain wall in Eq. (2.2) resembles the form which has been found to minimize the energy of a soli-

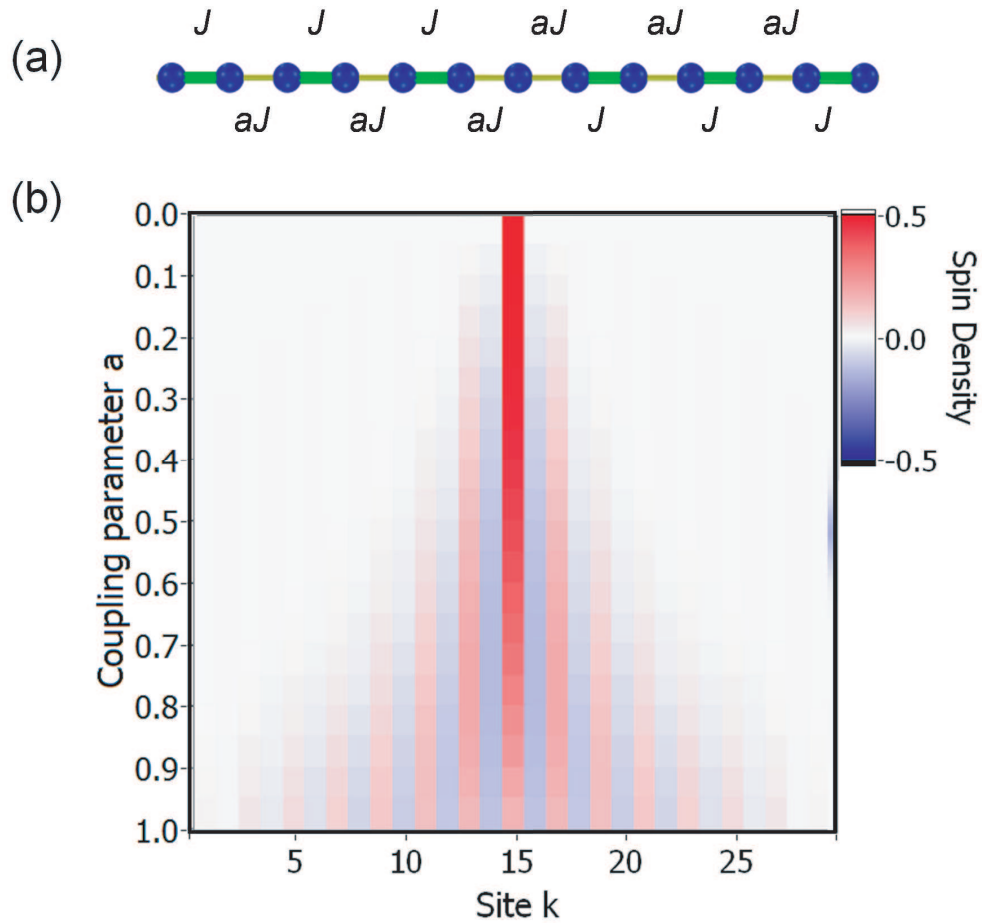


Figure 2.1: Dimerized Heisenberg spin- $\frac{1}{2}$  chains. (a) Schematic of an open Heisenberg-coupled spin chain ( $n_c = 13$ ) with a single defect at the center. (b) Plot of spin density for the  $S_Z = \frac{1}{2}$  ground state as a function of the dimer coupling parameter  $a$  for the case  $n_c = 29$ .

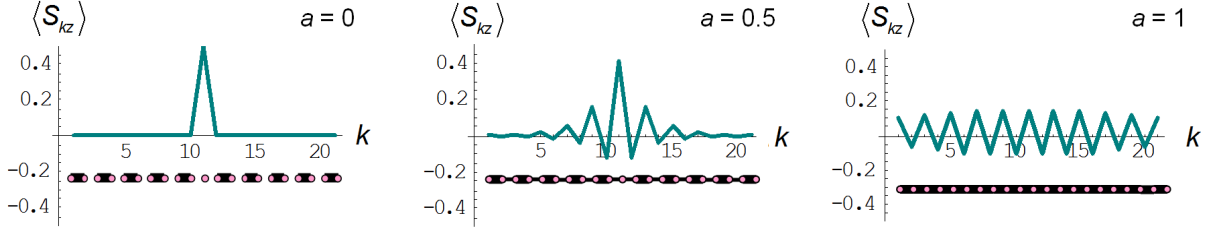


Figure 2.2: Spin density for an  $n_c = 21$  spin chain with a defect at the center as a function of  $a$ . Increasing  $a$  (shown from left to right) converts a single localized spin into a delocalized spin cluster state. The relative strengths of the exchange couplings between spins are indicated schematically below each plot.

ton in polyacetylene [147, 148, 149]. The spin density of the spin-up ground state is determined by numerical Lanczos diagonalization and is superimposed on the exchange profile, showing that localization coincides with the zero crossing of  $\alpha$ . This localization is retained when 50% multiplicative disorder is introduced into the exchange interaction strengths [Fig. 2.3(b)], illustrating the stability of the qubit with respect to local perturbations of the exchange profile.

By moving the domain wall, it is possible to transport logical spin qubits in a way that preserves the quantum information. The system will remain in the ground state, which represents the qubit, if a nonzero energy gap exists and the domain wall is displaced adiabatically with respect to this gap, i.e., over a time interval that satisfies the energy-time uncertainty principle [154, 155, 156]. Movement of the qubit state around the entire ring, achieved by letting  $k_0 \rightarrow k_0 + \Delta k$  and varying  $\Delta k$ , is shown in Fig. 2.3(c). To visualize the qubit, its spin density is plotted as a function of lattice site and domain wall displacement  $\Delta k$ . Note that two revolutions are required to achieve full periodicity for an  $n_c = \text{odd}$  spin ring. Variations in the energy gap  $E_1 - E_0$  between the ground state  $E_0$  and the first excited state  $E_1$  are small [ $\Delta(E_1 - E_0)/(E_1 - E_0)_{\min} \approx 0.23$ ].

For all domain wall positions shown in Fig. 2.3, the magnitude of the gap  $E_1 - E_0$  remains  $\sim J$ . The presence of a finite energy gap serves to protect the quantum information encoded in the ground state from decoherence due to noise [79, 80]. This protective effect is evident from an analysis of the system in the case of static disorder: Figure 2.3(d) shows that as the domain wall

center for the disordered system is displaced, the spatial localization of the qubit is preserved. Furthermore, because the exchange Hamiltonian in Eq. (2.1) conserves  $S^2$  and  $S_Z$ , these eigenvalues are unchanged by the introduction of noise into the exchange interaction strengths. Note that this reasoning is applicable in general, so that the finite gap  $E_1 - E_0$  and the conservation of  $S^2$  and  $S_Z$  will preserve the quantum information whether the noise is static or time dependent.

### 2.3 ANALYTICAL MODEL

General features of flying spin qubits emerge from an analysis of the simplest nontrivial case  $n_c = 3$ , for which exact solutions exist. The most general  $n_c = 3$  Hamiltonian in Eq. (2.1) can be reparametrized as

$$H_3 = \sum_{k=1}^3 \left\{ \tilde{J}_0 + \tilde{J}_1 \cos \left[ \frac{2\pi}{3}(k-1) - \varphi \right] \right\} \mathbf{S}_k \cdot \mathbf{S}_{k+1} \quad (2.3)$$

where  $\tilde{J}_0$  and  $\tilde{J}_1$  are constants, and  $\varphi$  represents the phase of the domain wall around the ring. The  $(S, S_Z) = (\frac{1}{2}, \frac{1}{2})$  subspace is two dimensional, spanned by the states  $|\pm\rangle = |001\rangle + e^{\pm 2\pi i/3} |010\rangle + e^{\pm 4\pi i/3} |100\rangle$ . (Here and in the following analysis, the states are defined up to an overall normalization factor.) Using this basis, we can re-express Eq. (2.3) as

$$H_3(\varphi) = \frac{\Delta}{2} (\Sigma_X \cos \varphi + \Sigma_Y \sin \varphi) - \frac{3\tilde{J}_0}{4} \mathbf{1}, \quad (2.4)$$

where the energy gap between the ground and first excited states is  $\Delta = 3\tilde{J}_1/2$  and

$$\Sigma_{X \pm iY} \equiv \frac{4}{3} \sum_{k=1}^3 e^{\pm 2\pi i(k-1)/3} \mathbf{S}_k \cdot \mathbf{S}_{k+1}.$$

Together with  $\Sigma_Z = -\frac{i}{2} [\Sigma_X, \Sigma_Y]$ , the operators  $\{\Sigma_X, \Sigma_Y, \Sigma_Z\}$  satisfy  $[\Sigma_a, \Sigma_b] = 2i\epsilon_{abc}\Sigma_c$ , and the states  $\{|\pm\rangle\}$  can be regarded as a pseudospin doublet [Fig. 2.4(a)]. This two-dimensional space is identical to the three-spin qubit proposed by DiVincenzo *et al.* in Ref. 87, but it does not represent the qubit; rather, it represents an orbital degree of freedom for the spin-up state. An isomorphic two-dimensional subspace exists for the spin-down state. These pseudospin spaces are described in more detail in Ch. 3. Spatially uniform exchange (parametrized by  $\tilde{J}_0$ ) does not couple to the

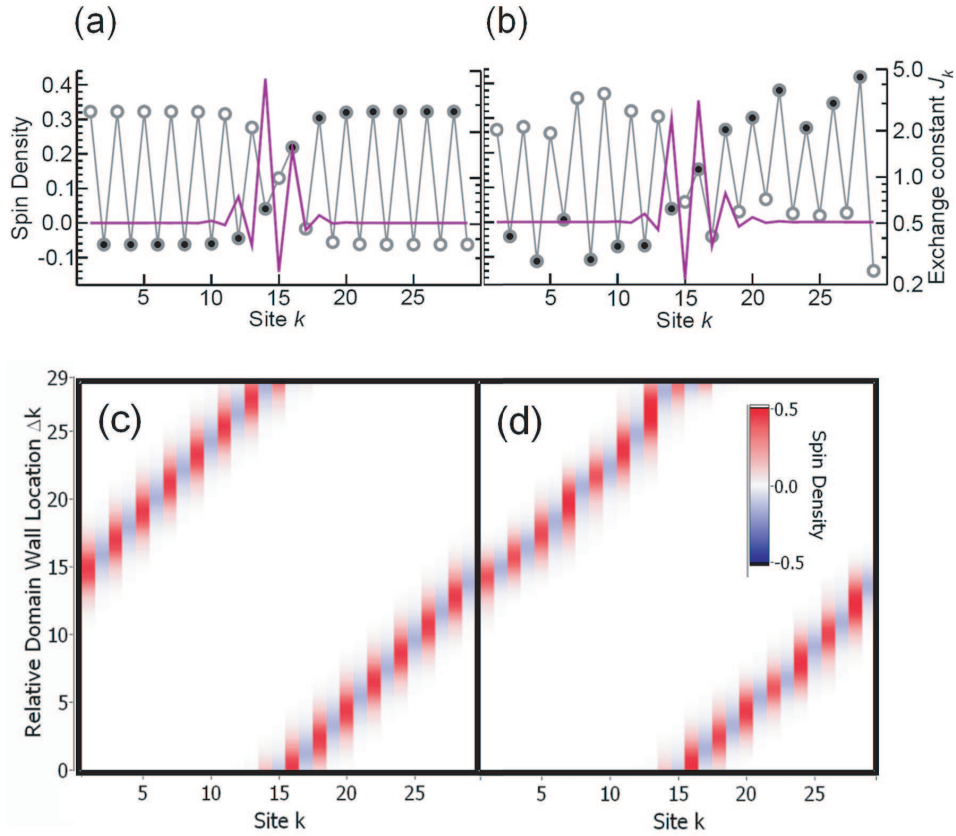


Figure 2.3: Generation of a flying spin qubit. (a) Exchange profile (circles) and spin density (line with no symbol) corresponding to the spin-up ground state for an  $n_c = 29$  spin ring containing a single soliton-like state. The filled circles represent even spin sites, and the empty circles represent odd spin sites. (b) Exchange profile and spin density for the spin-up ground state obtained when 50% multiplicative disorder is introduced into the exchange interaction strengths of the system in (a). (c) Adiabatic displacement of the qubit state shown in (a), achieved by shifting the domain wall center position by an amount  $\Delta k$  relative to its initial position  $k_0 = 15$ . The ground state is separated from the first excited state by a gap  $\sim J$  for all domain wall locations. (d) Adiabatic displacement of the qubit state for the disordered case shown in (b).

pseudospin states, and the ground state energy of  $H_3(\varphi)$  is independent of  $\varphi$ . We can interpret  $\{|\pm\rangle\}$  as right- and left-traveling spin-current Bloch states, eigenstates of the discrete translation operator  $D_2$  (defined by  $D_2\mathbf{S}_k \equiv \mathbf{S}_{k+2}D_2$ ) over two lattice sites. The ground state of  $H_3(\varphi)$  is given by  $|\varphi\rangle \equiv |+\rangle - e^{i\varphi}|-\rangle$ . The case  $\varphi = 0$  yields explicitly  $|\varphi = 0\rangle = |010\rangle - |100\rangle \equiv |SS0\rangle$ , which corresponds to spins 1 and 2 being in a singlet state, and spin 3 being in the “0” state. Adiabatic evolution of  $\varphi$  coherently moves the spin qubit around the ring, such that  $|\varphi = 2\pi/3\rangle = |001\rangle - |010\rangle \equiv |OSS\rangle$  and  $|\varphi = 4\pi/3\rangle = |001\rangle - |100\rangle \equiv |SOS\rangle$ . Note that these three states are not mutually orthogonal - they cannot be, since the space in which they evolve is two dimensional.

By letting  $\varphi = \omega t$ , the domain wall can be moved at a constant speed [Fig. 2.4(b)]. Because the Hamiltonian is now explicitly time-dependent, there are no longer stationary states; however, one may employ Bloch-Floquet theory [157] to understand the steady-state dynamics (as discussed in Sec. A.2). The time evolution is governed by a unitary operator  $U_t$  that satisfies the Schrödinger equation  $i\partial_t U_t = H(t)U_t$ , subject to the initial condition  $U_0 = \mathbf{1}$ . Floquet states are defined here to be the eigenstates of the combined time and space translation operators,  $F = D_2 U_{4\pi/n_c\omega}$ . Full translation around a closed spin chain by two revolutions (governed by the operator  $F^{n_c}$  or, equivalently,  $U_{4\pi/\omega}$ ) yields the same Floquet states as for  $F$ .

For the three-spin ring, we obtain (see Appendix A) the remarkable exact result for the Floquet state associated with the ground state:

$$|X+; \pm\omega\rangle = |SS0\rangle + \left( \frac{\omega}{\Delta} \pm \sqrt{1 + \left(\frac{\omega}{\Delta}\right)^2 \mp 1} \right) |\pm\rangle, \quad \omega > 0 \quad (2.5)$$

This state can be interpreted as a “snapshot” of the steady-state quantum dynamics at intervals in time  $t = 0, 2\pi/\omega, 4\pi/\omega, \dots$ , and is valid for all  $\omega$ . The adiabatic regime can be defined to be the range  $|\omega| < \Delta$ , in accordance with the energy-time uncertainty principle.

The exact results obtained for the three-spin ring extrapolate well to larger systems. To demonstrate, we consider an  $n_c = 9$  spin ring with a single domain wall given by  $J_k = J_0 + (-1)^k \alpha' (k - k_0)$ , where  $J_0 = 1$  and  $\alpha' (k - k_0) = a_0 \sin[\pi(k - k_0)/n_c - \omega t]$ . With  $k_0 \rightarrow k_0 + \frac{n_c}{\pi} \omega t$ , the staggered order parameter corresponds to Eq. (2.2) in the limit  $w \rightarrow n_c$ . Choosing  $a_0 = 0.1$  and  $k_0 = n_c/2$ , we obtain the Floquet states of the operator  $D_2 U_{2\pi/n_c\omega}$  for the  $n_c = 9$  spin ring. The ground state  $|\varphi_s^0\rangle$  is the analogue of the state  $|SS0\rangle$  in Eq. (2.5), where each spin in Eq. (2.5) has been replaced by a three-spin cluster qubit [91, 92]. The state  $|\varphi_s^0\rangle$  is determined by numerical diagonalization

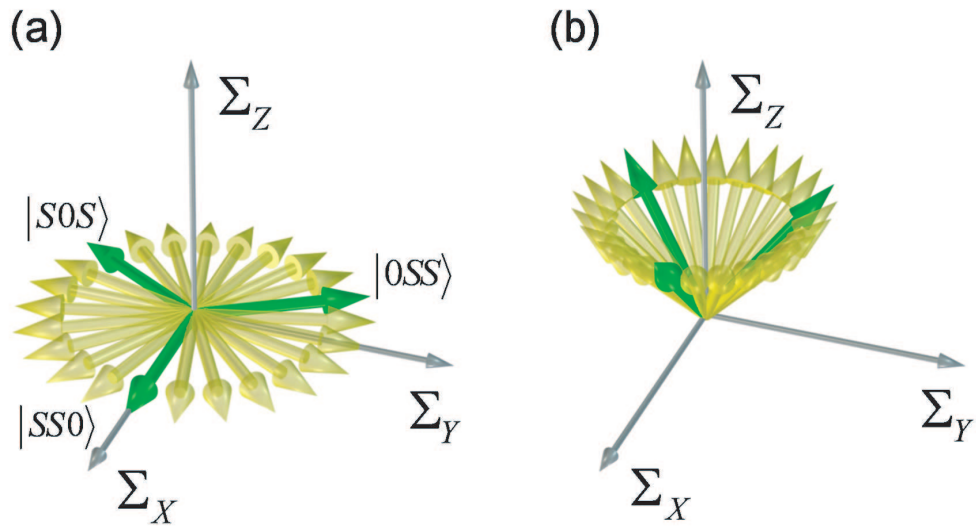


Figure 2.4: Analytical model for flying spin qubits. (a) Coherent evolution in the pseudo spin- $\frac{1}{2}$  space for an  $n_c = 3$  spin ring. Adiabatic evolution transports the spin state coherently between three nonorthogonal states shown as green arrows. (b) At high domain wall velocities, the Floquet states become distorted and eventually merge with eigenstates of  $\Sigma_Z$ .

of the initial Hamiltonian. We also find that the Floquet state  $|\varphi_s(\omega)\rangle$  associated with the ground state for  $\omega < \Delta E$  is well approximated (to within 1%) by the following expression:

$$|\varphi_s^{th}(\omega)\rangle = |\varphi_s^0\rangle + \frac{\omega}{\Delta E} |+\rangle, \quad (2.6)$$

where  $|+\rangle = \frac{1}{\sqrt{2}} (|u_1^0\rangle + i|u_2^0\rangle)$  is an eigenstate of  $D_2$  for the  $n_c = 9$  spin ring, and  $|u_1^0\rangle$  and  $|u_2^0\rangle$  are the ground states of this ring for the case  $J_k = 1$ . The energy gap  $\Delta E$  between the ground state and the first excited state is finite and is independent of the position of the domain wall. We note here that, for a given maximum value of the angular speed  $\omega$ , if the qubit speed is increased instantaneously to  $\omega$ , the error in the overlap  $|\langle\varphi_s(\omega)|\varphi_s^0\rangle|^2$  increases as  $\sim \omega^2$ . From Eq. (2.5), it can be seen that this  $\sim \omega^2$  dependence of the error also exists for the three-spin ring. Nevertheless, if the speed of the qubit is allowed to increase adiabatically to its maximum value  $\omega$  in small steps of  $\delta\omega \equiv \omega/N$ , where  $N$  is the number of steps, the error for each such step is proportional to  $\delta\omega^2 = (\omega/N)^2$ . Thus, provided  $\omega < \Delta E$ , as  $N$  is made very large,  $|\varphi_s(\omega)\rangle \rightarrow |\varphi_s^0\rangle$  and the fidelity of qubit transfer may be made arbitrarily close to unity.

## 2.4 EINSTEIN-PODOLSKY-ROSEN PAIR GENERATION

We now discuss a method of generating EPR pairs from a fully dimerized spin chain. Numerical investigations are performed for a closed chain with  $n_c = 30$  spins, using Lanczos diagonalization to determine the spin density and energies. The system is assumed to be initialized in the spin-singlet ground state ( $S = 0$ ). Two domain walls, denoted  $A$  and  $B$ , are created and moved in opposite directions [Fig. 2.5(a)]. The exchange profile describing this system is given by  $J_k = 0.55 - 0.45(-1)^k [1 + \alpha(k - k_A) - \alpha(k - k_B)]$ , where  $k_A = (n_c + s)/2$ ,  $k_B = (n_c - s)/2$ , and  $s$  is the separation between the two domain walls. Note that the exact quantitative form of the exchange profile is not crucial to this method of producing EPR pairs, provided the general characteristics which produce the domain walls are retained in the profile.

Because the Heisenberg exchange interaction conserves both  $S$  and  $S_Z$ , the two qubits associated with the domain walls must exist in a spin singlet or EPR pair:

$$|\Psi_0\rangle = \frac{1}{\sqrt{2}} (|\uparrow\rangle_A |\downarrow\rangle_B - |\downarrow\rangle_A |\uparrow\rangle_B).$$

In order to visualize this state, one can hybridize it with the first excited (triplet) state

$$|\Psi_1\rangle = \frac{1}{\sqrt{2}}(|\uparrow\rangle_A |\downarrow\rangle_B + |\downarrow\rangle_A |\uparrow\rangle_B)$$

and compute the spin density for  $\frac{1}{\sqrt{2}}(|\Psi_0\rangle - |\Psi_1\rangle) = |\downarrow\rangle_A |\uparrow\rangle_B$  [Fig. 2.5(b)]. The energies of the three lowest states behave as expected: there is an exchange splitting  $\Delta E = E_1 - E_0$  for the two spin qubits which decreases exponentially as the domain walls are moved apart [Fig. 2.5(c)]. The next excited state (energy  $E_2$ ) is given approximately by the one-magnon gap energy [158], which is largely unaffected by the domain wall states (i.e.,  $E_2 - E_0$  is approximately constant). Within a larger system, it would be possible to “radiate” multiple EPR pairs. Because they are entangled states, EPR pairs constitute an important physical resource for applications such as quantum teleportation [68].

## 2.5 PHYSICAL REALIZATION

The proposed mechanism for flying spin qubits must be capable of implementation in order to be relevant for quantum computing architectures. Here, we describe a specific realization using a one-dimensional array of elliptically shaped quantum dots, each containing one spin- $\frac{1}{2}$  electron (Fig. 2.6). Application of an electric field transverse to the array axis modulates the exchange interaction strength between each pair of nearest-neighbor quantum dots [Fig. 2.6(a)]. Each zero crossing of the electric field corresponds to a single (flying) spin qubit [Fig. 2.6(b)]. The “pseudodigital” nature [159] of  $J(E)$ , dependent on the detailed shape of the quantum dots, produces qubits that become more localized with increasing electric field amplitude. The electric field required to transport flying spin qubits may be implemented in a variety of ways, e.g., using a suitably designed coplanar waveguide.

The rate of qubit transfer  $R$  for such a device can be estimated in terms of the nominal exchange strength  $J$  between nearest-neighbor dots and the domain wall width  $w$ . The energy gap for the qubit states scales as  $\Delta \sim J/w$ , similar to that for spin cluster qubits [91, 92]. The qubit can travel  $w$  sites in a time  $\hbar/\Delta$  without violating the energy-time uncertainty principle. Taking  $D \approx 100$  sites for the spacing between domain walls, and using parameters relevant to Ge/Si quantum dots

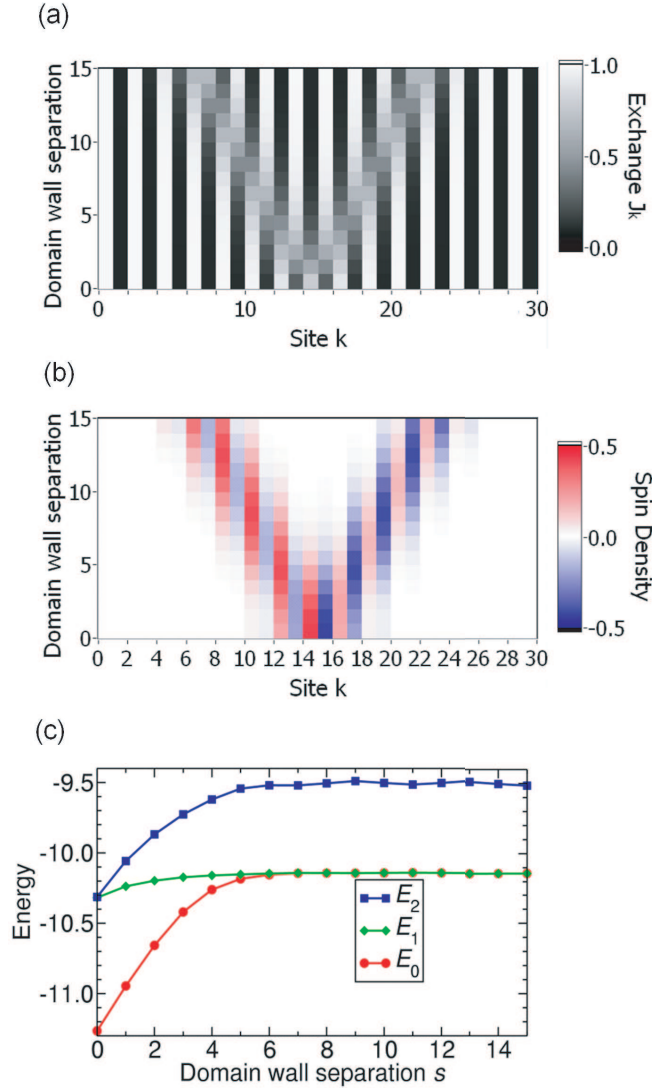


Figure 2.5: Generation of EPR pairs. (a) Exchange profile for an  $n_c = 30$  spin chain that is initially dimerized uniformly ( $J_{k=\text{odd}} = 1.0$ ,  $J_{k=\text{even}} = 0.1$ ). A domain wall pair is produced, and the walls move outward, creating an entangled pair of soliton-like states. (b) Spin density for a linear combination of the (spin-up) ground and first excited states, showing spatial separation of the qubit states as expected. (c) Lowest three energies (in units of  $J$ ) as a function of the domain wall separation  $s$ , showing the expected exchange splitting between  $E_0$  and  $E_1$ , and a relatively constant spin-wave gap between  $E_0$  and  $E_2$ .

[160] separated by  $d = 35$  nm and coupled by direct exchange  $J_0 \sim 500 \mu\text{eV}$  [161], one obtains  $R = J_0/\hbar D$  qubit  $\approx 7.6 \times 10^9$  qubit/s. Limitations on the switching speed for the electric field may reduce the qubit transfer rate from this maximum value; however, the mechanism of electric field propagation itself does not limit the rate. Sources of decoherence relevant to electron spins in quantum dots, such as fluctuating fields and coupling to nuclear spins, also apply to the systems considered here [47, 91].

Flying spin qubits should prove useful at all architectural levels, such as transporting “fresh qubits” for quantum error correction, carrying qubits to readout locations, implementing quantum gating between remote qubits, and other tasks.

## 2.6 CONCLUSION

In summary, we have demonstrated a mechanism by which flying spin qubits can be produced and moved controllably entirely within the solid state. Rapid, high fidelity transport of spin qubits is achieved by designing a quantum field with soliton-like domain walls that support localized spin states. The qubits created in this manner are topologically stable with respect to local perturbations of the exchange profile. By creating pairs of domain walls from a uniformly dimerized state, EPR pairs may be efficiently generated. Finally, we have proposed a scheme for implementing flying spin qubits in an array of elliptically shaped quantum dots.

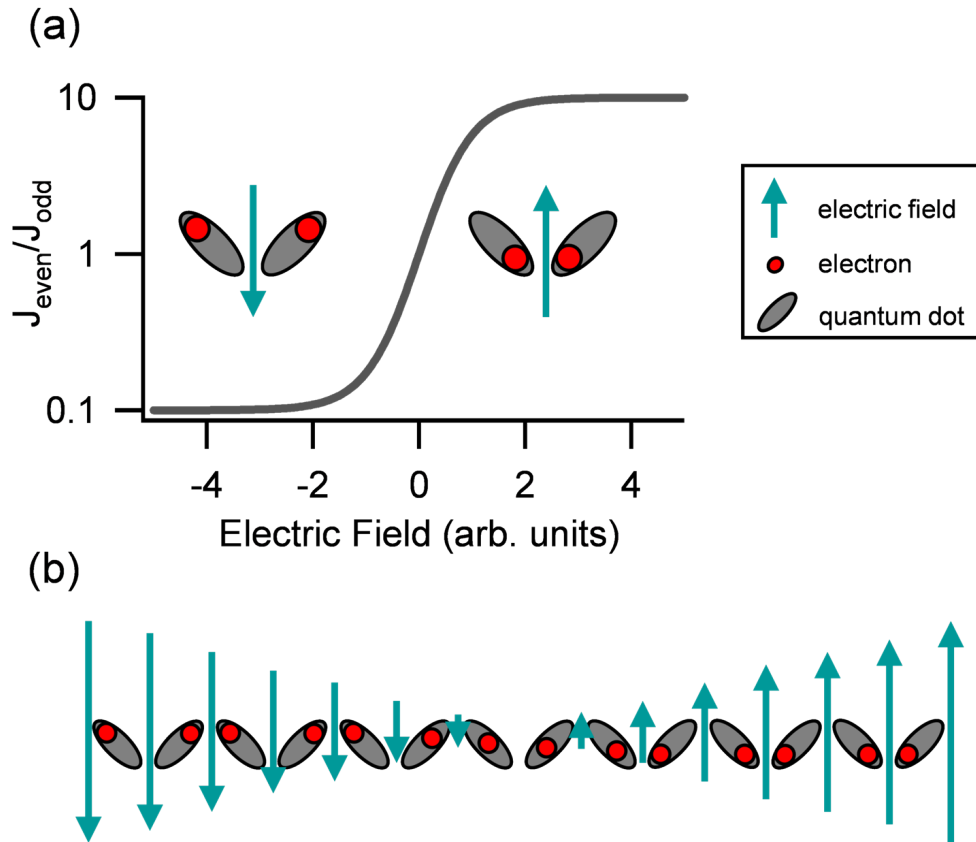


Figure 2.6: Experimental realization for flying spin qubits. (a) Dimerized exchange  $J(E)$  produced by elliptically shaped quantum dots in a transverse electric field. The field profile maps directly onto the staggered order parameter  $\alpha$ . (b) Zero crossings of the electric field correspond to single qubit states.

### 3.0 TAILORING EFFECTIVE EXCHANGE INTERACTIONS VIA DOMAIN WALLS IN COUPLED HEISENBERG RINGS

The nature of the exchange coupling variation in an AFM spin- $\frac{1}{2}$  system can be used to tailor its ground-state properties. In particular, we have seen in the previous chapter that dimerized Heisenberg rings containing domain walls have localized states that can serve as “flying spin qubits” when the domain walls are moved. Here, we show theoretically that when two of these rings are coupled, the movement of the domain walls leads to modulation of the effective exchange interaction between the qubits. Appropriately chosen configurations of domain walls can give rise to FM effective exchange. We describe how these spin rings may be used as basic building blocks to construct quantum spin systems whose properties are tunable by virtue of the exchange variation within the rings.<sup>1</sup>

#### 3.1 INTRODUCTION

While a single  $s = \frac{1}{2}$  spin is itself a qubit, we have seen how it may also be regarded as a fundamental building block that, together with interactions between spins, can be used to construct designer quantum materials with features that do not exist for the individual constituents. Among the types of quantum systems that may be constructed are single qubits formed from multiple spins interacting via Heisenberg exchange. As discussed in Sec. 1.4.3, the advantages of such qubits include the ability to perform universal quantum computation without requiring time-dependent external magnetic fields [81, 75, 82, 83, 84, 85] as well as with Heisenberg exchange as the sole physical interaction [87, 88, 89, 90], where the latter approach requires qubits composed of a minimum of

---

<sup>1</sup>The material in this chapter is adapted from Ref. [162].

three spins. We have also seen that uniform AFM Heisenberg chains of an odd number of spins can be used to define spin cluster qubits [91, 92], which are protected from decoherence by the presence of a finite energy gap above the qubit states [79, 80].

In addition to the number of spins, the exchange profile describing the set of interactions among spins may be varied. Collections of spins with modulated exchange give rise not only to stable qubits but also to systems capable of faithfully transporting quantum information [134, 135, 138, 130]. In particular, we have shown in Ch. 2 how it is possible to effectively construct a quantum field using a one-dimensional dimerized AFM Heisenberg spin- $\frac{1}{2}$  chain such that its topological excitations serve as qubits [130]. Introducing a domain wall that separates the two possible states of dimerization into the exchange profile produces a topologically stable logical qubit, whose spin density is localized at the domain wall. Movement of the domain wall within a large spin system allows the localized spin density to be propagated over arbitrary distances. While the qubit remains encoded in the spin- $\frac{1}{2}$  ground-state doublet of the entire system, the moving domain wall effectively changes the location from which the quantum information present in the form of nonzero spin density may be accessed, producing a “flying spin qubit” which is stable against local disorder in the exchange profile. This system therefore combines the stability properties of multi-spin qubits with the ability to transport the qubits within the very spin system in which they reside.

In order for quantum information processing to be possible with flying spin qubits, pairs of these qubits in their stationary form, which we refer to in the present work as domain-wall qubits, must be able to interact in a manner such that they become entangled. Entangling operations are essential elements of the set of quantum gates required to achieve universal quantum computation [35]. In order to explore methods for entangling domain-wall qubits, mechanisms by which they can be controllably coupled must first be understood. In this goal lies the motivation for the present work. Related work on methods for coupling qubits encoded in AFM molecular rings [163, 164] has involved switching on (off) the effective pairwise ring couplings by selectively exciting (deexciting) one of the rings in each pair to a state lying outside (inside) the qubit space. This scheme allows quantum gates to be performed by applying global fields to a chain of AFM rings alternating between two types, and qubit-qubit couplings can be switched off despite the existence of permanent spin-spin couplings. More recently, the advantages of applying this scheme to a chain of modulated AFM spin triangles have been discussed in the context of implementing quantum gates

between molecular qubits [165] and control over the effective coupling between molecular qubits via chemical modification of the intermolecular link has been demonstrated [166]. A method of entangling qubits via coupling to a uniform Heisenberg spin chain has also been proposed [167], where it was noted that the sign of the effective qubit-chain coupling depends on the spin site within the chain to which the qubit is coupled.

Here, we show that the exchange profiles for a pair of coupled dimerized AFM Heisenberg rings of  $s = \frac{1}{2}$  spins containing domain-wall qubits provide a means of tailoring the effective exchange interaction between the qubits. In this method, the system remains within the space spanned by the product states formed from the ground states of the rings. Tuning of the effective exchange is achieved by varying the positions of the domain walls within the rings. In all cases considered in the present work, the effective qubit-qubit exchange is found to be isotropic. Certain configurations of domain walls give rise to FM effective exchange despite the AFM nature of the spin-spin coupling between the rings. These features allow Heisenberg rings containing domain-wall qubits to serve as the building blocks of a new class of designer quantum materials, and we explore a few examples of such systems in the present work.

We first present basic features of an analytical model for a single AFM spin triangle containing a domain-wall qubit. This framework is then used to determine expressions for the effective qubit-qubit exchange as a function of the domain-wall positions within a pair of coupled AFM spin triangles. A direct connection between the spin-density variation within the rings and the effective exchange between the qubits is demonstrated. Extension of the results to larger coupled-ring systems is illustrated through numerical calculations for a pair of domain-wall qubits in coupled five-spin rings. Constructions of an effective three-qubit FM triangle, AFM rings of nine qubits with variable dimerization and a domain wall, and an effective spin-1 chain formed from qubits with alternating FM and AFM effective exchange are then demonstrated, using spin-triangle domain-wall qubits as the basic building blocks in each case. Finally, a possible physical realization of the spin-1 chain using quantum dots is described.

### 3.2 ANTIFERROMAGNETIC HEISENBERG SPIN RINGS

The Hamiltonian describing a one-dimensional system of  $n_c$  spin- $\frac{1}{2}$  objects coupled by nearest-neighbor Heisenberg (isotropic) exchange interactions is

$$H_{n_c} = \sum_{k=1}^{n_c} J_k (\mathbf{S}_k \cdot \mathbf{S}_{k+1}) \equiv \sum J_k (\mathbf{S}_k \cdot \mathbf{S}_{k+1}). \quad (3.1)$$

Here,  $\mathbf{S}_k = (S_k^x, S_k^y, S_k^z)$  is the vector operator for the  $k$ th spin and  $\hbar = 1$ . The constants  $\{J_k\}$  represent the strengths of the nearest-neighbor spin-spin-exchange interactions, whose AFM nature is incorporated into the model by assuming  $J_k > 0$  for all  $k$ . Periodic boundary conditions are included in Eq. (3.1) by letting  $k \pm n_c \equiv k$ . In the absence of external magnetic fields, both the square of the total spin angular momentum operator  $S^2 = (\sum \mathbf{S}_k)^2$  and the total  $z$  component  $S_Z = \sum S_k^z$  commute with  $H_{n_c}$ , so that state and operator representations can be defined for subspaces of definite  $S_Z$  and/or  $S^2$ .

The nature of the ground state of  $H_{n_c}$  depends on the form of the exchange profile, which is defined as the set of coupling constants  $\{J_k\}$ . To illustrate particular features of this dependence, we consider the smallest possible closed spin chain, which has  $n_c = 3$  spins. From Eq. (3.1), the Hamiltonian is  $H_3 = \sum_{k=1}^3 J_k (\mathbf{S}_k \cdot \mathbf{S}_{k+1})$ . The full Hilbert space for this Heisenberg spin triangle is spanned by  $2^3 = 8$  states and consists of subspaces characterized by energy eigenstates with fixed total spin quantum numbers  $S = \frac{3}{2}$  and  $S = \frac{1}{2}$ . The AFM spin-spin exchange gives rise to a ground state with the minimum possible total spin [91, 92], which is  $S = \frac{1}{2}$  for odd  $n_c$ . The space of  $S = \frac{1}{2}$  states can be divided into two subspaces  $(S, S_Z) = (\frac{1}{2}, \pm\frac{1}{2})$ , each of which is two dimensional and defines a pseudospin. We choose the particular exchange profile [130]

$$J_k = \tilde{J}_0 + \tilde{J}_1 \cos \left[ \frac{2\pi}{3}(k-1) - \varphi \right]. \quad (3.2)$$

The first term of this parametrization describes uniform exchange  $\tilde{J}_0$  and the second term is a sinusoidal modulation with an amplitude  $\tilde{J}_1$  and a phase  $\varphi$ . Here, we choose  $\tilde{J}_0 > 0$  and  $\tilde{J}_1 > 0$ . Equation (3.2) represents a typical exchange profile for the smallest possible spin system ( $n_c = 3$ ) that can contain a flying spin qubit. In this analytical model, a domain wall is centered around the position in the three-spin ring defined by the phase  $\varphi$  and varying  $\varphi$  corresponds to moving the spin qubit within the ring.

The spectrum of the spin-triangle Hamiltonian  $H_3$  is determined by the presence or absence of modulation in the exchange profile given in Eq. (3.2). For the case of uniform exchange,  $\tilde{J}_1 = 0$ , a set of eigenstates which spans the  $(S, S_Z) = (\frac{1}{2}, \frac{1}{2})$  subspace is

$$|\uparrow \pm\rangle \equiv \frac{1}{\sqrt{3}} \left( |001\rangle + e^{\pm 2\pi i/3} |010\rangle + e^{\pm 4\pi i/3} |100\rangle \right), \quad (3.3)$$

where  $|0\rangle \equiv |s = \frac{1}{2}, m_s = \frac{1}{2}\rangle$  and  $|1\rangle \equiv |s = \frac{1}{2}, m_s = -\frac{1}{2}\rangle$  are the single-spin basis states associated with the  $z$  component of spin. A corresponding set of eigenstates for the  $(S, S_Z) = (\frac{1}{2}, -\frac{1}{2})$  subspace is found by flipping all spins in Eq. (3.3),

$$|\downarrow \pm\rangle \equiv \frac{1}{\sqrt{3}} \left( |110\rangle + e^{\pm 2\pi i/3} |101\rangle + e^{\pm 4\pi i/3} |011\rangle \right). \quad (3.4)$$

The four states in Eqs. (3.3) and (3.4) are degenerate ground states for  $\tilde{J}_1 = 0$ . Introducing modulation into the exchange profile results in a splitting of the energies of the pseudospin states within each subspace of fixed  $S_Z$  (Fig. (3.1)). The  $S = \frac{1}{2}$  energy eigenstates become  $|\uparrow g_\varphi\rangle$ ,  $|\uparrow e_\varphi\rangle$ ,  $|\downarrow g_\varphi\rangle$ , and  $|\downarrow e_\varphi\rangle$ , where  $|\sigma g_\varphi\rangle = \frac{1}{\sqrt{2}} (|\sigma+\rangle - e^{i\varphi} |\sigma-\rangle)$  and  $|\sigma e_\varphi\rangle = \frac{1}{\sqrt{2}} (|\sigma+\rangle + e^{i\varphi} |\sigma-\rangle)$  for  $\sigma = \uparrow, \downarrow$ . The sets of eigenstates for the case  $\tilde{J}_1 \neq 0$  are therefore linear combinations of those in Eqs. (3.3) and (3.4), with the particular superpositions determined by the phase of the modulation  $\varphi$ . The degenerate ground states of the spin triangle are  $|\uparrow g_\varphi\rangle$  and  $|\downarrow g_\varphi\rangle$ , which have energy  $E_g = -3(\tilde{J}_0 + \tilde{J}_1)/4$  and are separated from the first excited states  $|\uparrow e_\varphi\rangle$  and  $|\downarrow e_\varphi\rangle$  with energy  $E_e = -3(\tilde{J}_0 - \tilde{J}_1)/4$  by a gap  $\Delta \equiv E_e - E_g = 3\tilde{J}_1/2$ . Note that both the energies  $E_g, E_e$  and the gap are independent of  $\varphi$  [130]. Within the ground-state subspace, the spin triangle can be regarded as a two-level system and serves as a single qubit [91, 92]. The finite gap present for all  $\varphi$  serves to protect this qubit from decoherence [88, 79].

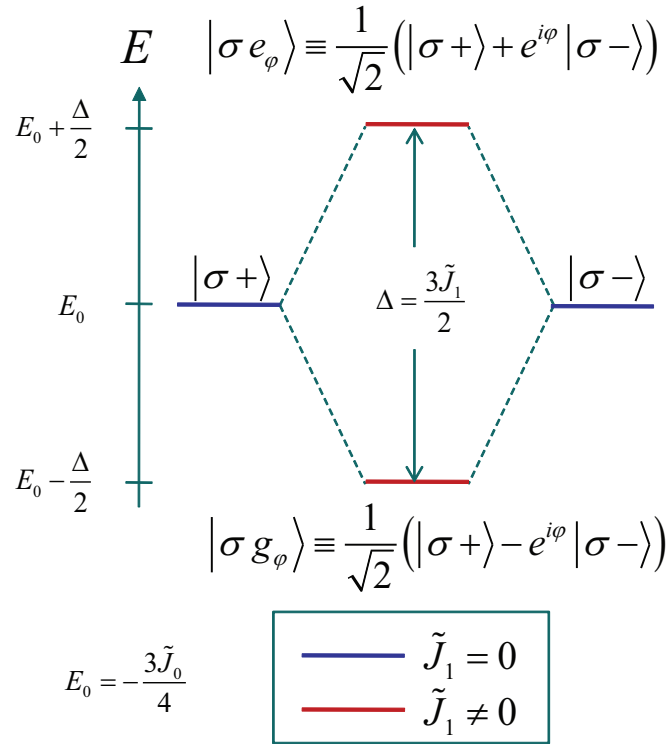


Figure 3.1: Energy level diagram illustrating the relationship between the energies of the pseudospin states  $|\sigma\pm\rangle$  and those of the states  $|\sigma g_\varphi\rangle$  and  $|\sigma e_\varphi\rangle$  for the three-spin ring with  $\sigma = \uparrow, \downarrow$ . The states  $|\sigma\pm\rangle$  are eigenstates for the case of uniform coupling ( $\tilde{J}_1 = 0$ ). Modulation of the exchange ( $\tilde{J}_1 \neq 0$ ) gives the eigenstates  $|\sigma g_\varphi\rangle$  and  $|\sigma e_\varphi\rangle$ , which are separated by an energy gap  $\Delta$ .

### 3.3 ANALYTICAL MODEL FOR EFFECTIVE EXCHANGE

We now consider a system of two coupled spin triangles with modulated nearest-neighbor exchange interactions (Fig. (3.2)). The exchange within each of the triangles is assumed to be given by the profile in Eq. (3.2). The Hamiltonian for this six-spin system can be written as  $H = H_0 + H'_{ij}$ , where

$$H_0 = \sum_{k=1}^3 \left\{ \left\{ \tilde{J}_0 + \tilde{J}_1 \cos \left[ \frac{2\pi}{3} (k-1) - \varphi_a \right] \right\} \mathbf{S}_{ka} \cdot \mathbf{S}_{(k+1)a} \right. \\ \left. + \left[ \tilde{J}_0 + \tilde{J}_1 \cos \left( \frac{2\pi}{3} (k-1) - \varphi_b \right) \right] \mathbf{S}_{kb} \cdot \mathbf{S}_{(k+1)b} \right\} \quad (3.5)$$

describes the coupling within the triangles (labeled  $a$  and  $b$ ), and  $H'_{ij} = J_r \mathbf{S}_{ia} \cdot \mathbf{S}_{jb}$  with  $J_r > 0$  denotes the intertriangle AFM spin-spin coupling. Figure (3.2) illustrates the particular cases  $H'_{ij} = H'_{33}$  and  $H'_{ij} = H'_{21}$ . The full Hilbert space for the system is spanned by the set of all possible product states of individual-spin-triangle basis states. For  $J_r = 0$  (uncoupled triangles), the gap between the ground state  $E_0 = 2E_g$  and the first excited state  $E_1 = 2E_e$  is  $E_1 - E_0 = 2\Delta$ . In the limit  $J_r \ll \Delta$ , the coupling between the rings  $H'_{ij}$  can be regarded as a perturbation relative to  $H_0$  [168, 169, 170], and the pair of triangles can be described within the subspace spanned by the product states of the spin-triangle ground states. To simplify the notation, we define  $|\uparrow(\varphi)\rangle = |\uparrow g_\varphi\rangle$  and  $|\downarrow(\varphi)\rangle = |\downarrow g_\varphi\rangle$ . The ground-state product basis can then be written as

$$\{ |\uparrow(\varphi_a)\rangle |\uparrow(\varphi_b)\rangle, |\uparrow(\varphi_a)\rangle |\downarrow(\varphi_b)\rangle, |\downarrow(\varphi_a)\rangle |\uparrow(\varphi_b)\rangle, |\downarrow(\varphi_a)\rangle |\downarrow(\varphi_b)\rangle \}. \quad (3.6)$$

The states in Eq. (3.6) are product states of the instantaneous ground states associated with the individual triangles for the set of domain-wall phases  $\{\varphi_a, \varphi_b\}$ . In a system in which the domain walls are in motion, choosing these states as a basis is similar to choosing a reference frame which rotates with the domain-wall positions. Here, we use basis (3.6) to analytically describe the variation in the *static* qubit states as a function of  $\varphi_a$  and  $\varphi_b$ .

Within the subspace defined by states (3.6), the Hamiltonian  $H_0$  in Eq. (3.5) is proportional to the identity operator  $\mathbf{1}$  (see Ref. 92) and the full Hamiltonian can be rewritten as

$$H_3^{\text{eff}} = -\frac{3}{2} (\tilde{J}_0 + \tilde{J}_1) \mathbf{1} + J_{\text{eff}}(J_r, \varphi_a, \varphi_b) \mathbf{S}_a^\Delta \cdot \mathbf{S}_b^\Delta. \quad (3.7)$$

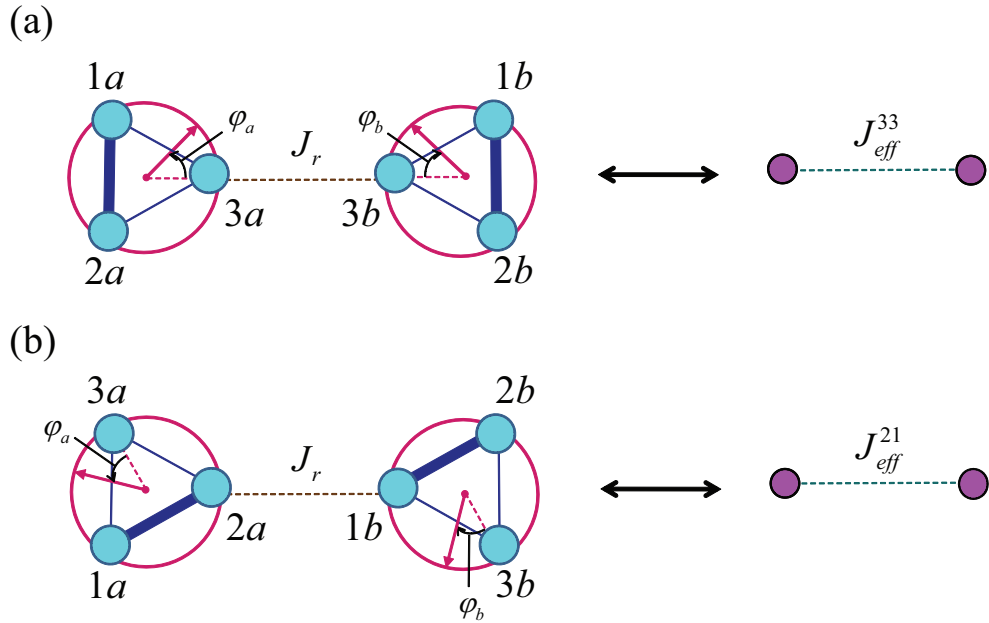


Figure 3.2: Pairs of spin triangles with exchange modulation parametrized by  $\{\varphi_a, \varphi_b\}$  and coupled by AFM exchange  $J_r > 0$ . The thicker and thinner lines drawn between the spins within the triangles indicate the stronger and weaker coupling strengths, respectively, for  $\varphi_a = \varphi_b = 0$ , which occurs when the domain walls are located at the site labeled “3” for each spin triangle. (a) Inter-triangle coupling  $H'_{33}$ . (b) Intertriangle coupling  $\hat{H}'_{21}$ . Within the ground-state product subspace, the triangle pairs in (a) and (b) are effectively pairs of qubits coupled by exchange  $J_{eff}^{33}$  and  $J_{eff}^{21}$ , respectively [Eqs. (3.8) and (3.9)], as shown on the right.

Here,  $\mathbf{S}_a^\Delta = \sum_{k=1}^3 \mathbf{S}_{ka}$  and  $\mathbf{S}_b^\Delta = \sum_{k=1}^3 \mathbf{S}_{kb}$  are the total spin operators for the individual triangles. The effective exchange  $J_{\text{eff}}$  is a function of the strength of the coupling between the triangles  $J_r$  as well as of the domain-wall phases  $\varphi_a$  and  $\varphi_b$ . Note that the nontrivial exchange term in Eq. (3.7) arises entirely from  $H'_{ij}$  and also that the exchange interaction remains isotropic within the subspace, as was found for spin cluster qubits [91, 92]. The form of  $J_{\text{eff}}(J_r, \varphi_a, \varphi_b)$  depends on the spins  $ia$  and  $jb$  involved in the coupling between the rings  $H'_{ij} = J_r \mathbf{S}_{ia} \cdot \mathbf{S}_{jb}$ . For  $H'_{33} = J_r \mathbf{S}_{3a} \cdot \mathbf{S}_{3b}$  [Fig. (3.2)(a)], the effective exchange is given by

$$J_{\text{eff}}^{33}(J_r, \varphi_a, \varphi_b) = \frac{J_r}{9} (1 + 2 \cos \varphi_a) (1 + 2 \cos \varphi_b), \quad (3.8)$$

while for  $H'_{21} = J_r \mathbf{S}_{2a} \cdot \mathbf{S}_{1b}$  [Fig. (3.2)(b)], the form of the effective exchange is

$$J_{\text{eff}}^{21}(J_r, \varphi_a, \varphi_b) = \frac{J_r}{9} \left( \cos \varphi_a - 1 + \sqrt{3} \sin \varphi_a \right) \left( \cos \varphi_b - 1 - \sqrt{3} \sin \varphi_b \right). \quad (3.9)$$

The origin of the exchange coupling variation in Eqs. (3.8) and (3.9) is directly related to the variation in the spin density at the sites  $ia$  and  $jb$ . We show this by deriving Eq. (3.7) for  $H'_{ij} = H'_{33}$ . To do so, we calculate the matrix elements of  $H'_{33}$  in the basis given in Eq. (3.6). The intertriangle interaction term can be rewritten as  $H'_{33} = J_r \mathbf{S}_{3a} \cdot \mathbf{S}_{3b} = J_r [S_{3a}^z S_{3b}^z + \frac{1}{2} (S_{3a}^+ S_{3b}^- + S_{3a}^- S_{3b}^+)]$ , where  $S_{k\lambda}^\pm = S_{k\lambda}^x \pm i S_{k\lambda}^y$  for  $\lambda = a, b$ . The first term of this expression has only diagonal nonzero elements and the second term has only off-diagonal nonzero elements [92]. Using the fact that  $\langle \downarrow(\varphi_\lambda) | S_{k\lambda}^z | \downarrow(\varphi_\lambda) \rangle = -\langle \uparrow(\varphi_\lambda) | S_{k\lambda}^z | \uparrow(\varphi_\lambda) \rangle$  and the representation defined by the order of the states in Eq. (3.6), we find

$$H'_{33} \rightarrow h_{11} \begin{pmatrix} 1 & 0 & 0 & 0 \\ 0 & -1 & 2 & 0 \\ 0 & 2 & -1 & 0 \\ 0 & 0 & 0 & 1 \end{pmatrix}, \quad (3.10)$$

where  $h_{11} \equiv J_r \langle \uparrow(\varphi_a) | S_{3a}^z | \uparrow(\varphi_a) \rangle \langle \uparrow(\varphi_b) | S_{3b}^z | \uparrow(\varphi_b) \rangle = J_r (1 + 2 \cos \varphi_a) (1 + 2 \cos \varphi_b) / 36$ . Setting the matrix in Eq. (3.10) equal to that for a Heisenberg exchange interaction between two spin- $\frac{1}{2}$  objects in the standard basis  $\{|00\rangle, |01\rangle, |10\rangle, |11\rangle\}$  gives  $H'_{33} \rightarrow J_{\text{eff}}^{33}(J_r, \varphi_a, \varphi_b) \mathbf{S}_a^\Delta \cdot \mathbf{S}_b^\Delta$ ,

which is the second term in Eq. (3.7) for the case  $H'_{ij} = H'_{33}$ . Here,  $J_{\text{eff}}^{33} = 4h_{11}$ , which agrees with Eq. (3.8) and may also be written as

$$J_{\text{eff}}^{33} = 4J_r \langle \uparrow(\varphi_a) | S_{3a}^z | \uparrow(\varphi_a) \rangle \langle \uparrow(\varphi_b) | S_{3b}^z | \uparrow(\varphi_b) \rangle. \quad (3.11)$$

The quantities  $\langle \uparrow(\varphi_a) | S_{3a}^z | \uparrow(\varphi_a) \rangle$  and  $\langle \uparrow(\varphi_b) | S_{3b}^z | \uparrow(\varphi_b) \rangle$  are none other than the values of the spin densities at sites  $3a$  and  $3b$  for the states  $|\uparrow(\varphi_a)\rangle$  and  $|\uparrow(\varphi_b)\rangle$ . We therefore find the result that the effective exchange between the spin-triangle qubits is directly proportional to the product of the spin densities at the sites participating in the intertriangle spin-spin coupling.

In particular, if these two spin densities are of opposite signs, the effective exchange is negative. With the convention chosen in the present work that positive values of the exchange are AFM, the negative sign corresponds to FM effective exchange. Note that this is true despite the AFM nature of the spin-spin coupling  $J_r$  between the triangles. Because the spin densities vary with the phases  $\{\varphi_a, \varphi_b\}$  of the domain walls within the triangles, these phases provide a method of controlling the effective coupling between the qubits. In other words, the *intertriangle* coupling can be tuned via the *intratriangle* coupling, and in particular, FM qubit-qubit coupling can in principle be realized with only AFM spin-spin coupling.

As an example, the variation in the effective exchange given by Eq. (3.8) for the coupled triangle pair in Fig. 3.2(a) is plotted in Fig. 3.3(a) as a function of  $\varphi_a$ , with  $J_r = 1$  and  $\varphi_b = 0$ . This variation is independent of the values of  $\tilde{J}_0$  and  $\tilde{J}_1$ . Note that as the domain wall in ring  $a$  is moved around the ring, the effective exchange changes from AFM to FM and back to AFM, which reflects the changing spin density at site  $3a$ . A maximum in the FM exchange strength occurs for  $\{\varphi_a = \pi, \varphi_b = 0\}$ , while for the domain-wall configurations  $\{\varphi_a = 2\pi/3, \varphi_b = 0\}$  and  $\{\varphi_a = 4\pi/3, \varphi_b = 0\}$ , the qubit-qubit coupling is effectively zero. The vanishing exchange can be understood by considering the spin density within the triangles. For both of these domain-wall configurations, the spin at site  $3a$  belongs to a relatively strongly coupled pair whose ground state is the  $S = 0$  singlet state  $\frac{1}{\sqrt{2}}(|01\rangle - |10\rangle)$  of two spins. The spin density at site  $3a$  is therefore zero, which results in the vanishing of the effective coupling in Eq. (3.11). Figure 3.3(b) shows the energies of the eight lowest states of the coupled spin-triangle pair as a function of  $\varphi_a$  for  $\tilde{J}_0 = 1$ ,  $\tilde{J}_1 = 1$ ,  $J_r = 0.1$ , and  $\varphi_b = 0$ . The effective exchange splitting is apparent in the energies of the lowest four states, three of which are triply degenerate and one of which is nondegenerate. The

presence of a relatively large gap between these lowest two energy levels and higher states for all values of  $\varphi_a$  confirms the validity of the effective exchange approximation.

The method of modifying the spin density within a Heisenberg ring in order to produce FM effective exchange which is described here is closely analogous to techniques that have been used to synthesize crystals of organic radicals with intermolecular FM exchange [171], which involve stacking radicals in orientations such that atoms with spin densities of opposite sign are neighboring each other. In these systems, the presence of the unpaired electron in a cyclic radical plays a role similar to the domain wall in the Heisenberg spin rings considered in the present work. In addition, the importance of the relative orientations of a pair of stacked radicals to the nature of the overall intermolecular effective exchange was shown to be related to the overlap of the atomic orbitals between the radicals [172], with large overlap corresponding to AFM exchange and small overlap to FM exchange. A similar but much less sophisticated relationship for the Heisenberg ring systems containing domain-wall qubits can be obtained by calculating the overlap  $|\langle \sigma(\varphi_a) | \sigma(\varphi_b) \rangle| = |\cos[(\varphi_a - \varphi_b)/2]|$  between the ground states of the two spin triangles, which can be regarded as orbital-like overlap by noting that moving the domain wall in each ring corresponds to changes within an orbital degree of freedom for each qubit [130]. For  $\varphi_b = 0$ , it is seen that a  $|\langle \sigma(\varphi_a) | \sigma(0) \rangle| \geq \frac{1}{2}$  for  $0 \leq \varphi_a \leq 2\pi/3$  and  $4\pi/3 \leq \varphi_a \leq 2\pi$ , which are the regions of AFM effective exchange [Fig. 3.3(a)] while  $|\langle \sigma(\varphi_a) | \sigma(0) \rangle| \leq \frac{1}{2}$  for  $2\pi/3 \leq \varphi_a \leq 4\pi/3$ , which corresponds to the range over which the exchange is FM. AFM (FM) effective exchange is therefore seen to occur for domain-wall locations associated with larger (smaller) orbital-like overlap values.

### 3.4 NUMERICAL STUDIES OF EFFECTIVE EXCHANGE

The discussion of effective exchange between domain-wall qubits has so far focused on a particular analytical model, in which the exchange profile is given by Eq. (3.2). To illustrate the generality of the results, we consider alternative forms of exchange profiles which give rise to domain walls in dimerized Heisenberg rings defined by Eq. (3.1) with  $n_c = 5$  and periodic boundary conditions. Numerical calculations are carried out in order to determine the effective exchange between the qubits, assuming that they are encoded in the ground states of the rings.

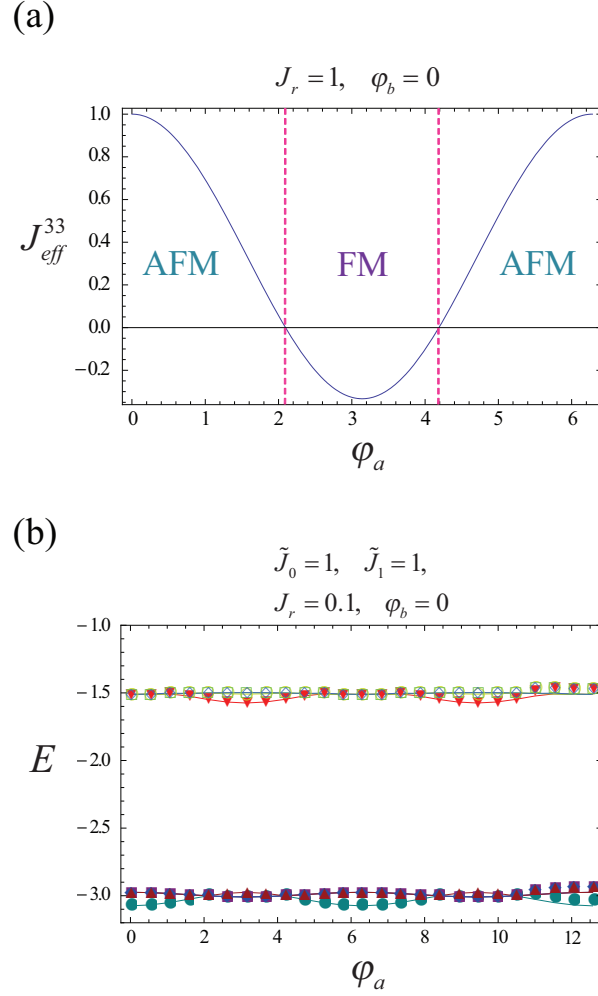


Figure 3.3: (a) Effective exchange  $J_{eff}^{33}(J_r = 1, \varphi_a, \varphi_b = 0)$  given by Eq. (3.8) for the coupled spin-triangle pair in Fig. 3.2(a), showing the ranges of domain-wall locations  $\varphi_a$  for which the exchange is AFM and FM. (b) Variation in the energies for the lowest eight states of the system in Fig. 3.2(a) as  $\varphi_a$  is changed from 0 to  $4\pi$  with  $\tilde{J}_0 = 1, \tilde{J}_1 = 1, J_r = 0.1,$  and  $\varphi_b = 0$ , showing the effective exchange splitting within the lowest two energies (four states, three of which are triply degenerate and one of which is nondegenerate) and a relatively large gap separating the lowest four states from higher levels for all values of  $\varphi_a$ .

For each five-spin ring, we initially consider an exchange profile formed from two exchange constants  $\bar{J}$  and  $J$ , with  $0 \leq J/\bar{J} \leq 1$ , in which there is a domain wall separating the two possible states of dimerization. General features of spin systems with such exchange profiles are discussed in Ref. [130]. We consider a pair of spin rings (labeled  $a$  and  $b$ ), which each have the exchange profile  $\{J_1 = J_4 = \bar{J}, J_2 = J_3 = J_5 = J\}$  and are coupled by AFM exchange  $J_r > 0$  [Fig. 3.4(a)]. This system has domain walls centered at sites  $3a$  and  $3b$ . The ground state doublet of a single AFM five-spin ring has  $(S, S_Z) = (\frac{1}{2}, \pm\frac{1}{2})$ . These two states define a qubit [91, 92, 130] and are determined by numerical diagonalization of the Hamiltonian in Eq. (3.1) for  $n_c = 5$ . The spin densities of the two ground states are plotted as a function of site  $k$  in Fig. 3.4(b) and show the spin density of the qubit localized around the domain wall at  $k = 3$ . Denoting the product basis constructed from the spin-ring ground states by

$$\{|\uparrow(a)\rangle|\uparrow(b)\rangle, |\uparrow(a)\rangle|\downarrow(b)\rangle, |\downarrow(a)\rangle|\uparrow(b)\rangle, |\downarrow(a)\rangle|\downarrow(b)\rangle\},$$

where  $\uparrow$  refers to the  $S_Z = \frac{1}{2}$  state and  $\downarrow$  to the  $S_Z = -\frac{1}{2}$  state, we determine the effective Hamiltonian within the subspace spanned by these states for  $\bar{J} = 1$ ,  $J/\bar{J} = 0.2$ , and  $J_r = 0.1$ . For the coupling depicted in Fig. 3.4(a) (where both domain walls are at the positions defined to be zero) we find the effective Hamiltonian  $-3.037 \mathbf{1} + 0.096 \mathbf{S}_a \cdot \mathbf{S}_b \equiv H_5^{\text{eff}}(0)$ , where  $\mathbf{S}_a$  and  $\mathbf{S}_b$  are the total spin operators of rings  $a$  and  $b$ , respectively. As was found for the coupled spin triangles and for spin cluster qubits [91, 92], the qubit-qubit exchange Hamiltonian is of the isotropic Heisenberg form (up to a term proportional to the identity, which simply corresponds to a uniform shift of all energies).

We now displace the domain wall within ring  $a$  by  $s$  sites in the direction of increasing site index with respect to the labeling in Fig. 3.4(a) by applying a discrete translation operator to  $|\uparrow(a)\rangle$  and  $|\downarrow(a)\rangle$ , and we calculate the effective Hamiltonian  $H_5^{\text{eff}}(s)$  in the shifted product basis for each distinct position of the domain wall. For the system in Fig. 3.4(a), there are three distinct positions, as seen by noting that the exchange profile is periodic with a period of  $n_c = 5$  sites, and further that the sites  $1a$  and  $5a$  are equivalent by symmetry, as are the sites  $2a$  and  $4a$  so that  $H_5^{\text{eff}}(1) = H_5^{\text{eff}}(4)$  and  $H_5^{\text{eff}}(2) = H_5^{\text{eff}}(3)$ . We find  $H_5^{\text{eff}}(s) = -3.037 \mathbf{1} + J_5^{\text{eff}}(s) \mathbf{S}_a \cdot \mathbf{S}_b$ , where the values of  $J_5^{\text{eff}}(s)$  are plotted in Fig. 3.4(c). Note the variation in the sign of  $J_5^{\text{eff}}(s)$ , indicating that the qubit-qubit exchange can be either AFM or FM, depending on the position of the domain

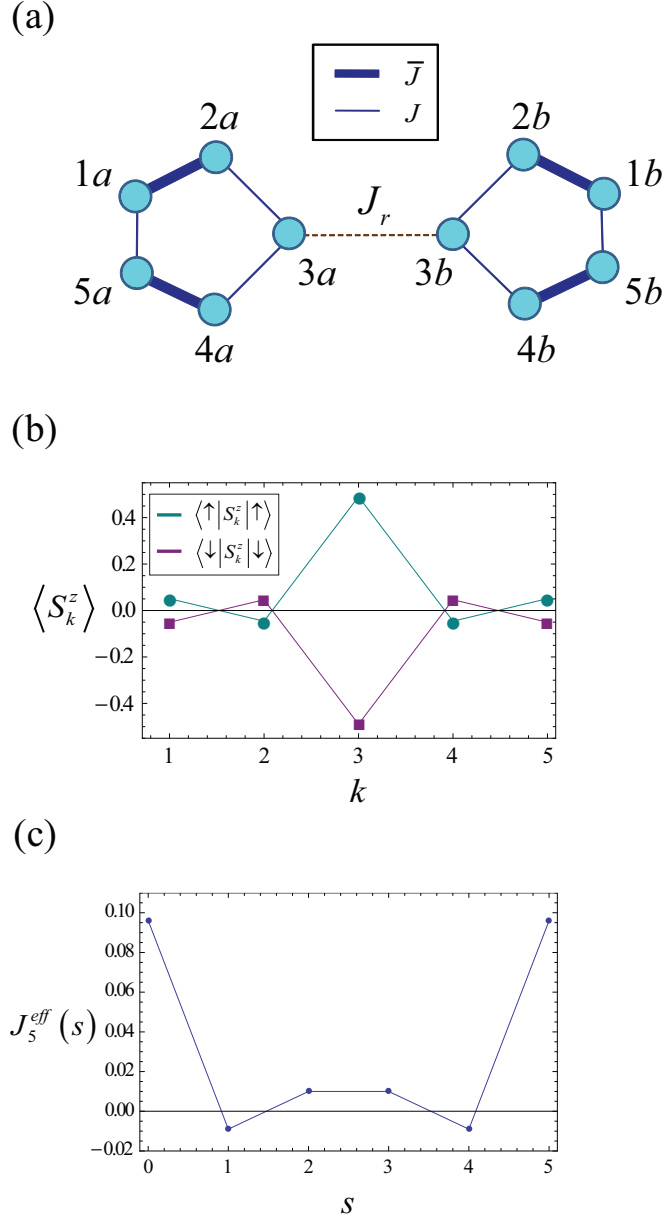


Figure 3.4: (a) Pair of  $n_c = 5$  spin rings having dimerized exchange and containing domain-wall qubits. The rings are coupled via AFM exchange  $J_r > 0$  and the coupling strength between each pair of spins within the rings is either  $\bar{J}$  or  $J$ , with  $0 \leq J/\bar{J} \leq 1$ . (b) Spin density of the  $(S, S_Z) = (\frac{1}{2}, \pm\frac{1}{2})$  ground states of a single  $n_c = 5$  spin ring of the type shown in a with  $\bar{J} = 1$  and  $J/\bar{J} = 0.2$ , showing localization of the qubit around the position of the domain wall at  $k = 3$ . (c) Effective exchange  $J_5^{\text{eff}}$  for  $J_r = 0.1$  as a function of the number of sites  $s$  by which the domain wall in ring  $a$  shown in (a) is displaced, with  $s = 0$  corresponding to the domain wall being located at site  $3a$ . The value of  $s$  is defined to increase in the direction of increasing spin index ( $3 \rightarrow 4 \rightarrow 5 \rightarrow 1 \rightarrow 2$ ).

wall within the five-spin ring. As in the case of the spin-triangle pair, the effective exchange variation results directly from the change in the spin density at site  $3a$  as the domain wall in ring  $a$  is displaced.

The relationship between the spin density within one of the  $n_c = 5$  spin rings and the effective exchange between the qubits can be made more apparent by moving the domain wall more continuously. For each ring, we therefore choose the particular exchange profile

$$J_k = \bar{J}(1 + J/\bar{J})/2 + [\bar{J}(1 - J/\bar{J})/2](-1)^k \alpha(k - k_0), \quad (3.12)$$

where the staggered order parameter is

$$\alpha(k - k_0) = \frac{1}{N} \sum_{r=-n}^n (-1)^r \tanh \left[ \frac{(k - k_0) - rn_c}{w} \right]$$

with  $k_0 = (n_c + 1)/2 + \Delta k$  denoting the position of the domain wall and

$$N = \sum_{r=-n}^n (-1)^r \tanh([n_c/2 - rn_c]/w).$$

Exchange profiles of this form can be used to produce flying spin qubits [130]. For the present case ( $n_c = 5$ ,  $k_0 = 3 + \Delta k$ ), we choose the parameter values  $\bar{J} = 1$ ,  $J/\bar{J} = 0.1$ ,  $w = 2$ , and  $n = 50$  along with  $J_r = 0.1$  for the spin-spin coupling between the rings. The effective exchange is determined numerically by diagonalizing the Hamiltonian for the coupled pair of rings within the ground-state product subspace

$$\{|\uparrow(\Delta k_a)\rangle|\uparrow(\Delta k_b)\rangle, |\uparrow(\Delta k_a)\rangle|\downarrow(\Delta k_b)\rangle, |\downarrow(\Delta k_a)\rangle|\uparrow(\Delta k_b)\rangle, |\downarrow(\Delta k_a)\rangle|\downarrow(\Delta k_b)\rangle\}$$

and calculating the energy gap between the singlet state (energy  $E_s$ ) and the triplet states (energy  $E_t$ ) of the two qubits associated with the rings in the above basis. The exchange splitting  $J_5^{\text{eff}}(\Delta k_a, \Delta k_b = 0) = E_t(\Delta k_a, \Delta k_b = 0) - E_s(\Delta k_a, \Delta k_b = 0)$  is shown in Fig. 3.5(a) as a function of  $\Delta k_a$ , where  $J_5^{\text{eff}} > 0$  corresponds to AFM exchange and  $J_5^{\text{eff}} < 0$  to FM exchange. Note that  $J_5^{\text{eff}}$  is periodic for two full revolutions of the domain wall around the ring, which arises from the fact that the staggered order parameter  $\alpha$  itself has a period of  $2n_c = 10$  sites. Figure 3.5(b) shows the variation in the spin density at site  $3a$  for the state  $|\uparrow(\Delta k_a)\rangle$  over the same range of values of  $\Delta k_a$ . We find that a relation analogous to Eq. (3.11) holds:

$$J_5^{\text{eff}} = 4J_r \langle \uparrow(\Delta k_a) | S_{3a}^z | \uparrow(\Delta k_a) \rangle \langle \uparrow(0) | S_{3b}^z | \uparrow(0) \rangle. \quad (3.13)$$

Applying Eq. (3.13) to the spin-density values in Fig. 3.5(b) with  $J_r = 0.1$  and  $\langle \uparrow(0) | S_{3b}^z | \uparrow(0) \rangle = \langle \uparrow(0) | S_{3a}^z | \uparrow(0) \rangle$  reproduces exactly Fig. 3.5(a). We also find that the ratio  $J_r/\Delta E$ , where  $\Delta E$  denotes the gap between the qubit states and the next excited state for a single ring, is small for all  $\Delta k_a$  values in Fig. 3.5, its maximum value being  $(J_r/\Delta E)_{\max} \approx 0.153$ . The effective exchange approximation therefore remains valid for the case of the coupled five-spin ring system.

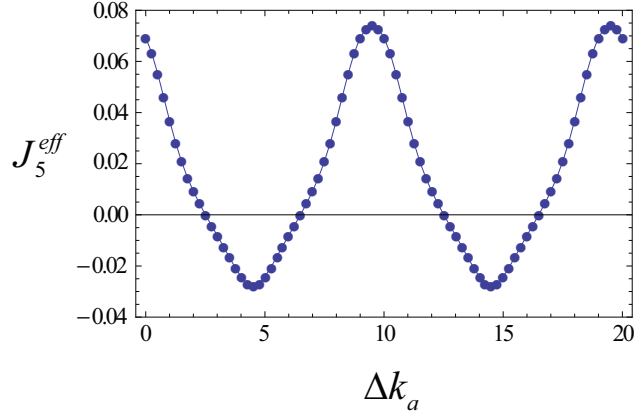
### 3.5 CONSTRUCTION OF QUANTUM SPIN SYSTEMS BY TAILORING OF THE EFFECTIVE EXCHANGE

We have shown that both the magnitude and the sign of the effective exchange between the qubits encoded in the ground states of two dimerized AFM Heisenberg rings containing domain walls can be tailored by suitable modification of the spin density within the rings. This ability to tune the nature of the exchange allows the spin rings to serve as building blocks for a wide variety of quantum spin systems. Here we demonstrate some examples of systems that can be constructed by virtue of this method. We use spin triangles of the type discussed in Secs. 3.2 and 3.3 as the basic building blocks in order to simplify the analytical description of the exchange profile and the resulting spin-density variation within each ring.

#### 3.5.1 FM triangle of qubits

As a first illustration, we consider the construction of an effective ferromagnetically coupled triangle of *qubits* using only AFM spin-spin couplings. This system requires  $n_\Delta = 3$  triangles with modulated exchange. The signs of the spin density at each site of a spin triangle having the exchange profile in Eq. (3.2) with  $\varphi = \pi/3$  are indicated in Fig. 3.6(a). Here, we show the signs of the spin density for the ground state  $|\uparrow(\varphi)\rangle$  of the spin triangle, but one can equally well consider the spin density for  $|\downarrow(\varphi)\rangle$ . In the latter case, all spin-density signs would simply be reversed. According to Eq. (3.11), it is the product of the spin densities at the sites involved in the spin-spin coupling between a pair of triangles that determines the sign of the effective exchange, which is independent of the pseudospin space ( $\uparrow$  or  $\downarrow$ ) chosen for the individual qubits (provided that the same

(a)



(b)

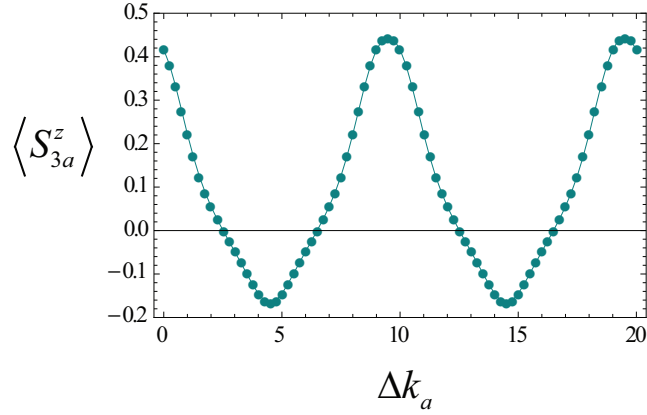


Figure 3.5: (a) Effective exchange and (b) spin-density variation at site  $3a$  for the state  $|\uparrow(\Delta k_a)\rangle$ , as a function of domain-wall displacement  $\Delta k_a$  for a pair of coupled  $n_c = 5$  spin rings of the type shown in Fig. 3.4, with  $J_r = 0.1$  and with the exchange profile for each ring given by Eq. (3.12), where  $\bar{J} = 1$ ,  $J/\bar{J} = 0.1$ ,  $w = 2$ , and  $n = 50$ .

space is chosen for all of them). One possibility for achieving FM effective exchange between two qubits is to couple a site labeled “2” in one triangle to a site labeled “1” in another triangle [Fig. 3.6(b)] so that the product of the spin-density values at the sites involved in each intertriangle spin-spin interaction is negative. The effective exchange for this case is given by Eq. (3.9). Since all three rings are of the type shown in Fig. 3.6(a),  $\varphi_a = \varphi_b = \varphi_c = \pi/3$ , and the effective exchange between each pair of rings is  $J_{\text{eff}}^{21}(J_r, \frac{\pi}{3}, \frac{\pi}{3}) = -2J_r/9$ . For  $J_r > 0$ , this results in a triangle of qubits with uniform FM effective exchange.

### 3.5.2 Dimerized Heisenberg triangle ring with domain wall

More complex systems of exchange-coupled qubits can also be constructed using the method discussed in the present work. In particular, it is possible to create a dimerized AFM Heisenberg ring of qubits containing a domain wall with spin triangles. Here, we show how this is possible using the domain-wall configurations and intertriangle couplings for  $n_\Delta = 9$  triangles (Fig. 3.7). The extreme case of a single isolated qubit and strongly coupled dimers is illustrated in Fig. 3.7(a). The basic spin-triangle building block for this case is shown, with sites of zero and positive spin density for the state  $|\uparrow(\varphi)\rangle$  indicated. The coupling between each pair of triangles  $a$  and  $b$  is given by  $H'_{31} = J_r \mathbf{S}_{3a} \cdot \mathbf{S}_{1b}$ , which leads to the effective exchange Hamiltonian in Eq. (3.7) within the space spanned by states (3.6), where

$$J_{\text{eff}}(J_r, \varphi_a, \varphi_b) = J_{\text{eff}}^{31}(J_r, \varphi_a, \varphi_b) = \frac{J_r}{9} (1 + 2 \cos \varphi_a) (1 - \cos \varphi_b + \sqrt{3} \sin \varphi_b). \quad (3.14)$$

The  $n_\Delta = 9$  qubit system with dimerized effective exchange and a domain wall is created using triangles with domain wall phases that alternate between  $\varphi_1 = 0 + \Delta\varphi$  and  $\varphi_2 = 2\pi/3 - \Delta\varphi$ , except where  $\varphi_1$  appears twice in a row, which creates a domain wall in the *effective* exchange profile. Figure 3.7(a) shows the  $n_\Delta = 9$  triangle ring for  $\Delta\varphi = 0$ . By setting  $\Delta\varphi = \pi/3$ , uniform AFM exchange can be achieved between the qubits. This case is depicted in Fig. 3.7(b), along with the basic spin-triangle building block and the spin-density signs associated with the exchange profile of the triangle. We note here that, due to the asymmetry of the exchange within the triangle at the domain wall relative to its neighboring triangles, the two effective AFM couplings between the isolated qubit and each of its neighboring dimers do not increase in an identical way as  $\Delta\varphi$  is

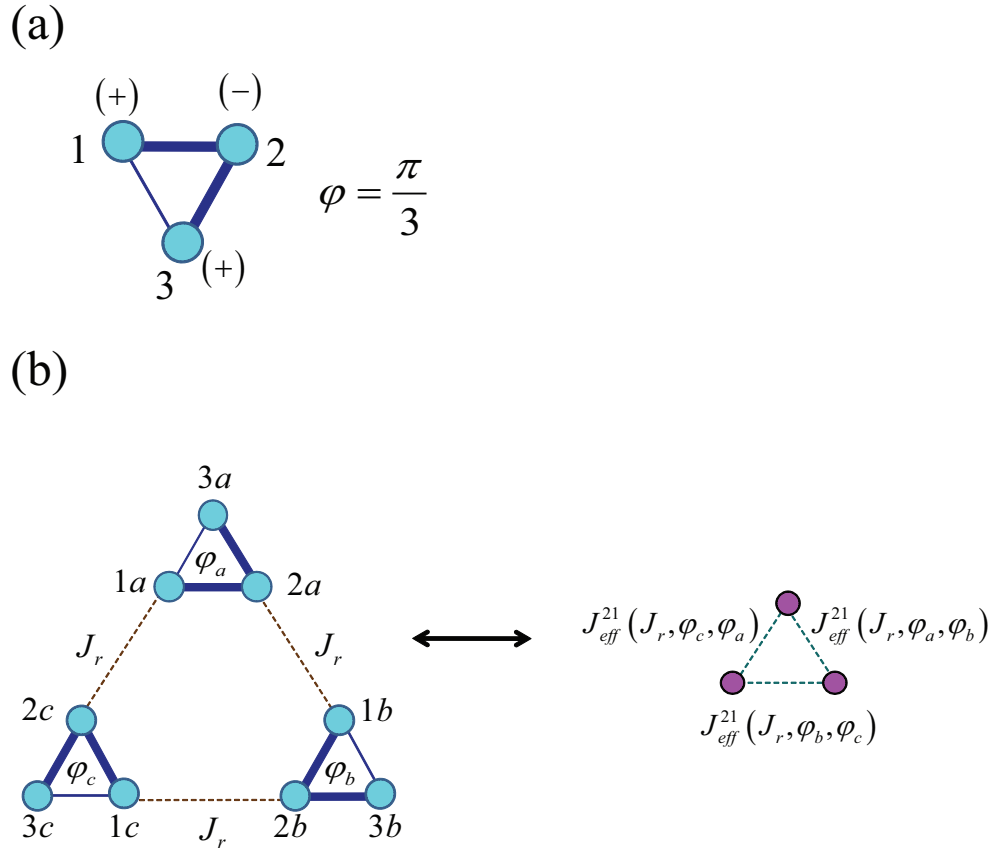


Figure 3.6: (a) Signs of spin density for the ground state  $|\uparrow(\varphi)\rangle$  of a spin triangle having the exchange profile given in Eq. (3.2) with  $\varphi = \pi/3$ . (b) Possible coupling configuration for three spin triangles of the type in a which gives rise to an effective uniform FM qubit triangle (illustrated on the right). Here,  $\varphi_a = \varphi_b = \varphi_c = \pi/3$ .

varied from 0 to  $\pi/3$ . Nevertheless, both couplings increase monotonically to their identical values at  $\Delta\varphi = \pi/3$ .

### 3.5.3 Effective spin-1 chain

We now demonstrate a possible construction of an effective spin-1 AFM Heisenberg chain. In general, a spin-1 chain can be formed from spin- $\frac{1}{2}$  objects with alternating FM and AFM exchange, in the limit where the FM exchange tends to infinity [173]. Using the method discussed in the present work, a spin-1 chain can be approximated by a chain of coupled triangle qubits in which the domain-wall configurations produce alternating FM and AFM exchange [Fig. 3.8(a)]. In order to determine a suitable set of domain-wall phases  $\{\varphi_a, \varphi_b\}$  we let the effective exchange function alternate between  $J_{\text{eff}}^{33}$  [Eq. (3.8)] and  $J_{\text{eff}}^{21}$  [Eq. (3.9)] and assume  $J_{\text{eff}}^{33}(J_r^{33}, \varphi_a, \varphi_b) < 0$  and  $J_{\text{eff}}^{21}(J_r^{21}, \varphi_b, \varphi_a) > 0$ . Assuming all spin-spin couplings are AFM, this leads to the conditions  $(1 + 2\cos\varphi_a)(1 + 2\cos\varphi_b) < 0$  and  $(\cos\varphi_b - 1 + \sqrt{3}\sin\varphi_b)(\cos\varphi_a - 1 - \sqrt{3}\sin\varphi_a) > 0$ . A set of domain-wall phases which satisfies these inequalities is  $\{\varphi_a = \frac{\pi}{3}, \varphi_b = \pi\}$ , which leads to  $J_{\text{eff}}^{33}(J_r^{33}, \frac{\pi}{3}, \pi) = -2J_r^{33}/9$  and  $J_{\text{eff}}^{21}(J_r^{21}, \pi, \frac{\pi}{3}) = 4J_r^{21}/9$ . With  $J_r^{33} > 0$  and  $J_r^{21} > 0$ , the chosen domain-wall phases produce the desired alternating FM and AFM effective exchange. In order for this system to closely approximate a spin-1 chain, one also requires the ratio  $|J_{\text{eff}}^{33}/J_{\text{eff}}^{21}| = J_r^{33}/2J_r^{21}$  to be large while ensuring that both  $J_r^{33}$  and  $J_r^{21}$  remain much smaller than the gap  $\Delta$ , which is proportional to the triangle modulation amplitude  $\tilde{J}_1$ . A schematic of the constructed system is shown in Fig. 3.8(b). Note that the variation in the spin density within the basic triangle building blocks is of the same form as that shown in Fig. 3.7(b).

To explore the properties of the approximate spin-1 chain constructed here, the Hamiltonian for a  $n_\Delta = 4$  triangle chain with  $\tilde{J}_0 = 10$ ,  $\tilde{J}_1 = 8$ ,  $\varphi_a = \pi/3$ ,  $\varphi_b = \pi$ ,  $J_r^{33} = 1$ ,  $0.05 \leq J_r^{21} \leq 0.5$ , and periodic boundary conditions was diagonalized using the Lanczos method [150]. Figure 3.8(c) shows the gap above the ground state,  $E_{\text{gap}}$ , as a function of the effective exchange ratio  $J_{\text{eff}}^{21}/J_{\text{eff}}^{33}$ . Note that a finite energy gap above the nondegenerate ground state is present for this spin-triangle qubit chain for all values of  $J_{\text{eff}}^{21}/J_{\text{eff}}^{33}$  shown. This finding agrees qualitatively with that expected for a spin-1 chain from Haldane's conjecture [13, 14], which suggests that an AFM Heisenberg integer spin chain possesses a finite gap above the ground state. The lowest gap is well approximated by

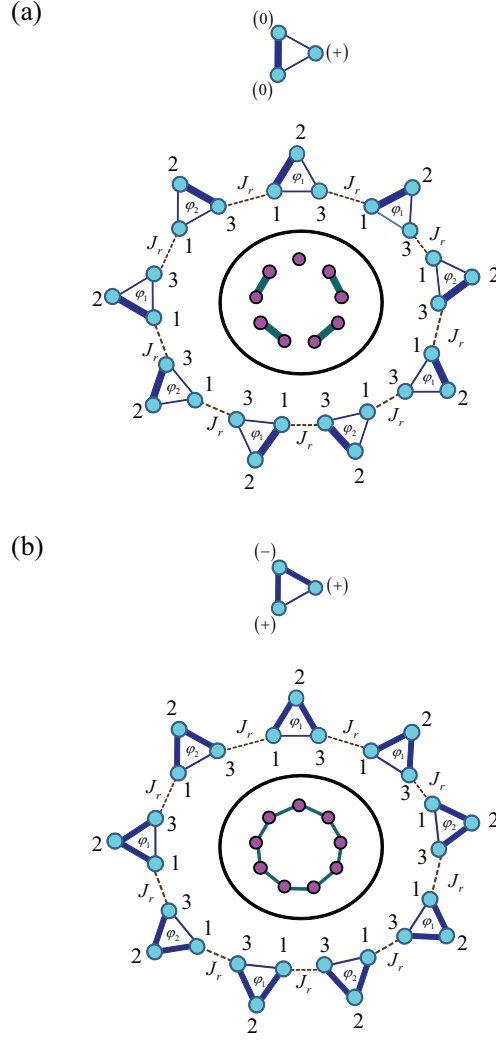


Figure 3.7: Effective AFM Heisenberg rings of  $n_{\Delta} = 9$  spin-triangle qubits with variable dimerization and a domain wall. The effective exchange between each pair of triangles is given by Eq. (3.14). (a) Basic spin-triangle building block, indicating zero and positive spin-density values within each qubit for the state  $|\uparrow(\varphi)\rangle$ , and constructed ring of coupled triangles giving rise to a single isolated qubit and strongly coupled dimers. Here,  $\varphi_1 = 0$  and  $\varphi_2 = 2\pi/3$ . (b) Basic spin-triangle building block, indicating positive and negative spin-density values within each qubit for the state  $|\uparrow(\varphi)\rangle$ , and constructed ring of coupled triangles giving rise to a uniform Heisenberg ring of qubits. For this case, all domain-wall phases are equal:  $\varphi_1 = \varphi_2 = \pi/3$ . Illustrations of the effective qubit systems for (a) and (b) are shown within the rings of triangles.

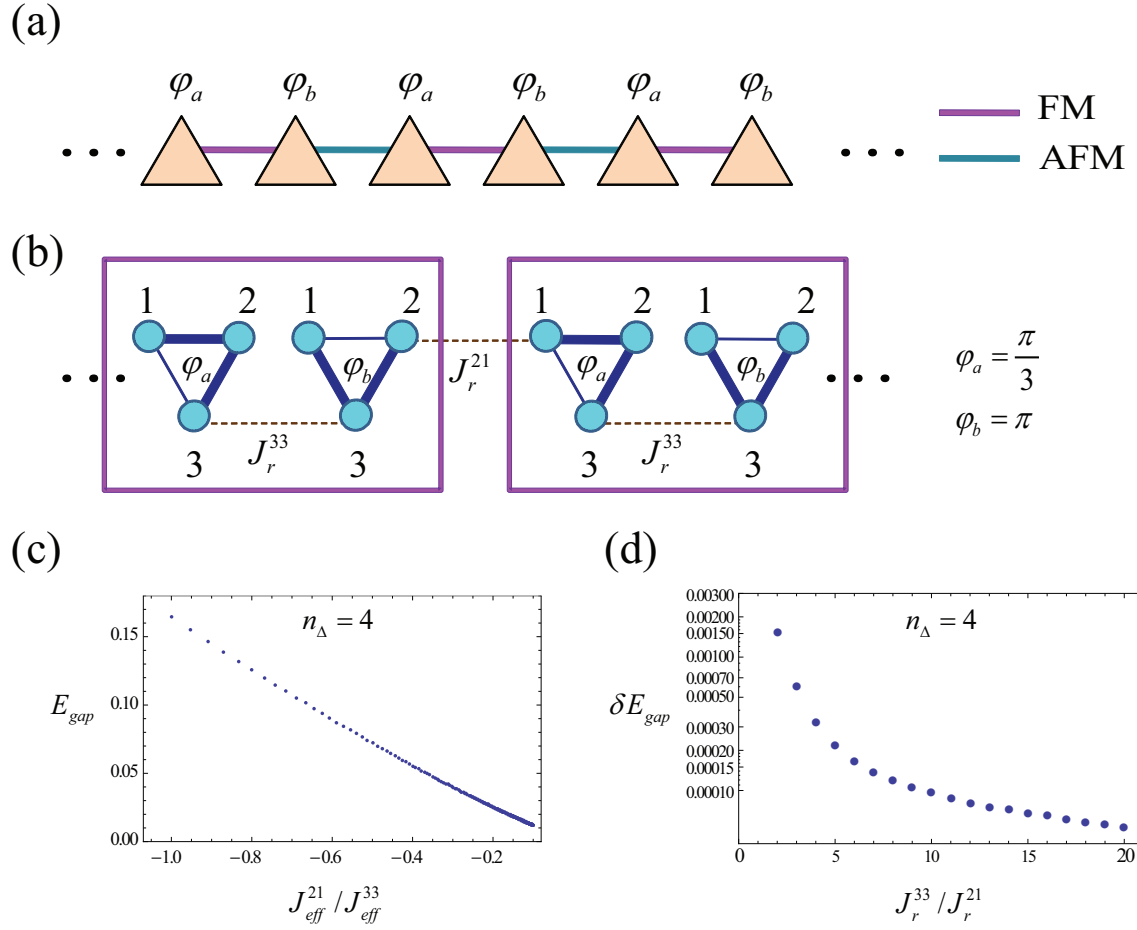


Figure 3.8: Effective spin-1 chain constructed from spin-triangle qubits via tailoring of the effective exchange by domain walls. (a) Required effective system for a chain of coupled triangles, consisting of alternating domain-wall phases  $\varphi_a$  and  $\varphi_b$  which produce alternating FM and AFM exchange in order to approximate a spin-1 chain. (b) Schematic of one possible solution for domain-wall configurations and intertriangle spin-spin coupling constants used to construct the effective spin-1 chain. The pairs of coupled triangles that act effectively as spin-1 objects are indicated by rectangles. (c) Lowest energy gap  $E_{\text{gap}}$  as a function of the effective exchange ratio  $J_{\text{eff}}^{21}/J_{\text{eff}}^{33}$  for a  $n_\Delta = 4$  triangle chain of the type shown in (b) with  $\tilde{J}_0 = 10$ ,  $\tilde{J}_1 = 8$ ,  $J_r^{33} = 1$ ,  $0.05 \leq J_r^{21} \leq 0.5$ , and periodic boundary conditions. (d) Difference  $\delta E_{\text{gap}}$  between the value of the lowest energy gap for the full 12-spin system and that calculated by diagonalizing the effective Hamiltonian in Eq. (3.15), as a function of the ratio  $J_r^{33}/J_r^{21}$ .

its value obtained from diagonalizing the effective Hamiltonian

$$H_{\Delta}^{\text{eff}} = -\frac{3n_{\Delta}}{4} (\tilde{J}_0 + \tilde{J}_1) \mathbf{1} + \sum_{m=1}^{n_{\Delta}/2} \left[ J_{\text{eff}}^{33}(J_r^{33}, \varphi_a, \varphi_b) \mathbf{S}_{2m-1}^{\Delta} \cdot \mathbf{S}_{2m}^{\Delta} + J_{\text{eff}}^{21}(J_r^{21}, \varphi_b, \varphi_a) \mathbf{S}_{2m}^{\Delta} \cdot \mathbf{S}_{2m+1}^{\Delta} \right] \quad (3.15)$$

with  $n_{\Delta} = 4$ , where the assumed periodic boundary conditions imply that  $m \pm n_{\Delta} \equiv m$ . The error [Fig. 3.8(d)] is seen to decrease rapidly with the increasing ratio  $J_r^{33}/J_r^{21}$  (corresponding to more weakly coupled effective spin-1 objects), and its relatively small value for all values of  $J_r^{33}/J_r^{21}$  shown indicates that the approximation of the four-triangle (12-spin) system with AFM spin-spin couplings by four qubits coupled via the appropriate effective exchange interactions remains valid.

### 3.6 PHYSICAL IMPLEMENTATION

In order to experimentally verify the effective exchange effects derived in the present work and attempt to construct spin systems such as those described in Sec. 3.5, it is necessary to find physical realizations of AFM Heisenberg spin rings with the appropriate exchange profiles. Here, we describe a possible implementation of the effective spin-1 chain described in Sec. 3.5.3 which involves an array of quantum dots, each containing a single electron. In the absence of external magnetic fields, AFM exchange interactions between electron spins in neighboring quantum dots are favored [72]. This suggests a potential advantage of the method discussed in the present work, since FM exchange between multi-spin qubits can be achieved using only AFM spin-spin couplings, without the additional magnetic fields that are required for FM coupling of single-electron-spin qubits in quantum dots. Another distinction between electron-spin qubits in quantum dots and domain-wall qubits arises in the context of a material in which spin-orbit coupling is present. Within a quantum dot array fabricated from such a material, the movement of the domain wall required to tailor the effective exchange by translating the spin density can in principle occur with negligible movement of the electrons contained in the quantum dots. As a result, the spin density can be transported without coupling to its spatial motion, which is not possible for the individual electrons themselves due to the spin-orbit interaction.

Figure 3.9(a) shows a configuration of spin triangles, which is modified relative to that shown in Fig. 3.8(b) but retains the alternating FM and AFM effective exchange interactions required to construct the spin-1 chain from the triangle qubits, as can be deduced from the spin-density signs. The quantum dot array for realizing the effective spin-1 chain is illustrated in Fig. 3.9(b). In this system, the required variation in the AFM electron-spin-exchange strengths can be achieved via the relative differences in the interdot separations. The creation of precisely controlled arrays of Ge/Si quantum dots (Fig. 3.10) has also been experimentally demonstrated [160], which in principle allows for the implementation of spin systems with AFM spin-spin exchange couplings of varying strengths.

Molecular magnets provide another potential means of realizing some of the systems discussed in the present work [164, 174]. In these systems, which often can be described by nearest-neighbor AFM Heisenberg exchange Hamiltonians, it is possible to synthesize exchange interaction strengths to desired values. Additionally, it has recently been shown [174] that the coupling of a uniform external electric field to the chiral degree of freedom that exists for the spin triangle  $\text{Cu}_3$  can modulate the exchange in a form equivalent to the exchange profile in Eq. (3.2).

The method of tailoring effective exchange interactions presented here may be of interest for quantum information processing, as it allows for controllable coupling between qubits that can additionally be converted to flying spin qubits by moving the domain walls, allowing for high-fidelity transport, and that can also be localized or delocalized by changing the dimerization strength of the exchange profile [130]. One possible scheme for controllably coupling domain-wall qubits within very large dimerized AFM Heisenberg rings of spins interacting over a relatively small region may be imagined as follows: moving the qubits as far apart as possible from the interaction region within their respective rings, and subsequently increasing (decreasing) the dimerization strength, results in smaller (larger) spin density in the region of interaction. Thus, when the spin density is delocalized, the effective coupling is “on,” while localization of the spin density effectively turns the coupling “off” due to the approximately zero spin density within the interaction region. The possibility of carrying out quantum entangling operations between domain-wall qubits which can give rise to universal quantum computing is the subject of current and future studies.

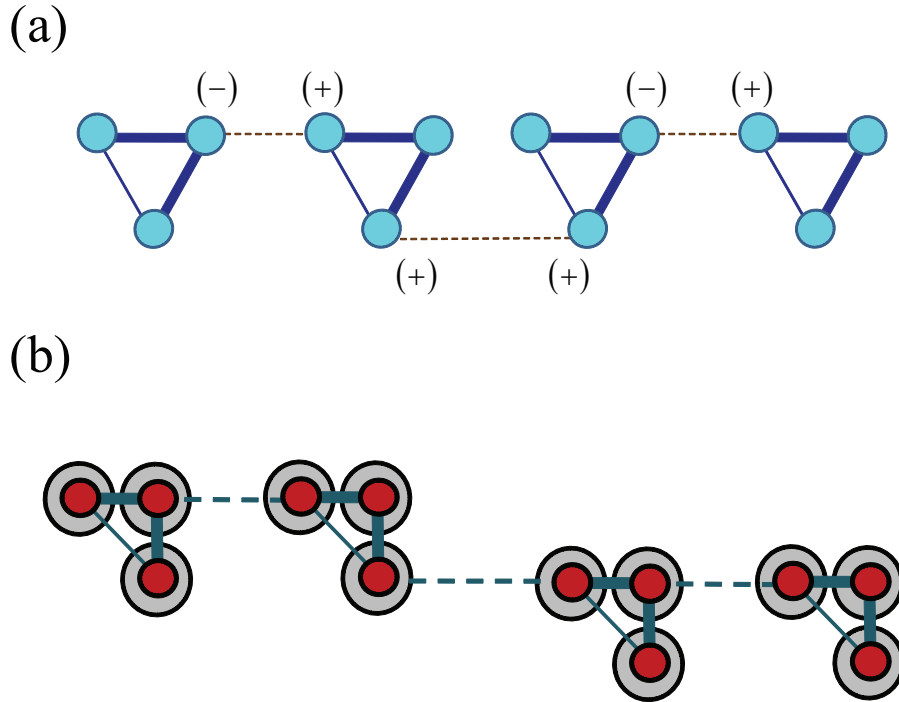


Figure 3.9: Possible physical realization of effective spin-1 chain. (a) Schematic diagram showing a coupling configuration for spin triangles which gives rise to alternating FM and AFM effective exchange. (b) Array of single-electron quantum dots for producing exchange coupling of the form shown in (a) in order to construct a spin-1 chain.

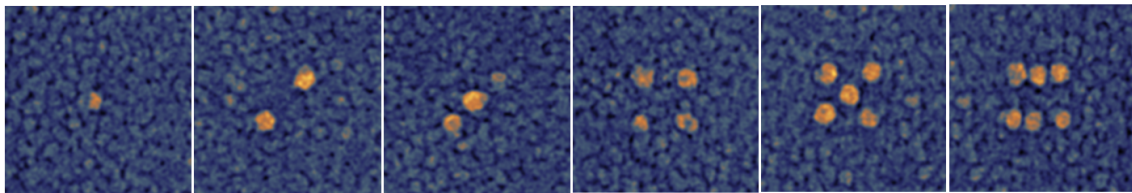


Figure 3.10: Arrays of Ge/Si quantum dots in configurations resembling dice faces. Unpublished result from D. Yang, C. Petz, J. Levy, and J. Floro.

### 3.7 CONCLUSION

We have demonstrated that the effective exchange between qubits encoded in the ground states of dimerized AFM Heisenberg spin rings containing domain walls may be tailored via the spin-spin-exchange variation within the rings. This method is based on the principle that the effective exchange originates from the spin-density distributions of the domain-wall qubits. By employing this method, we have shown that domain-wall qubits may be controllably coupled and that these qubits can serve as the building blocks of a wide variety of designer quantum materials. Finally, we have suggested a possible scheme for realizing an effective spin-1 chain based on an array of single-electron quantum dots.

## 4.0 RASHBA SPIN-ORBIT INTERACTION IN QUANTUM WIRES

One-dimensional and quasi-one-dimensional electronic systems such as quantum wires are particularly promising for the controlled manipulation of single spins via the spin-orbit interaction [95]. In particular, the strength of Rashba-type spin-orbit coupling can be controlled via electric fields produced by externally applied voltages and potentials built into tailored nanostructures. This chapter therefore explores aspects of Rashba spin-orbit coupling in quantum wires that are relevant for this thesis. We first describe basic spectral features of the continuum Rashba spin-orbit Hamiltonian in one dimension. The following section presents calculations we have performed in order to study some implications of the interplay between spin-orbit coupling and a magnetic field for the electronic energy subbands and zero-temperature ballistic conductance of quasi-one-dimensional quantum wires. In the last section of the chapter, a tight-binding model for Rashba spin-orbit coupling equivalent to the continuum model is discussed. An extension of this model to the case of spatially-varying spin-orbit coupling forms the basis for the analysis of the “spin-orbit superlattice quantum wires” we present in Ch. 5.

### 4.1 CONTINUUM MODEL

The three-dimensional motion of electrons in solids can be spatially confined along one or more directions using potential wells produced by artificial structures, effectively reducing the dimensions of the system in which the electrons are allowed to move. The reduced dimensionality arises because the spatial confinement results in quantization of the three-dimensional electronic energy bands such that *subbands* describing motion in the effective lower-dimensional systems are produced [175]. For example, a potential well along one of the three spatial directions can be formed

at the interface between the two distinct materials of a heterostructure. Each of the quantized levels produced by the confinement potential splits into subbands that correspond to states in which electrons move in two dimensions. For typical heterostructures, the confinement is strong enough such that the electrons exist only in a thin (10 nm) layer at the interface and the density of electrons is small enough such that only one two-dimensional subband is occupied [176]. Further confinement of this effective two-dimensional electron system along one direction, referred to as lateral confinement, results in a quantum wire. In this system, the subband spectrum consists of states describing one-dimensional electronic motion. If multiple subbands are occupied with electrons, the system is referred to as *quasi*-one-dimensional, while the case in which only a single one-dimensional subband is occupied can be regarded as purely one-dimensional. The extreme limit of confinement in all three spatial dimensions produces a quantum dot, which can therefore be thought of as a “zero-dimensional” system.

The properties of spatially uniform Rashba spin-orbit coupling in quantum wires have been widely investigated [95, 103, 104, 105, 106, 107, 108, 109, 110, 111, 112, 113, 114]. Basic features of this class of systems can be seen by considering a single-subband continuum model describing electrons which move in a one-dimensional quantum wire lying in the  $x - y$  plane, where the direction of propagation within the wire is chosen to be parallel to the  $y$  axis. Spin-orbit coupling of the Rashba form [28, 29] is assumed to be present due to a net potential gradient along the  $z$  axis. As discussed in Sec. 1.3, such a potential gradient can be produced across the interface of a heterostructure. The Hamiltonian describing this system can be written as [105, 107]

$$H_{1D} = H_0 + H_{so}, \quad (4.1)$$

where

$$H_0 = \frac{\hbar^2 k_y^2}{2m^*}, \quad (4.2)$$

$$H_{so} = -\alpha k_y \sigma_x. \quad (4.3)$$

Here,  $H_0$  is simply the Hamiltonian for a free particle in one dimension and gives a single parabolic energy subband that is two-fold degenerate due to the two possible components of the electron spin [Fig. 4.1(a)]. The spin-orbit term  $H_{so}$  describes an effective magnetic field of magnitude proportional to  $\alpha k_y$  and directed along the  $x$  axis, perpendicular to the propagation ( $y$ ) direction.

We can therefore choose the representation consisting of the eigenstates of  $\sigma_x$ , which correspond to the spin components along the effective magnetic field. Noting that  $[H_{1D}, k_y] = 0$  in order to replace the operator  $k_y$  by its eigenvalue and that  $H_0$  is proportional to the identity operator in spin space then yields the eigenvalues of  $H_{1D}$ ,

$$E_{\pm} = \frac{\hbar^2 k_y^2}{2m^*} \pm \alpha k_y. \quad (4.4)$$

Eq. (4.4) describes parabolic subbands associated with the two components of spin along the  $x$  axis, with  $E_-$  ( $E_+$ ) corresponding to the eigenstate  $|\uparrow\rangle_x$  ( $|\downarrow\rangle_x$ ). These energies can also be written in the alternative form [105, 107]

$$E_{\pm} = \frac{\hbar^2}{2m^*} (k_y \pm k_{so})^2 - \Delta_{so}, \quad (4.5)$$

where the characteristic spin-orbit wavevector  $k_{so} \equiv m^* \alpha / \hbar^2$  is proportional to the Rashba spin-orbit coupling strength  $\alpha$  and  $\Delta_{so} \equiv \hbar^2 k_{so}^2 / 2m^* = m^* \alpha^2 / 2\hbar^2$  describes the uniform (i.e., same for all  $k_y$ ) shift of the free-electron energy subbands along the energy axis due to the spin-orbit interaction. The characteristic length scale associated with the spin-orbit interaction is given by  $l_{so} = 1/2k_{so} = \hbar^2 / 2m^* \alpha$ . Eq. (4.5) indicates that a spin-splitting of the initially degenerate free-electron energy subbands occurs in opposite directions along the momentum axis. This splitting of the subbands is illustrated in Fig. 4.1(b) and reflects the momentum dependence of the effective magnetic field associated with spin-orbit coupling. The magnitude of the energy splitting also depends on  $k_y$  and is seen from Eq. (4.4) to be  $E_+ - E_- = 2\alpha k_y$ . In particular, this splitting is zero at  $k_y = 0$ .

## 4.2 INTERPLAY OF SPIN-ORBIT AND ZEEMAN INTERACTIONS

The splitting of energies for states of different spin can also arise due to the Zeeman interaction [Eq. (1.18)] that describes the coupling of spin to external magnetic fields. Unlike the splitting due to the effective magnetic field associated with the Rashba spin-orbit interaction, which shifts the subbands for different spin components along the momentum axis (Fig. 4.1), the spin splitting due to an external magnetic field is independent of the momentum and shifts the subbands along the

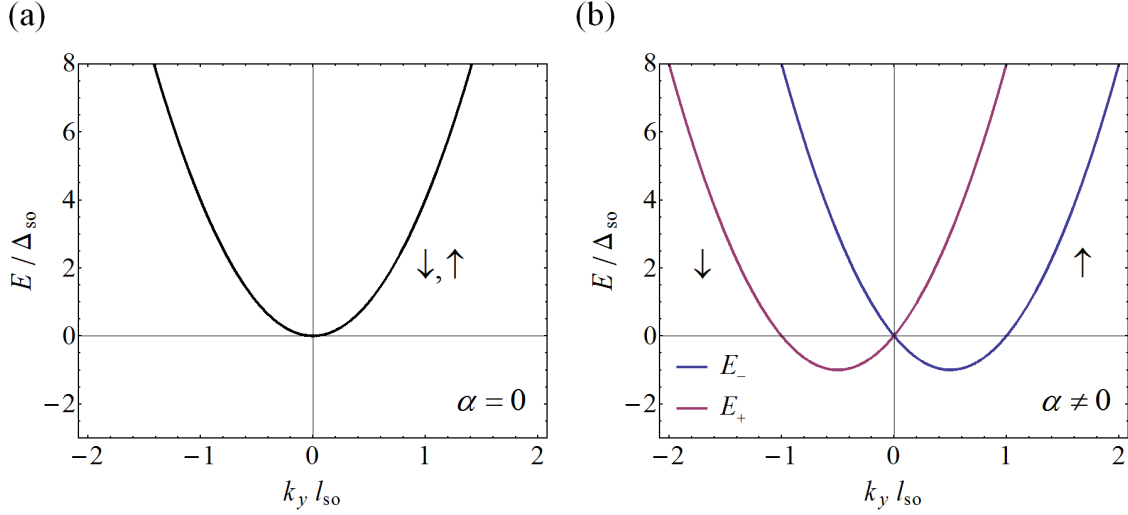


Figure 4.1: One-dimensional electronic energy subbands for a quantum wire (a) without spin-orbit coupling and (b) in the presence of Rashba spin-orbit coupling. Arrows indicate the spin component along the  $x$  axis.

energy axis [107]. In the presence of both Rashba spin-orbit and Zeeman interactions, new types of features can arise in the subband spectra of quantum wires. Some of these features involve multiple subbands, so we now consider *quasi*-one-dimensional quantum wires.

One spectral feature that appears due to the combined effects of the spin-orbit and Zeeman interactions is a so-called “spin-orbit gap,” which refers to an energy gap between subbands that occurs at  $k_y = 0$  (using the coordinate system of the previous section for the quantum wire). It has been shown theoretically that this gap can be produced when the external and spin-orbit fields are in perpendicular directions [106]. In order to explore further the parameter space in which a spin-orbit gap occurs, we follow the approach of Refs. 108 and 109 to calculate the quasi-one-dimensional electronic energy subbands for a quantum wire as a function of both Rashba spin-orbit coupling of strength  $\alpha$  and an external magnetic field of magnitude  $B$  applied perpendicular to the plane containing the wire. The total Hamiltonian describing this system is given by

$$H_{\text{Q1D}} = H'_0 + H'_{so}, \quad (4.6)$$

where

$$H'_0 = \frac{\hbar^2}{2m^*} \left[ k_x^2 + \left( k_y + \frac{eB}{\hbar} x \right)^2 \right] + \frac{1}{2} m^* \omega_0^2 x^2 + \frac{1}{2} g\mu_B B \sigma_z, \quad (4.7)$$

$$H'_{\text{so}} = \alpha \left[ \left( k_y + \frac{eB}{\hbar} x \right) \sigma_x - k_x \sigma_y \right]. \quad (4.8)$$

Here, the quasi-one-dimensional description of the quantum wire is incorporated via the second term in Eq. (4.7), which is a potential describing lateral confinement along the  $x$  direction. The momentum  $k_x$  along this direction therefore also appears in  $H_{\text{Q1D}}$ . The lateral confinement is harmonic with frequency  $\omega_0$  and has an associated characteristic length scale  $l_0 \equiv \sqrt{\hbar/m^*\omega_0}$ . In addition to its presence in the Zeeman term, the external magnetic field  $\mathbf{B} = B\hat{z}$  also appears in the Hamiltonian through a vector potential  $\mathbf{A}$  that modifies the momentum. The choice of this vector potential is not unique, since different choices for  $\mathbf{A}$  can produce the same magnetic field  $\mathbf{B}$  via  $\mathbf{B} = \nabla \times \mathbf{A}$ . Here, we choose the Landau gauge  $\mathbf{A} = (0, Bx, 0)$  [176].

In order to calculate the spectrum of  $H_{\text{Q1D}}$ ,  $H'_{\text{so}}$  can be treated as a perturbation to  $H'_0$ . In what follows, we outline how this calculation proceeds. The time-independent Schrödinger equation (TISE) can be written as

$$H_{\text{Q1D}}\Psi(x, y) = E\Psi(x, y), \quad (4.9)$$

where the two-dimensional wavefunction  $\Psi(x, y) = \phi(x) e^{ik_y y}$  is expressed as a product of a function  $\phi(x)$  in the confinement ( $x$ ) direction and plane waves  $e^{ik_y y}$  in the propagation ( $y$ ) direction for the wire. By substituting this form for the wavefunction into Eq. (4.9) and using the fact that  $[H_{\text{Q1D}}, k_y] = 0$  to replace the operator  $k_y$  with its eigenvalue, it can be shown [176, 108] that the eigenvalues of  $H'_0$  are given by

$$E_{n\sigma}^{(0)} = \hbar\omega \left( n + \frac{1}{2} \right) + \frac{\hbar^2}{2m^*} \frac{\omega_0^2}{\omega^2} k_y^2 + \sigma \frac{g\mu_B}{2} B, \quad (4.10)$$

and the corresponding eigenstates for the  $x$  direction are

$$\phi_{n\sigma}(x) = \frac{1}{\sqrt{b}} \frac{\pi^{-1/4}}{\sqrt{2^n n!}} H_n \left( \frac{x - \bar{x}_0}{b} \right) e^{-(x - \bar{x}_0)^2 / 2b^2} \chi_\sigma. \quad (4.11)$$

In Eqs. (4.10) and (4.11),  $\omega = \sqrt{\omega_c^2 + \omega_0^2}$  where  $\omega_c = eB/m^*$  is the cyclotron frequency,  $b = \sqrt{\hbar/m^* \omega}$ ,  $\bar{x}_0 = (\omega_c/\omega_0)^2 (-\hbar k_y/eB)$ ,  $H_n(x)$  is the  $n$ th-degree Hermite polynomial, and  $\chi_\sigma$  is the spinor corresponding to the spin component  $\sigma = \pm 1$  along the  $z$  direction such that

$$\chi_{+1} = \begin{pmatrix} 1 \\ 0 \end{pmatrix}, \chi_{-1} = \begin{pmatrix} 0 \\ 1 \end{pmatrix}. \quad (4.12)$$

From the forms of Eqs. (4.10) and (4.11), it is seen that the spin-independent parts of the energies  $E_{n\sigma}^{(0)}$  and states  $\phi_{n\sigma}(x)$  essentially describe a harmonic oscillator with characteristic frequency  $\omega$  and lengthscale  $b$  that is shifted along the  $x$  axis by  $\bar{x}_0$ . Expanding  $\phi(x)$  in terms of the eigenstates of  $H'_0$  as

$$\phi(x) = \sum_{n,\sigma} a_{n,\sigma} \phi_{n\sigma}(x) \quad (4.13)$$

(where  $\sum_{n,\sigma} |a_{n,\sigma}|^2 = 1$ ) and dividing by  $\hbar\omega_0$  to remove dimensions leads to the following set of equations which are equivalent to the TISE [Eq. (4.9)]:

$$\sum_{m,\sigma'} \frac{(H'_{so})_{nm}^{\sigma\sigma'}}{\hbar\omega_0} a_{m\sigma'} = E a_{n\sigma}. \quad (4.14)$$

Here,  $(H'_{so})_{nm}^{\sigma\sigma'}$  denotes the matrix elements of the spin-orbit term [Eq. (4.8)] in the basis of the states  $\phi_{n\sigma}(x)$  in Eq. (4.11). We can write these matrix elements as

$$\frac{(H_{so})_{nm}^{\sigma\sigma'}}{\hbar\omega_0} = \frac{E_{n\sigma}^{(0)}}{\hbar\omega_0} \delta_{nm} \delta_{\sigma\sigma'} + \left( \frac{H_{nm}^{\sigma\sigma'}}{\hbar\omega_0} \delta_{nm} + \frac{H_{n,n+1}^{\sigma\sigma'}}{\hbar\omega_0} \delta_{n,m-1} + \frac{H_{n,n-1}^{\sigma\sigma'}}{\hbar\omega_0} \delta_{n,m+1} \right) (1 - \delta_{\sigma\sigma'}) \quad (4.15)$$

where

$$\frac{E_{n\sigma}^{(0)}}{\hbar\omega_0} = \sqrt{1 + \omega_r^2} \left( n + \frac{1}{2} \right) + \frac{q^2}{2(1 + \omega_r^2)} + \sigma \frac{g}{4} m \omega_r, \quad (4.16)$$

$$\frac{H_{nm}^{\sigma\sigma'}}{\hbar\omega_0} = \frac{l_r q}{2(1 + \omega_r^2)}, \quad (4.17)$$

$$\frac{H_{n,n+1}^{\sigma\sigma'}}{\hbar\omega_0} = \frac{l_r}{2} \left[ \frac{\omega_r + \sigma \sqrt{1 + \omega_r^2}}{(1 + \omega_r^2)^{1/4}} \right] \sqrt{\frac{n+1}{2}}, \quad (4.18)$$

$$\frac{H_{n,n-1}^{\sigma\sigma'}}{\hbar\omega_0} = \frac{l_r}{2} \left[ \frac{\omega_r - \sigma \sqrt{1 + \omega_r^2}}{(1 + \omega_r^2)^{1/4}} \right] \sqrt{\frac{n}{2}}. \quad (4.19)$$

In Eqs. (4.16)-(4.19), we have defined the dimensionless magnetic field strength  $\omega_r = \omega_c/\omega_0$ , the dimensionless wavevector  $q = k_y l_0$ , the dimensionless spin-orbit strength  $l_r = l_0/l_{\text{so}}$ , and the dimensionless effective mass  $m_r = m^*/m_e$ . We use the matrix elements  $(H'_{\text{so}})_{nm}^{\sigma\sigma'}$  and choose a maximum value  $n_{\text{max}}$  for  $n$  in order to obtain a  $2n_{\text{max}}$ -dimensional matrix that can be numerically diagonalized (where the factor of 2 is due to the spin degree of freedom).

In order to proceed with the numerical calculation of the subbands, specific parameter values must be chosen. In experiments performed by our research group at the University of Pittsburgh, nanowires with widths  $\lesssim 10$  nm are created at the interface of a heterostructure formed from the two oxides LaAlO<sub>3</sub> and SrTiO<sub>3</sub> [177, 178]. While LaAlO<sub>3</sub> and SrTiO<sub>3</sub> are insulators, the interface between them can be conducting [179] and a transition between the insulating and metallic character of the interface can be induced by controlling the thickness of the LaAlO<sub>3</sub> layer or through applied voltages [180]. In a heterostructure with a particular LaAlO<sub>3</sub> thickness chosen to be just below that at which the insulator-to-metal transition for the entire two-dimensional interface occurs, Cen *et al.* have demonstrated that narrow conducting regions can be formed via a *local* insulator-to-metal transition that is induced at the LaAlO<sub>3</sub>/SrTiO<sub>3</sub> interface by a voltage applied to the surface of LaAlO<sub>3</sub> using an atomic force microscope probe. Using this method, a Hall effect device in which the main conducting channel is 6 nm wide has been created [181]. Adopting parameters relevant to the quantum wires created at the interface of LaAlO<sub>3</sub> /SrTiO<sub>3</sub> systems, we choose  $l_0 = 6$  nm,  $m^* = 1.1m_e$ , and  $g = 2$ . We use  $n_{\text{max}} = 10$  and numerically solve the TISE to obtain the subband spectrum  $E(q)/\hbar\omega_0$  as a function of  $B$  (or  $\omega_r$ ) and  $\alpha$  (or  $l_r$ ). Figures 4.2(a) and 4.2(b) show the lowest few subbands for  $\alpha = 5.3 \times 10^{-12} \text{eV} \cdot \text{m}$  ( $l_r = 1$ ) and  $\alpha = 1.1 \times 10^{-11} \text{eV} \cdot \text{m}$  ( $l_r = 2$ ), respectively, at  $B = 15$  T ( $\omega_r = 0.82$ ). A distinct local maximum appears in the lowest subband for the larger spin-orbit coupling value that produces a spin-orbit gap [Fig. 4.2(b)].

As shown in Ref. [106] and recently demonstrated experimentally for holes in GaAs/AlGaAs quantum wires [113], a spin-orbit gap gives rise to an effect that is observable in measurements of the ballistic conductance of a quantum wire<sup>1</sup>. The ballistic conductance changes in quantized steps as a function of  $B$  and the Fermi energy  $E_F$  (which is directly related to the density of electrons in the wire and typically determines its transport properties). [176, 175]. The quantization of the

---

<sup>1</sup>Here, ballistic conductance refers to the transport of electrons through the quantum wire in the absence of scattering from impurities. This approximation is valid when the width of the wire is smaller than the mean free path of the electron characterizing the distance between scattering events [176].

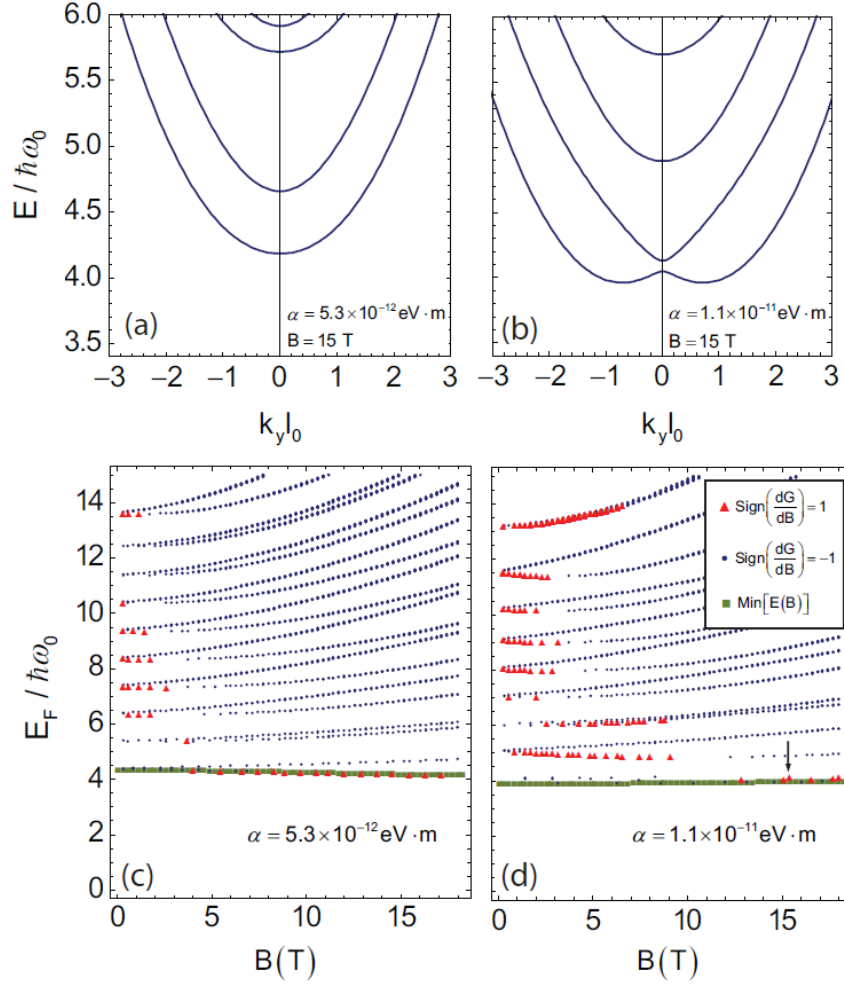


Figure 4.2: (a) Lowest few quasi-one-dimensional electronic energy subbands of a quantum wire for  $\alpha = 5.3 \times 10^{-12} \text{ eV} \cdot \text{m}$  and  $B = 15 \text{ T}$ . (b) Lowest few subbands for  $\alpha = 1.1 \times 10^{-11} \text{ eV} \cdot \text{m}$  and  $B = 15 \text{ T}$ , showing a local maximum in the lowest subband. (c) Plots of points for which  $\text{Sign}(dG/dB) = 1$  (red points) and  $\text{Sign}(dG/dB) = -1$  (blue points) as a function of  $B$  and  $E_F$  for the Rashba spin-orbit coupling strength in (a). The lowest energy minimum of all subbands for each value of  $B$  is also indicated (green points). (d) Same as (c), but for the Rashba spin-orbit coupling strength in (b). The arrow indicates a point at  $B \sim 15 \text{ T}$  which corresponds to a spin-orbit gap.

conductance reflects the fact that the energy spectrum consists of discrete subbands. These subbands give rise to a fixed number of conducting modes at the Fermi energy  $M(E_F)$  that completely determine the conductance  $G$  at zero temperature via the Landauer formula [182, 176],

$$G = \frac{e^2}{h} M(E_F). \quad (4.20)$$

In writing Eq. (4.20), we have assumed for simplicity that the probabilities for transmission of the electrons through the wires are equal to 1 for all conducting modes. Because the ballistic conductance can be given in terms of a fixed number of propagating modes, the quantum wire essentially acts as an “electron waveguide.” The number of conducting modes  $M(E_F)$  can be determined by counting the number of subband local maxima and minima which lie below  $E_F$  in the spectrum [106]. This leads to the following relation for the zero-temperature ballistic conductance of the quantum wire:

$$G(\alpha, B, E_F) = \frac{e^2}{h} \left\{ \sum_{l,i} \theta \left[ E_F - E_{\min,i}^{(l)}(\alpha, B) \right] - \sum_{l,j} \theta \left[ E_F - E_{\max,j}^{(l)}(\alpha, B) \right] \right\}. \quad (4.21)$$

Here,  $E_{\min,i}^{(l)}(\alpha, B)$  and  $E_{\max,j}^{(l)}(\alpha, B)$  denote the energies of the  $i$ th minimum and the  $j$ th maximum, respectively, in the  $l$ th subband of the spectrum for a Rashba spin-orbit coupling strength  $\alpha$  and magnetic field strength  $B$ , and  $\theta$  is the Heaviside unit step function. For a fixed value of  $E_F$ , increasing  $B$  causes the local minima and maxima to shift in energy. According to Eq. (4.21),  $G$  increases by  $e^2/h$  for each  $E_{\min,i}^{(l)}(\alpha, B) < E_F$  and decreases by  $e^2/h$  for each  $E_{\max,j}^{(l)}(\alpha, B) < E_F$ . Therefore, shifts of the local maxima associated with spin-orbit gaps from below  $E_F$  to above  $E_F$  can produce positive jumps in  $G$ . These jumps do not occur in the absence of a spin-orbit gap. In Figs. 4.2(c) and 4.2(d), we plot  $\text{Sign}(dG/dB)$  as a function of  $B$  and  $E_F$  for  $l_r = 1$  and  $l_r = 2$ , respectively. The points for which  $\text{Sign}(dG/dB) = 1$  correspond to positive jumps in  $G$  with increasing  $B$ . Some of these points can be neglected because they coincide with the minima of lowest energy in the spectrum and therefore cannot correspond to maxima associated with spin-orbit gaps. For the smaller value of  $\alpha$  shown [Fig. 4.2(c)], the nontrivial conductance jumps appear at lower magnetic field values. Increasing  $\alpha$  tends to shift the distribution of these points to higher magnetic field strengths, reflecting the fact that larger spin-orbit splittings are able to compete with larger Zeeman splittings in order to produce spin-orbit gaps.

We note that, in experiments performed with the 6 nm Hall effect device created at the interface of a  $\text{LaAlO}_3/\text{SrTiO}_3$  heterostructure, dips in the Hall resistance  $R_H = 1/G$  (which correspond to positive jumps in  $G$ ) have been observed at high magnetic field strengths (15 T and  $-17$  T). These dips are believed to occur due to strong spin-orbit coupling at the interface. While previous work [183, 184] has suggested that this spin-orbit coupling may be of the Rashba type, very recent experimental results obtained for both two-dimensional electron systems [185] and nanowires created by our group provide strong evidence that atomic spin-orbit coupling [186] plays the dominant role in bringing about effects such as the Hall resistance dips observed for  $\text{LaAlO}_3/\text{SrTiO}_3$  systems.

### 4.3 SPATIALLY-VARYING SPIN-ORBIT INTERACTION AND TIGHT-BINDING MODEL

The designer quantum materials we propose in this thesis are based on both uniform and spatially-varying spin-orbit coupling. The consequences of a spatially-modulated spin-orbit interaction have been considered in multiple contexts, including spin-dependent transport [115], spin precession [116], and spin relaxation [129] in quantum wires. The modulation of Rashba spin orbit coupling due to the periodic potential of a one-dimensional superlattice has also been investigated, both fundamentally in terms of the resulting spin-dependent band structure of the superlattice [187] and for its role in a device used to couple conducting states with different definite spin that exist at the edges of an integer quantum Hall system due to a perpendicular magnetic field [188]. In the latter work, the coupling is achieved by matching the wavevector associated with the superlattice periodicity to the difference in the wavevectors of the two conducting states. These studies describe the spatial variation in the spin-orbit coupling using a *continuum* Hamiltonian in which the momentum is a continuous quantity, such as those given in the last two sections [Eqs. (4.3) and (4.8)].

In order to describe the spatially-varying spin-orbit interaction in designer quantum materials based on the “spin-orbit superlattice quantum wires” discussed in Ch. 5, we find it useful to consider a tight-binding Hamiltonian that represents a discretized version of the continuum Hamiltonian  $H_{\text{so}}$  and can be used to obtain an equivalent description of systems with uniform spin-orbit coupling [104, 189]. Recently, such a tight-binding model has also been applied to the description

of spatially-varying spin orbit coupling in a quantum wire [117, 118], where it was shown that a Peierls-like [152] metal-insulator transition can be induced when the wavevector of this modulation approaches twice the electron Fermi wavevector and a band gap appears in the spectrum.

To illustrate features of the tight-binding model for spin-orbit coupling, we show how this model can be obtained for the continuum Hamiltonian  $H_{1D}$  [Eqs. (4.1)-(4.3)] that describes an ideal one-dimensional quantum wire. A tight-binding description can be obtained by discretizing space on a lattice. Setting  $y = na$ , where  $n$  is an integer, effectively represents the wire by a one-dimensional lattice of  $N$  sites with uniform spacing given by the lattice constant  $a$ . A single-band tight-binding model is obtained by using the complete and orthogonal basis  $\{|n, \sigma\rangle\}$  to describe a single electron in this system, where the state  $|n, \sigma\rangle$  describes an electron at site  $n$  with spin  $\sigma$ . This description implies that there is only one electronic orbital state per lattice site, which gives rise to a single band for the  $N$ -site lattice. Assuming that an electron at a particular site moves or “hops” only to nearest-neighbor sites, the kinetic energy term  $H_0$  [Eq. (4.2)] can be expressed as

$$H_0 = -t_0 \sum_{n,\sigma} (|n+1, \sigma\rangle \langle n, \sigma| + |n, \sigma\rangle \langle n+1, \sigma|) \quad (4.22)$$

where the “hopping amplitude”  $t_0 = \hbar^2/2m^*a^2$  represents the kinetic energy associated with hopping of the electron between neighboring lattice sites. This hopping can also be expressed in terms of the fermion creation and annihilation operators, denoted  $c_{n,\sigma}^\dagger$  and  $c_{n,\sigma}$ , respectively. These operators satisfy the fermion anticommutation relations  $\{c_{n,\sigma}, c_{n',\sigma'}^\dagger\} \equiv c_{n,\sigma}c_{n',\sigma'}^\dagger + c_{n',\sigma'}^\dagger c_{n,\sigma} = \delta_{n,n'}\delta_{\sigma,\sigma'}$  and  $\{c_{n,\sigma}, c_{n',\sigma'}\} \equiv c_{n,\sigma}c_{n',\sigma'} + c_{n',\sigma'}c_{n,\sigma} = 0$ . Their action is defined such that  $c_{n,\sigma}^\dagger$  ( $c_{n,\sigma}$ ) creates (annihilates) an electron at site  $n$  with spin  $\sigma$ . In terms of these operators, Eq. (4.22) can be written in the equivalent form

$$H_0 = -t_0 \sum_{n,\sigma} \left( c_{n+1,\sigma}^\dagger c_{n,\sigma} + \text{H.c.} \right),$$

where “H.c.” indicates the Hermitian conjugate of all terms appearing before it.

The tight-binding Hamiltonian for the spin-orbit coupling term  $H_{so} = -\alpha k_y \sigma_x$  [Eq. (4.3)] can be obtained by determining the action of  $H_{so}$  on a general state

$$|\Psi\rangle = \sum_{\sigma} \int dy |y, \sigma\rangle \langle y, \sigma| \Psi\rangle. \quad (4.23)$$

Eq. (4.3) gives

$$\langle y, \sigma | H_{\text{so}} | \Psi \rangle = -\alpha \sum_{\sigma'} (\sigma_x)_{\sigma\sigma'} \int dy' \langle y | k_y | y' \rangle \langle y', \sigma' | \Psi \rangle,$$

where  $(\sigma_x)_{\sigma\sigma'} \equiv \langle \sigma | \sigma_x | \sigma' \rangle$ . Using  $\langle y | k_y | y' \rangle = -i(\partial/\partial y) \delta(y - y')$  then leads to

$$\langle y, \sigma | H_{\text{so}} | \Psi \rangle = i\alpha \sum_{\sigma'} (\sigma_x)_{\sigma\sigma'} \frac{\partial \psi_{\sigma'}(y)}{\partial y}, \quad (4.24)$$

where  $\psi_{\sigma}(y) = \langle y, \sigma | \Psi \rangle$ . In order to obtain the tight-binding model of  $H_{\text{so}}$ , the derivative with respect to the continuous coordinate  $y$  in the above expression must be discretized on the lattice defined by setting  $y = na$ . Here, this discretization is carried out by rewriting  $|\Psi\rangle$  in the discretized basis  $\{|n, \sigma\rangle\}$  as

$$|\Psi\rangle = \sum_{n, \sigma} \psi_{n, \sigma} |n, \sigma\rangle, \quad (4.25)$$

where  $\psi_{n, \sigma} = \langle n, \sigma | \Psi \rangle$ , and using the approximation

$$\frac{\partial \psi_{\sigma}(y)}{\partial y} \approx \frac{\psi_{n+1, \sigma} - \psi_{n-1, \sigma}}{2a}. \quad (4.26)$$

This discrete derivative gives

$$\begin{aligned} \langle n, \sigma | H_{\text{so}} | \Psi \rangle &= i\alpha \sum_{\sigma'} (\sigma_x)_{\sigma\sigma'} \frac{\psi_{n+1, \sigma'} - \psi_{n-1, \sigma'}}{2a}, \\ &= i\frac{\alpha}{2a} \sum_{\sigma'} (\sigma_x)_{\sigma\sigma'} (\langle n+1, \sigma' | \Psi \rangle - \langle n-1, \sigma' | \Psi \rangle), \end{aligned}$$

which is equivalent to

$$H_{\text{so}} |n, \sigma\rangle = -i\frac{\alpha}{2a} \sum_{\sigma'} (\sigma_x)_{\sigma'\sigma} (|n+1, \sigma'\rangle - |n-1, \sigma'\rangle). \quad (4.27)$$

$H_{\text{so}}$  can be expanded in terms of the basis  $\{|n, \sigma\rangle\}$  as

$$H_{\text{so}} = \sum_{n, \sigma} \sum_{n', \sigma'} |n', \sigma'\rangle \langle n', \sigma' | H_{\text{so}} |n, \sigma\rangle \langle n, \sigma|, \quad (4.28)$$

where the matrix element  $\langle n', \sigma' | H_{\text{so}} |n, \sigma\rangle$  is found from Eq. (4.27) and the orthogonality relation  $\langle n', \sigma' | n, \sigma\rangle = \delta_{n', n} \delta_{\sigma', \sigma}$  to be

$$\langle n', \sigma' | H_{\text{so}} |n, \sigma\rangle = -i\frac{\alpha}{2a} (\sigma_x)_{\sigma'\sigma} (\delta_{n', n+1} - \delta_{n', n-1}).$$

Substituting this expression into Eq. (4.28), performing some manipulation of the summation indices, and simplifying yields

$$H_{\text{so}} = -t_{\text{so}} \sum_{n,\sigma,\sigma'} [(i\sigma_x)_{\sigma'\sigma} |n+1, \sigma'\rangle \langle n, \sigma| + (-i\sigma_x)_{\sigma\sigma'} |n, \sigma\rangle \langle n+1, \sigma'|],$$

which is equivalent to

$$H_{\text{so}} = -t_{\text{so}} \sum_{n,\sigma,\sigma'} [c_{n+1,\sigma'}^\dagger (i\sigma_x)_{\sigma'\sigma} c_{n,\sigma} + \text{H.c.}]. \quad (4.29)$$

Here, the hopping amplitude  $t_{\text{so}} \equiv \alpha/2a$ . Eq. (4.29) is the tight-binding model corresponding to the continuum Rashba Hamiltonian in Eq. (4.3). While the kinetic energy term  $H_0$  given above involves a hopping that occurs without changing the spin, the tight-binding model for the spin-orbit interaction [Eq. (4.29)] describes a spin-dependent hopping for which the hopping amplitude is directly proportional to the spin-orbit coupling strength  $\alpha$  and inversely proportional to the lattice constant  $a$ .

We now obtain the spectrum of this tight-binding model by diagonalizing the full Hamiltonian  $H = H_0 + H_{\text{so}}$  for an  $N$ -site lattice with periodic boundary conditions, which are incorporated by assuming  $n \pm N \equiv n$ . Because the spin-orbit coupling is uniform,  $[H, k_y] = 0$ ; i.e.,  $H$  is invariant with respect to translations along the wire ( $y$ ) axis. The periodic boundary conditions determine a finite set of allowed quasimomenta [23], which are given by  $k_y = 2\pi l/Na$  with  $l$  an integer such that  $-N/2 \leq l < N/2$ . The diagonalization can then be carried out using a discrete Fourier transform of the fermion operators defined by

$$\tilde{c}_{l,\sigma} = \frac{1}{\sqrt{N}} \sum_{n=1}^N e^{-i\frac{2\pi}{N}l(n-1)} c_{n,\sigma}. \quad (4.30)$$

and the corresponding expression for  $\tilde{c}_{l,\sigma}^\dagger$ . Figure 4.3 shows the energy bands of the tight-binding Hamiltonian for zero and nonzero  $t_{\text{so}}$ . Without spin-orbit coupling ( $t_{\text{so}} = 0$ ), the spectrum is described by a single tight-binding band that is two-fold degenerate due to spin. This band splits into two bands of opposite spin when uniform spin-orbit coupling is present ( $t_{\text{so}} \neq 0$ ). As in the case of the subbands in the spectrum for the continuum model shown in Fig. 4.1, tight-binding bands of opposite spin are shifted in opposite directions along the quasimomentum axis. The tight-binding

description thus provides an alternative representation of the Rashba spin-orbit interaction in one-dimensional systems and can also be extended to higher dimensions [104, 189]. In Ch. 5, we use a generalized version of this tight-binding model in order to describe a quantum wire with both uniform and spatially-varying spin-orbit interactions in orthogonal directions and show that spin resonance can in principle be achieved without any external magnetic fields in these systems.

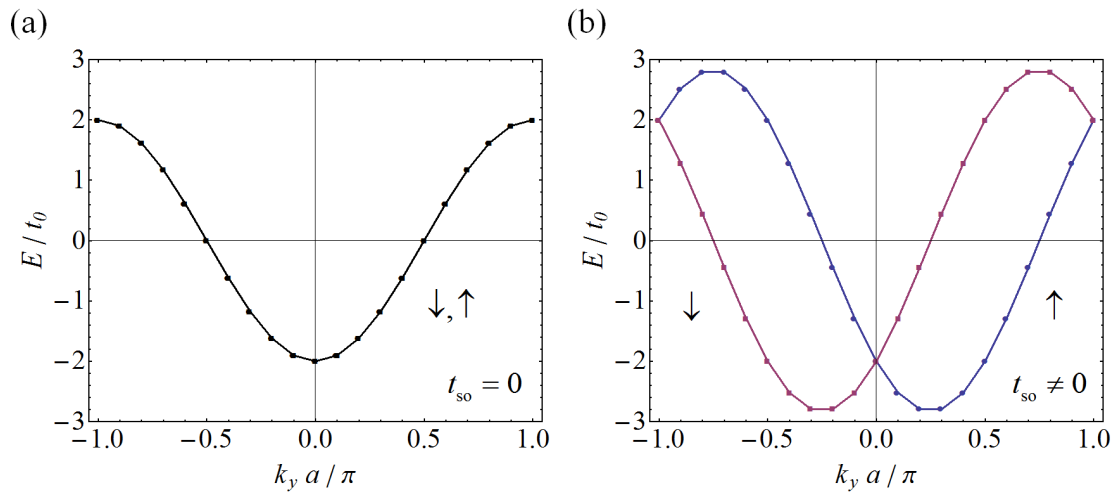


Figure 4.3: Spectrum of the single-band tight binding model for spatially uniform Rashba spin-orbit coupling in a quantum wire. (a) For  $t_{so} = 0$ , the spectrum consists of one two-fold degenerate tight-binding band. (b) In the presence of uniform spin-orbit coupling ( $t_{so} \neq 0$ ), spin-split tight-binding bands exist which are shifted in opposite directions along the quasimomentum axis.

## 5.0 SPATIAL ANALOGUE OF QUANTUM SPIN DYNAMICS VIA SPIN-ORBIT INTERACTION

We map electron spin dynamics from time to space in quantum wires with spatially uniform and oscillating Rashba spin-orbit coupling. The presence of the spin-orbit interaction introduces pseudo-Zeeman couplings of the electron spins to effective magnetic fields. We show that by periodically modulating the spin-orbit coupling along the quantum wire axis, it is possible to create the spatial analogue of spin resonance, without the need for any real magnetic fields. The mapping of time-dependent operations onto a spatial axis suggests a new mode for quantum information processing in which gate operations are encoded into the band structure of the material. We describe a realization of such materials within nanowires at the interface of  $\text{LaAlO}_3/\text{SrTiO}_3$  heterostructures.<sup>1</sup>

### 5.1 INTRODUCTION

Quantum dynamics lies at the heart of modern physics. While the evolution of a quantum mechanical system is governed by the time-dependent Schrödinger equation (TDSE), the mapping of this evolution from time to space has given rise to fundamental advances through the development of powerful theoretical techniques. One familiar example is provided by Feynman's path integral method [191], in which a description equivalent to the TDSE is obtained by recasting time evolution in terms of space-time paths. This approach finds applicability in a wide variety of contexts ranging from relativistic quantum mechanics to the braiding of quasiparticles that forms the basis for topological quantum computation [59]. World lines associated with quasiparticle braiding in two dimensions can be mapped to flux lines in three dimensions [192] if time itself is treated as

---

<sup>1</sup>The material in this chapter is adapted from Ref. [190].

a spatial coordinate by analytical continuation to imaginary time. In general, combining imaginary time with  $d$  spatial dimensions defines a  $(d + 1)$ -dimensional Euclidean space that provides a correspondence between quantum field theory and statistical mechanics [193]. Similarly, a connection between quantum field theory and quantum gravitational theory emerges through holographic mapping of a  $(d + 1)$ -dimensional combined space-time description to a  $d$ -dimensional one [194].

In the present work, we explore a mapping of spin dynamics from time to space, motivated by its potentially fundamental relevance to methods for coherent spin manipulation in solid-state systems [67] and physical realizations of spin-based quantum computing [35, 195]. Addressing these challenges involves harnessing the interactions of spin with spatial as well as external degrees of freedom. We show here that the coupling between spin and space can in fact be used to map the spin evolution from a temporal axis to a spatial one. Conceptually, instead of the TDSE (for  $\hbar = 1$ ),

$$i\partial_t U(t) = H(t)U(t), \quad (5.1)$$

the evolution is governed by a spatial analogue, which we write as

$$i\partial_y \tilde{U}(y) = K(y)\tilde{U}(y). \quad (5.2)$$

The coordinate-dependent “quasimomentum operator”  $K(y)$  in Eq. (5.2) plays a role similar to a time-varying Hamiltonian. The time-to-space mapping of spin dynamics then entails identifying a form for  $K(y)$  that generates a unitary transformation  $\tilde{U}(y)$  describing a simultaneous spatial translation and spin rotation. This identification can be made by considering the spatial analogues of time-dependent Hamiltonians  $H(t)$  which generate spin dynamics.

Electron spin resonance enables three-dimensional dynamical manipulation of single electron spins and therefore plays a central role in their promise as natural candidates for solid-state qubits [47, 66]. As discussed in Sec. 1.4.4, while the Zeeman interaction is typically used to carry out ESR, applying the local magnetic fields required for selectively addressing individual electron spin qubits is challenging in practice. The implementation of ESR using electric fields has therefore been widely investigated, leading to methods such as g-tensor modulation resonance (g-TMR) [96], electric dipole spin resonance (EDSR) [97, 98, 119, 120, 100], and ballistic spin resonance (BSR) [121]. A basic resource in both EDSR and BSR is the spin-orbit interaction: recall (Sec.

1.3) that time-varying spin-orbit coupling (which is generated by an external driving voltage in EDSR and internal electron dynamics in BSR) replaces the oscillating magnetic field required for ESR in these methods. We have also seen (Sec. 1.4.4) that several proposals for single-qubit gates rely on the effective magnetic field due to spin-orbit coupling [122, 123, 124, 125, 126, 127].

Here, we describe a mechanism for spin resonance that relies on *spatially*-varying spin-orbit coupling and the associated effective magnetic field, without employing any real magnetic fields. This method maps the spin evolution from time to space and is therefore not subject to the typical time-dependent constraints imposed in quantum computing for the purpose of preserving coherence [35, 195]. We show theoretically that this “spin spatial resonance” can be achieved by creating a superlattice within a quantum wire via periodically-modulated asymmetry in the lateral confinement potential. Rather than being controlled by time-dependent external fields, spin spatial resonance is built into the spin-dependent band structure [187, 111] of the superlattice. Segments of this “designer quantum material” having fixed lengths can be used to apply spatial “pulses” that execute single-qubit gate operations on the spins of electrons which travel through the wires. Because the system is one-dimensional and gate operations are determined only by the spatial coordinate of an electron, these single-qubit gates are intrinsically “fault-tolerant” with respect to backscattering, as we discuss below.

## 5.2 SPIN-ORBIT SUPERLATTICE QUANTUM WIRES

In order to show how ESR can be mapped to space using the spin-orbit interaction alone, we first describe a “spin-orbit superlattice quantum wire,” i.e., a one-dimensional system with built-in spatially uniform and oscillating spin-orbit coupling in perpendicular directions [Fig. 5.1(a)]. For specificity, we choose the coupling to be of the Rashba form [28, 29], although it may be possible to realize the mapping presented here with other types of spin-orbit interaction. We assume a zero-temperature independent-electron description and represent the quantum wire confining the electronic motion to one spatial dimension using a single-band tight-binding model. In Sec. 4.3 we showed that, in addition to a term  $H_0$  describing the kinetic hopping of the electron along the wire, a tight-binding Hamiltonian for the Rashba spin-orbit interaction via a spin-dependent hopping

can be written by discretizing the interaction on a lattice [104, 189]. Inspired once again by the Su-Schrieffer-Heeger model [147, 148, 149], which includes a site-dependent hopping amplitude, we now extend this tight-binding model in order to incorporate spatially-varying Rashba spin-orbit coupling. The full Hamiltonian for a wire represented by  $N$  sites with lattice constant  $a$  is given by

$$H = H_0 + H_{\text{so}}^{\text{unif}} + H_{\text{so}}^{\text{osc}}, \quad (5.3)$$

where

$$H_0 = -t_0 \sum_{n,\sigma} \left( c_{n+1,\sigma}^\dagger c_{n,\sigma} + \text{H.c.} \right), \quad (5.4)$$

$$H_{\text{so}}^{\text{unif}} = -t_{\text{so}}^{\text{unif}} \sum_{n,\sigma,\sigma'} \left[ c_{n+1,\sigma'}^\dagger (i\sigma_x)_{\sigma'\sigma} c_{n,\sigma} + \text{H.c.} \right], \quad (5.5)$$

$$H_{\text{so}}^{\text{osc}} = -t_{\text{so}}^{\text{osc}} \sum_{n,\sigma,\sigma'} \left[ \varphi_n c_{n+1,\sigma'}^\dagger (i\sigma_z)_{\sigma'\sigma} c_{n,\sigma} + \text{H.c.} \right]. \quad (5.6)$$

Here, the operators  $c_{n,\sigma}^\dagger$  and  $c_{n,\sigma}$  create and annihilate, respectively, an electron at site  $n$  with spin  $\sigma$ , and  $t_0 = \hbar^2/2m^*a^2$ , where  $m^*$  is the effective mass of the electron. The spin-dependent hopping amplitude  $t_{\text{so}}^{\text{unif}} = \alpha_\perp/2a$  describes spatially uniform Rashba spin-orbit coupling of strength  $\alpha_\perp$  generated by the potential gradient perpendicular to the plane containing the wire (defined to be the  $xy$  plane). Spatially-varying Rashba spin-orbit coupling with amplitude  $\alpha_\parallel$  due to the potential asymmetry in the  $xy$  plane but perpendicular to the propagation direction ( $y$  axis) of the wire is incorporated via a hopping described by an amplitude  $t_{\text{so}}^{\text{osc}} = \alpha_\parallel/2a$  together with a site-dependent factor  $\varphi_n$ . The summations in Eqs. (5.4)-(5.6) run over  $n = 1, \dots, N$  and  $\sigma, \sigma' = \uparrow, \downarrow$ . Here, we assume periodic boundary conditions so that  $n \pm N \equiv n$ . Note that we choose the uniform [Eq. (5.5)] and oscillating [Eq. (5.6)] effective magnetic fields to lie along the  $x$  and  $z$  axes, respectively. In the present work, we therefore define  $|\sigma\rangle \equiv |\sigma\rangle_x$ ; i.e., we choose the basis  $\{|\uparrow\rangle_x, |\downarrow\rangle_x\}$  associated with the components of spin along the  $x$  axis in order to describe the spin orientation with respect to the effective magnetic field due to the uniform spin-orbit interaction [Eq. (5.5)]. The matrix elements of the Hamiltonian defined by Eqs. (5.3)-(5.6) in the basis  $\{|n, \sigma\rangle\}$  are given by

$$\langle n', \sigma' | H_0 | n, \sigma \rangle = -t_0 (\delta_{n',n+1} + \delta_{n',n-1}) \delta_{\sigma'\sigma}, \quad (5.7)$$

$$\langle n', \sigma' | H_{\text{so}}^{\text{unif}} | n, \sigma \rangle = -it_{\text{so}}^{\text{unif}} \sigma (\delta_{n',n+1} - \delta_{n',n-1}) \delta_{\sigma'\sigma}, \quad (5.8)$$

$$\langle n', \sigma' | H_{\text{so}}^{\text{osc}} | n, \sigma \rangle = -it_{\text{so}}^{\text{osc}} (\varphi_n \delta_{n',n+1} - \varphi_{n'} \delta_{n',n-1}) (1 - \delta_{\sigma'\sigma}). \quad (5.9)$$

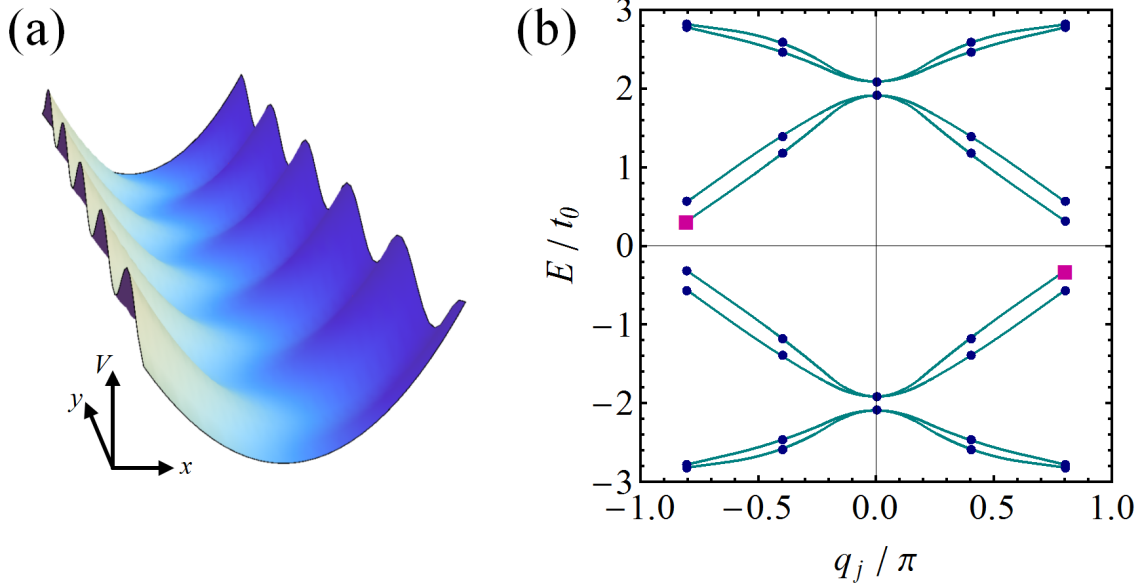


Figure 5.1: Spin-orbit superlattice quantum wire. (a) Schematic of a quantum wire with periodically-varying lateral confinement asymmetry which gives rise to a spin-orbit superlattice within the wire. (b) Spectrum as a function of electron quasimomentum  $q_j$  in the presence of both spatially uniform and oscillating Rashba spin-orbit coupling in perpendicular directions for  $N = 20$ ,  $m = 4$ ,  $t_{\text{so}}^{\text{unif}}/t_0 = 1$ , and  $t_{\text{so}}^{\text{osc}}/t_0 = 0.125$ . Filled squares indicate the eigenstates used to form the wavepacket state  $|\Psi_{\text{wp}}\rangle$  discussed in the text. Lines are guides to the eye.

In the presence of only uniform spin-orbit coupling ( $t_{\text{so}}^{\text{osc}} = 0$ ), the energy spectrum for the Hamiltonian consists of two tight-binding bands [Fig. 4.3(b)]. We have seen that these bands are shifted in opposite directions along the quasimomentum axis with respect to the energy band for  $H_0$  [Fig. 4.3(a)] due to the momentum dependence of the effective magnetic field associated with the spin-orbit interaction. If the modulated Rashba spin-orbit coupling term in Eq. (5.6) is included in the Hamiltonian ( $t_{\text{so}}^{\text{osc}} \neq 0$ ), the translational symmetry of the system is reduced. To map ESR spatially, we introduce periodically-varying spin-orbit coupling via  $\phi_n = \cos(2\pi n/m)$ . The Hamiltonian in Eq. (5.3) then retains a periodicity over  $m$  lattice sites. In this case, the energy eigenstates can be characterized by the eigenvalues of an operator  $D_m$ , which is defined to be the discrete translation operator over  $m$  sites and for which  $[H, D_m] = 0$ . The eigenvalues of  $D_m$  are of the form  $e^{iq_j}$ , where the associated dimensionless quasimomenta are  $q_j \equiv 2\pi j/N'$ , with  $N' \equiv N/m$  and  $j$  an integer such that  $-N'/2 \leq j < N'/2$ . Letting  $n = mn' + l$ , we express the Hamiltonian in terms of the operators

$$\tilde{c}_{j,l,\sigma} \equiv \frac{1}{\sqrt{N'}} \sum_{n'=0}^{N'-1} e^{-iq_j(mn'+l)} c_{mn'+l,\sigma} \quad (5.10)$$

and  $\tilde{c}_{j,l,\sigma}^\dagger$ . Subsequently transforming to the representation given by

$$d_{j,p,\sigma} \equiv \frac{1}{\sqrt{m}} \sum_{l=1}^m e^{-iQ_p l} \tilde{c}_{j,l,\sigma} \quad (5.11)$$

and  $d_{j,p,\sigma}^\dagger$ , where  $Q_p \equiv 2\pi p/m$  with  $p$  an integer such that  $-m/2 \leq p < m/2$ , leads to the following equivalent forms for Eqs. (5.4)-(5.6):

$$H_0 = -2t_0 \sum_{j,p,\sigma} \cos(q_j + Q_p) d_{j,p,\sigma}^\dagger d_{j,p,\sigma}, \quad (5.12)$$

$$H_{\text{so}}^{\text{unif}} = -2t_{\text{so}}^{\text{unif}} \sum_{j,p,\sigma} \sigma \sin(q_j + Q_p) d_{j,p,\sigma}^\dagger d_{j,p,\sigma}, \quad (5.13)$$

$$H_{\text{so}}^{\text{osc}} = -t_{\text{so}}^{\text{osc}} \sum_{j,p,\sigma,\sigma'} (1 - \delta_{\sigma',\sigma}) \sin\left(q_j + Q_p + \frac{\pi}{m}\right) \left( e^{-i\pi/m} d_{j,p+1,\sigma'}^\dagger d_{j,p,\sigma} + \text{H.c.} \right). \quad (5.14)$$

These expressions are derived in Appendix B. From Eqs. (5.12)-(5.14), it is evident that the kinetic hopping term  $H_0$  and the uniform spin-orbit coupling term  $H_{\text{so}}^{\text{unif}}$  are diagonal in the basis corresponding to the operators  $d_{j,p,\sigma}^\dagger$  and  $d_{j,p,\sigma}$ , where  $j$  indicates the quasimomentum  $q_j$ ,  $p$  is a band index, and  $\sigma$  represents the spin component along the  $x$  axis [defined to be 1 (-1) for  $\uparrow$  ( $\downarrow$ )

when used to explicitly represent the eigenvalue of  $\sigma_x$ , as in Eq. (5.13)]. The expression for  $H_{\text{so}}^{\text{osc}}$  in this basis implies that the periodically-modulated spin-orbit interaction couples “adjacent” ( $\Delta p = 1$ ) bands having opposite spin ( $\sigma' \neq \sigma$ ). The symmetry associated with this coupling of basis states gives rise to  $m$ -dimensional representations of the Hamiltonian (see Appendix B). To obtain the full spectrum for Eq. (5.3), we numerically diagonalize the Hamiltonian matrix within each of the two  $m$ -dimensional subspaces associated with each value of  $q_j$ . As in standard ESR, we treat the oscillating effective magnetic field as a perturbation relative to the uniform effective field and choose  $t_{\text{so}}^{\text{osc}}/t_0 \ll t_{\text{so}}^{\text{unif}}/t_0$ . Figure 1(b) shows the spectrum as a function of  $q_j$  for  $N = 20$ ,  $m = 4$ ,  $t_{\text{so}}^{\text{unif}}/t_0 = 1$ , and  $t_{\text{so}}^{\text{osc}}/t_0 = 0.125$ , illustrating the coupling between the bands due to  $H_{\text{so}}^{\text{osc}}$ .

### 5.3 SPIN SPATIAL RESONANCE

To demonstrate that signatures of spin resonance exist in the band structure of a spin-orbit superlattice quantum wire, we form a superposition of two energy eigenstates with equal and opposite quasimomenta  $q_j$  [indicated by squares in Fig. 5.1(b)]. Expressing these eigenstates using the notation  $|j, \mathbf{v}\rangle$ , where  $\mathbf{v} = 0, 1, \dots, 7$  represents a combined spin-orbital index that is defined to increase with increasing energy  $E$ , we define a “wavepacket”  $|\Psi_{\text{wp}}\rangle \equiv \frac{1}{\sqrt{2}} (|-2, 4\rangle + e^{-i\phi} |2, 3\rangle)$ . Note that the variation of  $\phi$ , which changes the relative phase between the two eigenstates, is equivalent to the time evolution of  $|\Psi_{\text{wp}}\rangle$  and simply results in a shift of the phase of the oscillation in the spin polarization. We therefore fix  $\phi$  and calculate the spin polarization as a function of site  $n$  for the wavepacket by determining the expectation values  $\langle S_{n\tau} \rangle \equiv \langle \Psi_{\text{wp}}^{(n)} | S_{\tau} | \Psi_{\text{wp}}^{(n)} \rangle$ , where  $\Psi_{\text{wp}}^{(n)}$  is the normalized spinor at site  $n$  for  $|\Psi_{\text{wp}}\rangle$  and  $\tau = x, y, z$ . In the following, we let  $\hbar = 1$ . We use the discrete Fourier transform  $F_d$ , defined by  $\langle l | F_d | n \rangle \equiv (1/\sqrt{N}) e^{-2\pi i l(n-1)/N}$ , to calculate the distribution of the Fourier modes in  $\langle S_{nx} \rangle$  as a function of  $t_{\text{so}}^{\text{unif}}/t_0$ . The absolute value of the amplitude of the  $l = 1$  Fourier mode,  $|a_1|$  [Fig. 5.2(a)], has a peak for  $t_{\text{so}}^{\text{unif}}/t_0 = 1$ . A calculation of the spin polarization components ( $\langle S_{nx} \rangle, \langle S_{ny} \rangle, \langle S_{nz} \rangle$ ) for the wavepacket corresponding to this peak [Fig. 5.2(b)] reveals that, while  $\langle S_{ny} \rangle$  and  $\langle S_{nz} \rangle$  vary rapidly over space,  $\langle S_{nx} \rangle$  exhibits a more gradual oscillation with one full cycle over the length of the wire. The corresponding spatial dependence of the spin polarization vector is illustrated above the plot of the spin polarization components in

Fig. 5.2(b). The Bloch-sphere evolution of the spin vector [Fig. 5.2(c)] follows a spiraling path typical of ESR. Here, however, the evolution of the spin occurs with respect to a spatial coordinate - the distance along the  $y$  axis. Analogous calculations performed for a wavepacket constructed from the two ground states  $|\pm 2, 0\rangle$  [Fig. 5.3] reveal nearly the same results, with a peak in  $|a_1|$  at  $t_{\text{so}}^{\text{unif}}/t_0 = 1$ .

The above analysis based on the tight-binding model defined in Eqs. (5.3)-(5.6) is well described by an analytical model obtained from a mapping of the standard spin resonance formalism for a two-state system from time to space via Eq. (5.2) (see Appendix A). Based on the continuum version of Eq. (5.3) for  $\varphi_n = \cos(2\pi n/m)$ , we choose the form

$$K(y) \equiv \frac{k_0}{2} \sigma_x - k_1 \cos(ky) \sigma_z \quad (5.15)$$

for the quasimomentum operator. Here,  $k \equiv 2\pi/\lambda$  is the spatial frequency associated with oscillating spin-orbit coupling of wavelength  $\lambda$ . Eq. (5.15) has a form analogous to a spin resonance Hamiltonian, with time replaced by the spatial coordinate  $y$  along the wire and temporal frequencies replaced by their spatial counterparts. The spin polarization components can be written in terms of the matrix elements of the solution  $\tilde{U}(y)$ , which can be determined using spatial analogues of a transformation to a rotating frame and the rotating wave approximation (see Appendix A for details). Choosing  $\lambda = 4a$ ,  $k_0 = (\pi/2a) (t_{\text{so}}^{\text{unif}}/t_0)$ , and  $k_1 = (4\pi/5a) (t_{\text{so}}^{\text{osc}}/t_0)$  in order to make a correspondence with the wavepacket state used in the tight-binding calculation described above, we let  $y = (n-1)a$  and evaluate the spin polarization as a function of  $n$ . The case  $t_{\text{so}}^{\text{unif}}/t_0 = 1$ ,  $t_{\text{so}}^{\text{osc}}/t_0 = 0.125$ , which corresponds to the spatial resonance condition  $k = k_0$  and the fundamental spatial frequency  $k_1 = \pi/10a$ , is shown in Fig. 5.2(d). This analytical result for the spin polarization components possesses qualitative features similar to the numerical result based on diagonalization of the tight-binding model for the same values of  $t_{\text{so}}^{\text{unif}}/t_0$  and  $t_{\text{so}}^{\text{osc}}/t_0$  [Fig. 5.2(b)]. The distortion of  $\langle S_{nx} \rangle$  in Fig. 5.2(b) relative to the smooth sinusoidal variation in the continuum analytical model of Fig. 5.2(d) is due to the fact that the subspace of  $|j, p, \sigma\rangle$  basis states for the tight-binding calculation consists of  $m = 4$  rather than two states (see Appendix B), all of which contribute to  $|\Psi_{\text{wp}}\rangle$ . In addition, the finite size of the system used in the tight-binding calculation results in a reduced amplitude of variation in  $\langle S_{ny} \rangle$  and  $\langle S_{nz} \rangle$  compared to the analytical result of Fig. 5.2(d). For illustration, the spectrum and spin polarization components for a system with

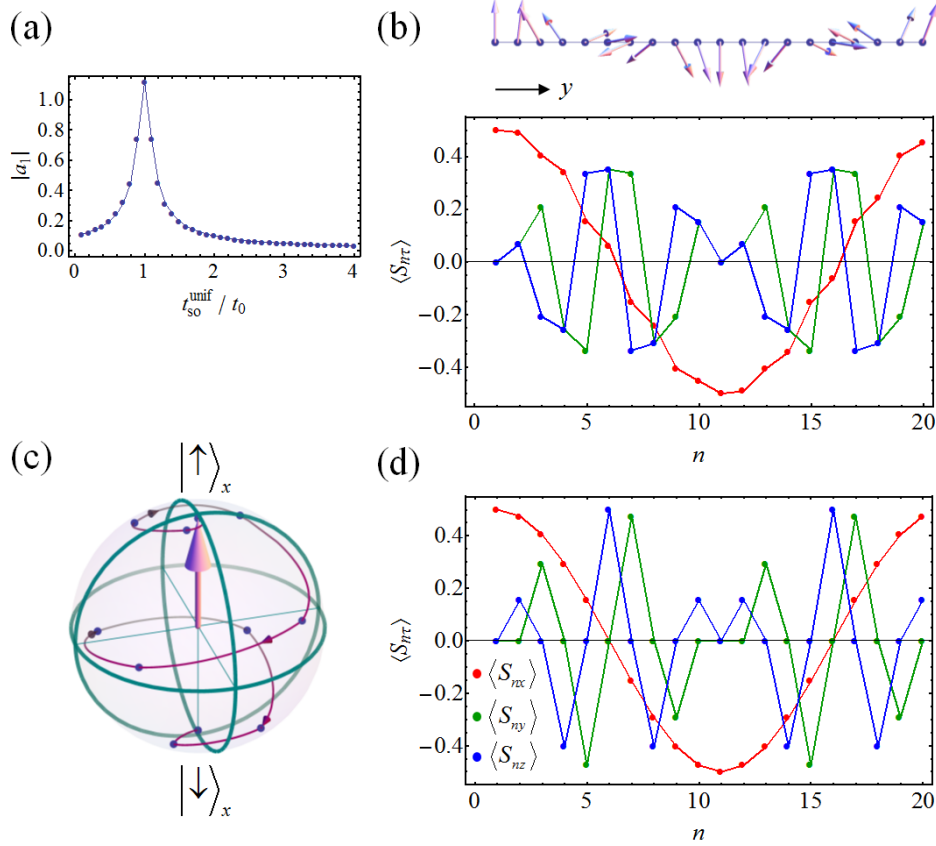


Figure 5.2: Spin spatial resonance. (a) Amplitude for the lowest nonzero ( $l = 1$ ) Fourier mode of the oscillation in  $\langle S_{nx} \rangle$  as a function of  $t_{\text{so}}^{\text{unif}}/t_0$ , showing a peak at  $t_{\text{so}}^{\text{unif}}/t_0 = 1$ . (b) Spin polarization (in units of  $\hbar$ ) for the state  $|\Psi_{\text{wp}}\rangle$  at  $t_{\text{so}}^{\text{unif}}/t_0 = 1$  as a function of spatial coordinate along the propagation direction ( $y$  axis) of the wire. (c) Bloch-sphere representation of the spin polarization in (b). As a function of the spatial coordinate  $y$  along the wire, the spin polarization follows a spiraling trajectory typical of spin resonance. Points indicated along the trajectory correspond to lattice sites. (d) Spin polarization components as a function of spatial coordinate for the continuum analytical model based on Eqs. (5.2) and (5.15).

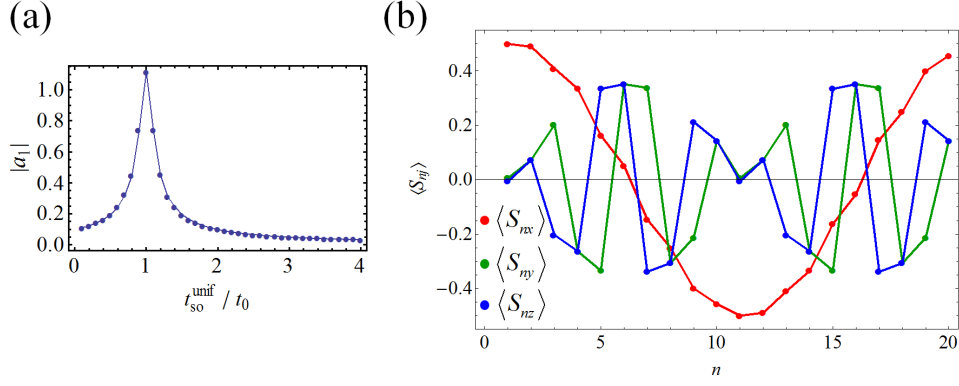


Figure 5.3: Spin spatial resonance for a wavepacket state constructed as a superposition of the two ground states  $|\pm 2, 0\rangle$ . (a) Amplitude for the  $l = 1$  Fourier mode of the oscillation in  $\langle S_{nx} \rangle$  as a function of  $t_{\text{so}}^{\text{unif}}/t_0$ , again showing a peak at  $t_{\text{so}}^{\text{unif}}/t_0 = 1$ . (b) Spin polarization for the ground-state wavepacket at  $t_{\text{so}}^{\text{unif}}/t_0 = 1$  as a function of spatial coordinate along the propagation direction of the wire.

$N = 40$ ,  $m = 8$ ,  $t_{\text{so}}^{\text{unif}}/t_0 = \sqrt{2} - 1$ , and  $t_{\text{so}}^{\text{osc}}/t_0 = 1/16$  are shown in Fig. 5.4. In this case, the amplitudes of the spin polarization components for the tight-binding model closely resemble those for the continuum model. The analytically-obtained signatures of ESR are nevertheless evident in the tight-binding results for the spin-orbit superlattice quantum wire, demonstrating that it is indeed possible to achieve ESR entirely from spin-orbit coupling and map spin resonance from time to space.

We now describe a possible physical implementation of a spin-orbit superlattice quantum wire at the interface of a  $\text{LaAlO}_3/\text{SrTiO}_3$  heterostructure. In this system, a local voltage-induced metal-insulator transition has been used to demonstrate both the fabrication of nanowires with widths  $\sim 2$  nm [177, 178] and the incorporation of highly asymmetric potential profiles along the nanowires [196]. In principle, the same method can be used to create nanowires with built-in lateral confinement asymmetry, and periodic variation of the asymmetry of the applied pulse along the wire can give rise to spatially oscillating spin-orbit coupling. The corresponding oscillating effective magnetic field will be oriented perpendicular to the plane containing the wire (i.e., along the  $z$

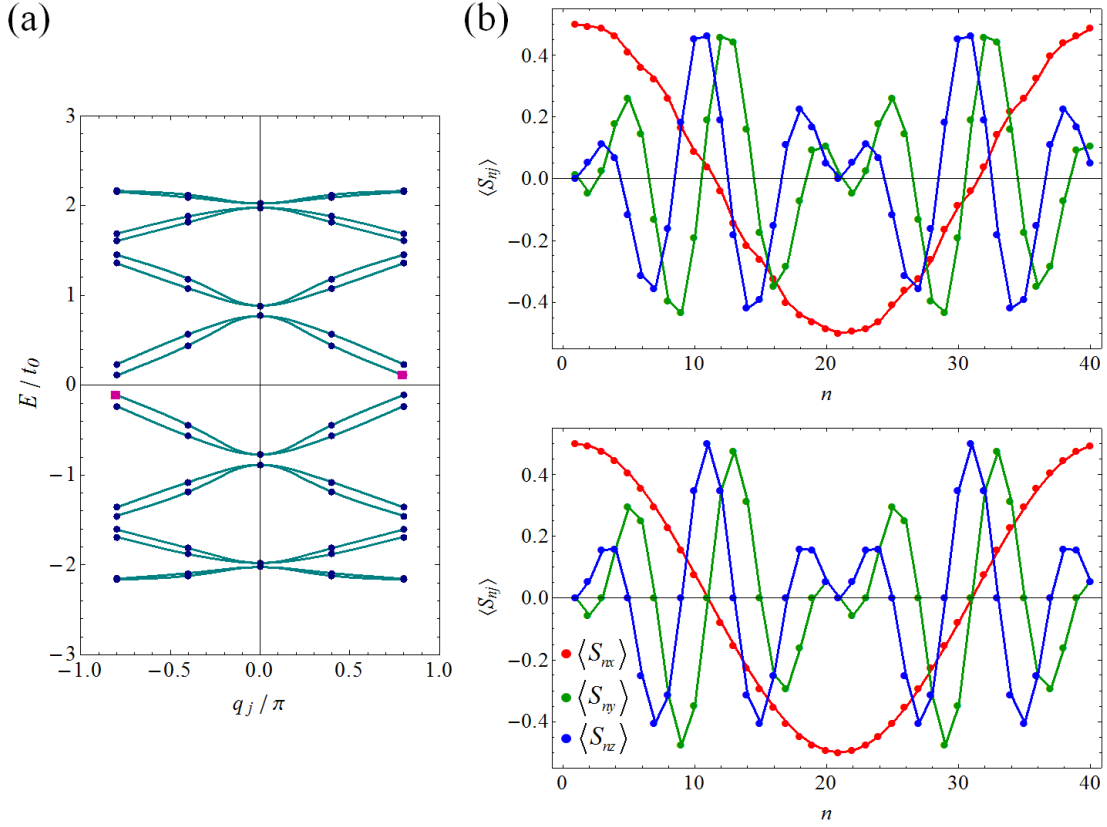


Figure 5.4: Spin spatial resonance for a spin-orbit superlattice quantum wire with  $N = 40$ ,  $m = 8$ ,  $t_{\text{so}}^{\text{unif}}/t_0 = \sqrt{2} - 1$ , and  $t_{\text{so}}^{\text{osc}}/t_0 = 1/16$ . (a) Spectrum with the eigenstates used to form a wavepacket state indicated by filled squares. Lines are guides to the eye. (b) Comparison of spin polarization components obtained from the tight-binding (upper panel) and continuum analytical (lower panel) models for the wavepacket state indicated in (a) at resonance.

axis). Together with an orthogonal effective field due to uniform spin-orbit coupling at the interface [183, 184, 185], this would allow for the creation of a spin-orbit superlattice quantum wire. The resonance condition  $t_{\text{so}}^{\text{unif}}/t_0 = 1$  can be used to estimate the length and spatial period of the superlattice. Using the definitions of  $t_0$  and  $t_{\text{so}}^{\text{unif}}$ , we find  $a = \hbar^2/m^*\alpha_{\perp}$ . With  $\alpha_{\perp} = 8 \times 10^{-12}$  eV · m and  $m^* = 1.1m_e$ , where  $m_e$  is the free electron mass,  $a = 300$  nm. For  $m = 4$ , this corresponds to  $\lambda = ma = 4a \sim 1 \mu\text{m}$  for the oscillating spin-orbit coupling [Eq. (5.6)].

#### 5.4 SPATIALLY-ENCODED SINGLE-QUBIT GATE SEQUENCE

The spatial mapping of ESR using only spin-orbit coupling implies that single-qubit gates can also be mapped to space. These gates are built into the spin-dependent band structure of the superlattice. Because the spin polarization is determined by the distance the electron travels along the wire, segments of spin-orbit superlattice quantum wires having fixed lengths can be thought of as spatial “pulses” applied to an electron which traverses them. As one application of this idea, we map a spin-echo pulse sequence of the form [197]

$$T_0 - \frac{\pi}{2} - T - \pi - T - \frac{\pi}{2} - T_0 \quad (5.16)$$

from time to space. In Eq. (5.16),  $T_0$  and  $T$  are time intervals in which the electron is allowed to evolve “freely” in the presence of a uniform magnetic field (i.e., without any manipulation by ESR pulses) and the ESR pulses labeled “ $\pi$ ” and “ $\pi/2$ ” indicate rotations by these angles about different axes of the Bloch sphere, i.e., single-qubit gates. Pulse sequences of this form are used in experiments involving spin manipulation to reverse the effects of decoherence due to unwanted couplings between spins and inhomogeneous magnetic fields [197]. For example, if the components of a spin “dephase,” or lose their definite phase relationship, during the first free evolution time  $T$  due to magnetic field variations, the spin-echo pulse sequence in Eq. (5.16) causes the evolution to proceed in the reverse direction after the  $\pi$  pulse, canceling the effects of the dephasing and effectively “refocusing” the spin.

Here, we use the spin-echo pulse sequence in Eq. (5.16) to illustrate that several single-qubit gates may be carried out in sequence by a corresponding series of spatial “pulses.” Fig. 5.5

shows the spatial mapping of the pulse sequence. Here,  $T_0$  and  $T$  are *pseudo*-time intervals of free evolution under the uniform effective magnetic field ( $t_{\text{so}}^{\text{osc}} = 0$ ). The pulses are spin-orbit superlattice quantum wire segments ( $t_{\text{so}}^{\text{osc}} \neq 0$ ), where the length of the  $\pi$  pulse segment is taken to be twice that of the  $\pi/2$  pulse segment. This pulse sequence can be built directly into the Hamiltonian [Eq. (5.3)] of the system via the site-dependent hopping factor  $\varphi_n$  in Eq. (5.6). We plot  $\varphi_n$  [Fig 5.5(a)] and the resulting spin polarization for a superposition of the two ground states as a function of the spatial coordinate [Fig. 5.5(b)] for  $N = 80$ ,  $t_{\text{so}}^{\text{unif}}/t_0 = 1$ , and  $t_{\text{so}}^{\text{osc}}/t_0 = 0.186$ . The forms  $\varphi_{n'} = \pm \cos(2\pi n'/m)$  with  $m = 4$  (where the site  $n'$  is labeled with respect to the beginning of each segment) were used for the  $\pi/2$  and  $\pi$  pulses, respectively. The degenerate ground states for this case are obtained via numerical diagonalization by identifying a symmetry operator  $S$  for the Hamiltonian such that  $[H, S] = 0$ . The symmetry operator used for the pulse sequence in Eq. (5.16) with the given parameters can be expressed as  $S = -D_2 R \sigma_z$ , where  $D_2$  is the discrete translation operator over two lattice sites and  $R$  is a “reflection” operator that transforms each site  $n$  according to  $n \rightarrow N - (n - 1)$ . As seen in Fig. (5.5), the spin polarization exhibits the spatial evolution expected for the series of quantum gates in the corresponding time-dependent spin echo sequence.

A degree of robustness to spin qubit gate errors caused by backscattering of the electrons exists in this class of systems by virtue of the fact that they are one-dimensional, so that any change in spin polarization due to backscattering can be undone if the electron again scatters into its original propagation direction. In addition, errors due to randomness in the material do not continuously degrade the quantum information over time - they are instead built into the state along with the desired spin dynamics via the spatial mapping described here. The essentially static nature of these errors enables their detection and correction without imposing a time limit, in contrast to systems in which a finite decoherence time exists for the spin of an electron which rotates over time as it moves in a random environment.

## 5.5 CONCLUSION

While ESR, quantum gates, and pulse sequences are typically regarded as time-dependent processes, the mapping of these building blocks for spin manipulation onto a *spatial* axis as described

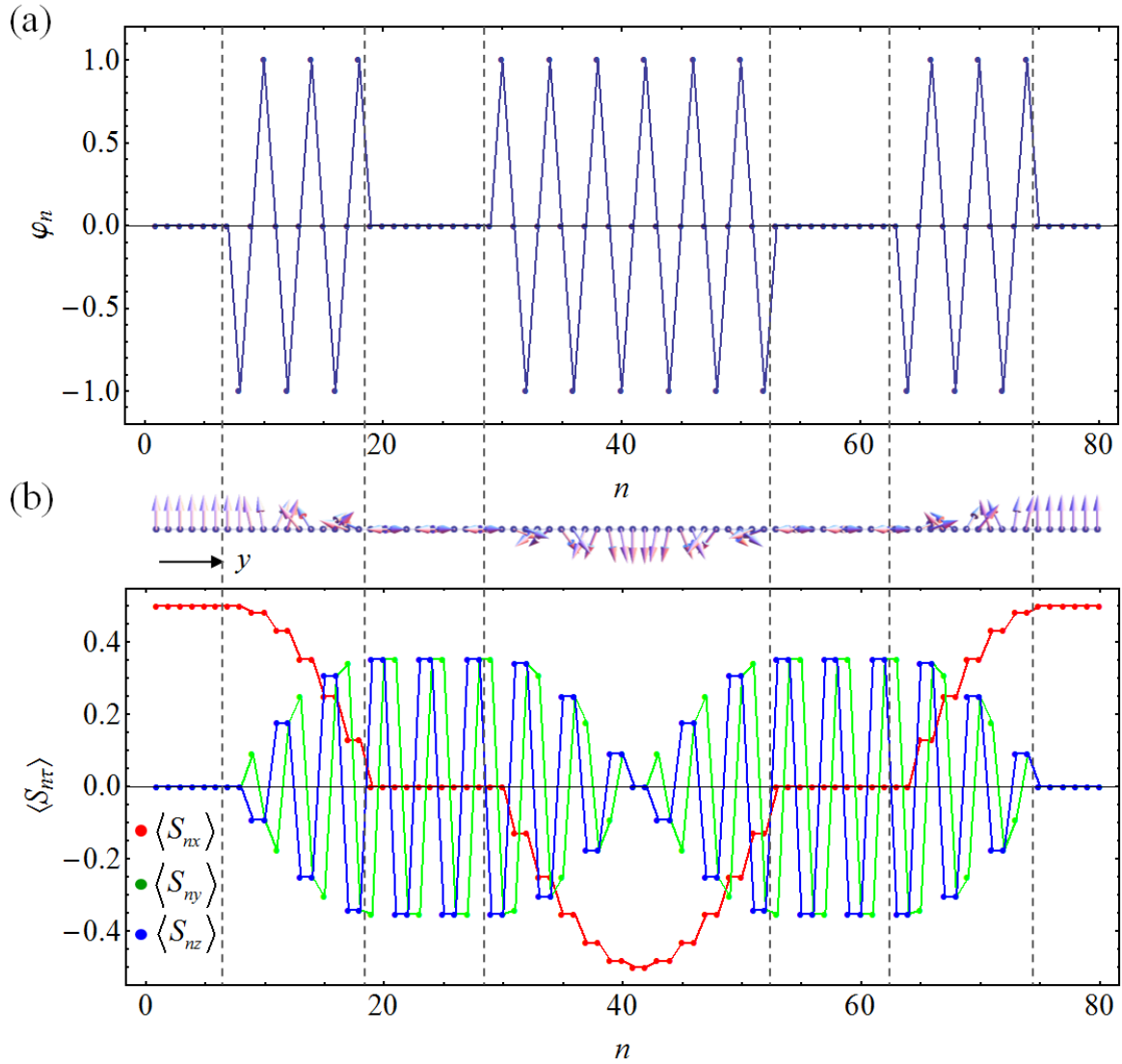


Figure 5.5: Spatial mapping of a spin echo pulse sequence. (a) Site-dependent hopping factor  $\varphi_n$  used to incorporate the pulse sequence into the Hamiltonian in Eq. (5.3) for  $N = 80$ ,  $t_{\text{so}}^{\text{unif}}/t_0 = 1$ , and  $t_{\text{so}}^{\text{osc}}/t_0 = 0.186$ . Regions of oscillating hopping amplitude correspond to spin-orbit superlattice quantum wire segments of fixed lengths and act as the spatial analogues of ESR pulses. (b) Site dependence of the spin polarization for the Hamiltonian described in (a), showing the spatial mapping of the spin dynamics expected for a spin-echo pulse of the form in Eq. (5.16).

in the present work suggests a new paradigm for quantum information processing. In this framework, a spin-orbit superlattice quantum wire represents a designer quantum material with a single-qubit gate encoded into its band structure. Generalization of the ideas presented here to two or more qubits would pave the way for achieving universal quantum computing via spatial encoding of quantum dynamics.

## 6.0 SUMMARY AND FUTURE PROSPECTS

In this thesis, we have presented two classes of designer quantum materials based on spatially-varying exchange and spin-orbit interactions. These systems enable quantum mechanics “by construction,” with spins and their interactions acting as naturally-existing building blocks. We have aimed to demonstrate the relevance of the new resources which emerge in these constructed quantum systems in the context of spin manipulation and spin-based quantum information processing.

Within dimerized Heisenberg spin systems, we have seen that the movement of domain walls can produce topologically-stable flying spin qubits (Ch. 2). Pairs of these domain walls also allow for the generation and transport of EPR pairs of entangled qubits. Coupling two Heisenberg rings containing domain walls leads to exchange between the two domain-wall qubits that can be tuned via the spin density variation within the rings (Ch. 3). This effective exchange can be ferromagnetic even when all exchange couplings between spins are antiferromagnetic. As a result, Heisenberg spin rings with domain walls can themselves be used as building blocks of a variety of quantum spin systems. We have also proposed physical implementations of these exchange-coupled spin systems within quantum dot arrays. Ongoing experimental efforts in the Levy research group involve Ge/Si quantum dots and have demonstrated the fabrication of dot configurations with precisely-controlled positions.

For quantum wires with spatially-varying spin-orbit interaction, we have shown how a mapping of quantum spin dynamics from time to space can be achieved. In this thesis, we considered the specific example of spatially-mapped ESR within a spin-orbit superlattice quantum wire (Ch. 5). This system represents a material with a spin-dependent band structure into which single-qubit gates can be encoded. In addition, the versatility of the local metal-insulator transition method developed in the Levy group suggests an implementation of spin-orbit superlattice quantum wires within nanowires having tailored lateral confinement asymmetry at the interface of  $\text{LaAlO}_3/\text{SrTiO}_3$

heterostructures. The mapping we describe allows for the manipulation of spins using only spin-orbit coupling and without any external magnetic fields.

Viewed from another perspective, the work presented in this thesis explores methods for the manipulation of spin via *internal* and *symmetry-maintaining* interactions: the Heisenberg exchange interaction preserves  $S^2$  and  $S_Z$  as well as time-reversal symmetry, and the spin-orbit interaction also preserves time-reversal symmetry. This is in contrast to *external* magnetic fields, which are often used for spin manipulation but *break* both total spin symmetry (if the magnetic field is inhomogeneous) and time-reversal symmetry.

The discussion in this thesis also emphasizes the fundamentally new phenomena and resources that emerge in designer quantum materials due to the connection between spin and spatial degrees of freedom. As was described in the introductory chapter, spin cluster qubits can be thought of as systems which effectively distribute a single spin- $\frac{1}{2}$  object over a finite region of space. In our work on coupled Heisenberg spin rings containing domain walls, we found that the exchange between the two domain-wall qubits is determined by the values of the spin density at the sites involved in the spin-spin coupling. This result is directly relevant to the method of producing flying spin qubits we present here: specifically, it provides confirmation that the transport of the localized nonzero spin density achieved by moving the domain wall also spatially transports the spin information encoded in the spin- $\frac{1}{2}$  ground-state doublet for the entire spin system. Since the sites with zero spin density do not contribute to the qubit coupling, they are effectively not associated with the measurable spin information. In the case of quantum wires with spin-orbit coupling, an interaction between spin and spatial degrees of freedom provides a pathway for mapping quantum spin dynamics to space. The spatial degree of freedom therefore provides robust methods for both transporting and manipulating spin.

A variety of possibilities exists for future work that can be built upon the foundation laid in this thesis. As one example, the fact that ferromagnetic interactions between logical qubits (which can be regarded as *effective* spins) can be produced using only antiferromagnetic interactions between individual spins suggests the potential for switching between antiferromagnetic and ferromagnetic materials within the *same* constructed system via electrical control of the exchange strengths. We have also shown that topological features such as domain walls can be explicitly incorporated into exchange-coupled spin systems. We may imagine extending this idea by introducing analo-

gous domain walls in systems with spatially-varying spin-orbit coupling. Alternatively, topological properties of designer quantum materials which are not intentionally introduced but which emerge as an end result of the construction may be explored.

Another direction for future investigation involves extending the scope of the spatial analogues of quantum dynamics introduced in this thesis. Such an extension might be achieved by, e.g., constructing designer quantum materials using both the exchange interaction and the spin-orbit interaction. The construction of this new class of hybrid quantum materials may enable a generalization of spatially-mapped single-qubit gates to two-qubit gates, or perhaps even full quantum algorithms, that are encoded into the band structure of the materials. By combining a two-qubit gate with appropriate single-qubit gates, it may be possible to achieve a new paradigm for universal quantum gating that is based on spatially-encoded spin manipulation. An interplay of the exchange and spin-orbit interactions within this class of designer quantum materials may also allow the construction of quantum spin systems with anisotropic exchange coupling. Additionally, methods may be explored by which the flying spin qubits, EPR pairs, and spatially-encoded quantum gates described in this thesis can be combined with elements arising in new classes of designer quantum materials in order to achieve a full architecture that addresses all seven DiVincenzo criteria for the physical realization of quantum information processing.

The wealth of new resources which emerge by constructing quantum materials from spins and their interactions, together with the multitude of possible future directions to explore, suggest that the quest for new designer quantum materials will be both worthwhile and exciting.

## APPENDIX A

### QUANTUM SPIN DYNAMICS

#### A.1 UNITARY TIME EVOLUTION OPERATOR

Here, we recall some general aspects of quantum dynamics useful for describing the time evolution of the spin systems considered in this thesis. The nonrelativistic description of quantum spin dynamics is based on the time-dependent Schrödinger equation (TDSE),

$$i\partial_t U(t) = H(t)U(t), \quad (\text{A.1})$$

where  $\partial_t \equiv \partial/\partial t$  and the evolution is generated by the (spin-dependent) Hamiltonian  $H(t)$  describing the system, which in general may also change with time. The unitary time evolution operator  $U(t)$  is the solution to Eq. (A.1) with the initial condition  $U(0) = \mathbf{1}$  and determines the time evolution of a state  $|\Psi(t)\rangle$  via

$$|\Psi(t)\rangle = U(t)|\Psi(0)\rangle. \quad (\text{A.2})$$

In general, obtaining an exact expression for  $U(t)$  given an arbitrary Hamiltonian  $H(t)$  is not possible. The analysis can be simplified if the Hamiltonian contains time-independent terms. In the limit of a Hamiltonian  $H$  which has no time dependence at all, the unitary time evolution operator is  $U(t) = e^{-iHt}$  and corresponds to stationary states  $|\Psi_i(t)\rangle = e^{-iE_i t} |\psi_i\rangle$ , where  $E_i$  and  $|\psi_i\rangle$  satisfy the time-independent Schrödinger equation  $H|\psi_i\rangle = E_i|\psi_i\rangle$ .

If the full Hamiltonian  $H(t)$  depends on time but contains a time-independent term of the form  $H_0 \propto \mathbf{1}$ , where  $\mathbf{1}$  is the identity operator in spin space, the Hamiltonian can be written as

$H(t) = H_0 + H_1(t)$ . Since  $H_0$  is proportional to the identity matrix, it commutes with the time-dependent term  $H_1(t)$ . As a result, the solution  $U(t)$  can be expressed as a product of the time evolution operators obtained by solving the TDSE for  $H_0$  and  $H_1(t)$  separately [198]. This method gives  $U(t) = e^{-iH_0t}U^1(t)$ , where  $U^1(t)$  is the solution to the TDSE for  $H_1(t)$ . Substituting this factored form for  $U(t)$  along with  $H(t) = H_0 + H_1(t)$  into Eq. (A.1), applying the operator identity [199]

$$e^A B e^{-A} = B + [A, B] + \frac{1}{2!} [A, [A, B]] + \dots \quad (\text{A.3})$$

with  $A = iH_0t$  and  $B = H_1(t)$ , and using the fact that  $[H_0, H_1(t)] = 0$  results in the vanishing of all commutators in Eq. (A.3) leads to the TDSE for  $U^1(t)$ ,

$$i\partial_t U^1(t) = H_1(t) U^1(t), \quad (\text{A.4})$$

with the initial condition  $U^1(0) = U(0) = \mathbf{1}$ . Since  $H_0$  is proportional to the identity matrix, the additional exponential factor  $e^{-iH_0t}$  in the full time evolution operator simply multiplies the solution  $|\Psi(t)\rangle$  by a global phase that does not change the physical meaning of  $|\Psi(t)\rangle$ .  $H_1(t)$  therefore generates the nontrivial spin dynamics through Eq. (A.4).

For the case in which the Hamiltonian depends on time but satisfies  $[H(t_1), H(t_2)] = 0$  for any two times  $t_1$  and  $t_2$ , the unitary time evolution operator can be written as

$$U(t) = \exp \left[ -i \int_0^t H(t') dt' \right]. \quad (\text{A.5})$$

For example, Eq. (A.5) applies to Hamiltonians of the form  $H(t) = C(t)A$ , in which the operator  $A$  is time-independent and all time dependence is contained in the factor  $C(t)$ . This case is relevant for the single-spin and two-spin unitary time evolution operators that are considered in Sec. 1.4.2.

## A.2 FLOQUET STATES FOR THREE-SPIN RING

For a time-varying Hamiltonian  $H(t)$ , stationary states cannot exist because  $H(t)$  in general does not possess a single set of energy eigenstates for all  $t$ . In the specific case of Hamiltonians that are periodic in time, Floquet theory can be applied [157]. This formalism is analogous to the Bloch theory for spatially-periodic Hamiltonians [23]. Here, we use this method to analyze the time evolution in the pseudospin space for flying spin qubits described in Ch. 2 and derive the Floquet state given in Eq. (2.5).

Substituting  $\varphi = \omega t$  into the Hamiltonian for the three-spin ring in the pseudospin representation  $\{|\pm\rangle\}$  [Eq. (2.4)] gives a time-dependent Hamiltonian of the form  $H_3(t) = H_3^0 + H_3^1(\Delta, \omega t)$ , where  $H_3^0 = (-3\tilde{J}_0/4) \mathbf{1}$  and

$$H_3^1(\Delta, \omega t) = \frac{\Delta}{2} (\Sigma_X \cos \omega t + \Sigma_Y \sin \omega t) = \frac{\Delta}{2} \begin{pmatrix} 0 & e^{-i\omega t} \\ e^{i\omega t} & 0 \end{pmatrix}. \quad (\text{A.6})$$

Since  $H_3^0 \propto \mathbf{1}$ ,  $H_3^1(\Delta, \omega t)$  generates the nontrivial dynamics (see Sec. A.1). Comparing Eq. (A.6) with the Zeeman Hamiltonian for a single spin- $\frac{1}{2}$  particle in a magnetic field  $\mathbf{B}$  [Eq. (1.18)] reveals that  $H_3^1(\Delta, \omega t)$  represents the coupling of the pseudospin to an effective magnetic field

$$\mathbf{B}_{\text{ps}} = -\frac{\Delta}{g\mu_B} (\cos \omega t \hat{x} + \sin \omega t \hat{y}). \quad (\text{A.7})$$

Eq. (A.7) describes a *pseudomagnetic* field rotating with frequency  $\omega$  in the  $xy$  plane of the Bloch sphere (Fig. 1.3) for the pseudospin basis  $\{|\pm\rangle\}$ . This field has an exchange-dependent strength determined by  $\Delta = 3\tilde{J}_1/2$ , where  $\tilde{J}_1$  is the exchange modulation amplitude [see Eq. (3.2)]. The splitting due to this pseudomagnetic field is illustrated in Fig. 3.1.

Although the Hamiltonian in Eq. (A.6) varies continuously in time, it repeats at regular time intervals  $T = 2\pi/\omega$  such that  $H_3^1(\Delta, \omega t + 2\pi) = H_3^1(\Delta, \omega t)$ . This corresponds to the fact that the domain wall returns to its original location within the three spin-ring after one full revolution, during which  $\varphi$  changes by  $2\pi$ . Because of this temporal periodicity, the eigenstates of the Hamiltonian for  $t = 0$  can be associated with dynamic states of the system at later times  $rT$ , where  $r$  is the number of complete revolutions of the domain wall around the ring.

Using Eq. (A.2), we can write the TDSE as  $i\partial_t |\Psi(t)\rangle = H(t) |\Psi(t)\rangle$ . In general, for a Hamiltonian with period  $T$  such that  $H(t+T) = H(t)$ , Floquet's theorem states that there exist solutions to the TDSE of the form  $|\Psi_m(t)\rangle = e^{-i\varepsilon_m t} |\phi_m(t)\rangle$ , where  $|\phi_m(t)\rangle$  has the property  $|\phi_m(t+T)\rangle = |\phi_m(t)\rangle$ . Using the relation  $|\Psi_m(t)\rangle = U(t) |\Psi_m(0)\rangle$  leads to  $|\phi_m(t)\rangle = e^{i\varepsilon_m t} U(t) |\phi_m(0)\rangle$ . Since  $|\phi_m(0)\rangle = |\phi_m(T)\rangle = |\phi_m(2T)\rangle = \dots = |\phi_m(rT)\rangle$ , it follows that  $|\phi_m(rT)\rangle = e^{i\varepsilon_m rT} U(rT) |\phi_m(0)\rangle$  can be rewritten in the form

$$U(rT) |\phi_m(T)\rangle = e^{-i\varepsilon_m rT} |\phi_m(T)\rangle. \quad (\text{A.8})$$

This is an eigenvalue equation which shows that the eigenvectors of  $U(rT)$  are the states  $|\phi_m(T)\rangle$ . In what follows, these eigenvectors are referred to as Floquet states. Note that the Floquet states are the same for all values of  $r$ . The corresponding eigenvalues  $\{\lambda_m = e^{-i\varepsilon_m rT}\}$  are complex numbers of unit modulus, and  $\varepsilon_m = i \ln \lambda_m / rT$  is called the quasienergy associated with the Floquet state  $|\phi_m(T)\rangle$ . Eq. (A.8) signifies that the Floquet states and quasienergies for the evolution of a system over a time interval  $rT$  can be determined by diagonalizing the operator  $U(rT)$ . The Floquet states obtained in this way serve to characterize the dynamics of the system in situations where the concept of stationary states is not applicable but temporal periodicity exists.

To determine the Floquet states associated with the domain wall dynamics in the three-spin ring, we first use Eq. (A.4) with  $H(t) = H_3^1(\Delta, \omega t)$  to solve for  $U^1(t)$ . Let the matrix elements of  $U^1(t)$  in the pseudospin basis be denoted by  $u_{ab}(t) = \langle a | U^1(t) | b \rangle$ , where  $a, b = \pm$ . Using Eq. (A.4) and Eq. (A.6) gives two pairs of complex coupled differential equations:

$$\begin{aligned} i \frac{du_{++}(t)}{dt} &= \frac{\Delta}{2} e^{-i\omega t} u_{-+}(t), \\ i \frac{du_{-+}(t)}{dt} &= \frac{\Delta}{2} e^{i\omega t} u_{++}(t), \end{aligned} \quad (\text{A.9})$$

and a second pair of equations obtained by making the replacements  $u_{++} \rightarrow u_{+-}$  and  $u_{-+} \rightarrow u_{--}$  in (A.9). In what follows, we derive the solutions to the system in Eq. (A.9) in order to obtain the first column of  $U^1(t)$ ; the same method can be used to obtain the second column. Applying the initial condition  $U^1(0) = \mathbf{1}$  gives  $u_{++}(0) = 1$  and  $u_{-+}(0) = 0$ . The equations in (A.9) can be solved analytically by a transformation to a coordinate system rotating with the pseudomagnetic

field  $\mathbf{B}_{\text{ps}}$  at the frequency  $\omega$ . [200] This transformation is given by rewriting Eq. (A.9) in terms of the new functions

$$\begin{aligned} v_{++} &\equiv e^{-i\omega t/2} u_{++}, \\ v_{-+} &\equiv e^{i\omega t/2} u_{-+}. \end{aligned} \quad (\text{A.10})$$

The transformed versions of Eq. (A.9) yield

$$i \frac{d}{dt} \begin{pmatrix} v_{++} \\ v_{-+} \end{pmatrix} = H_{\text{rot}} \begin{pmatrix} v_{++} \\ v_{-+} \end{pmatrix}, \quad (\text{A.11})$$

where the corresponding time-*independent* Hamiltonian  $H_{\text{rot}}$  in the rotating frame is given by

$$H_{\text{rot}} = \frac{1}{2} \begin{pmatrix} -\omega & \Delta \\ \Delta & \omega \end{pmatrix} = \frac{1}{2} (-\omega \Sigma_Z + \Delta \Sigma_X). \quad (\text{A.12})$$

With this form for  $H_{\text{rot}}$ , Eq. (A.11) is equivalent to the TDSE for the coupling of the pseudospin to a static magnetic field. Since  $H_{\text{rot}}$  is independent of time, the corresponding time evolution operator  $V(t)$  constructed from the matrix elements  $v_{ab}(t) = \langle a|V(t)|b\rangle$  is given by  $V(t) = e^{-iH_{\text{rot}}t}$ . To calculate this operator, we recall a useful identity for spin rotation operators [74]: a rotation about an axis defined by a unit vector  $\hat{\mathbf{n}}$  of the Bloch sphere by an angle  $\theta$  can be written in the form

$$R_{\hat{\mathbf{n}}}(\theta) = e^{i\theta \hat{\mathbf{n}} \cdot \boldsymbol{\sigma}/2} = \cos\left(\frac{\theta}{2}\right) \mathbf{1} + i \sin\left(\frac{\theta}{2}\right) \hat{\mathbf{n}} \cdot \boldsymbol{\sigma}. \quad (\text{A.13})$$

Eq. (A.12) has the form  $H_{\text{rot}} = -\mathbf{b} \cdot \boldsymbol{\Sigma}$ , where  $\mathbf{b} \equiv (-\Delta \hat{x} + \omega \hat{z})/2$  is proportional to the static effective magnetic field. Since the pseudospin operators  $\{\Sigma_X, \Sigma_Y, \Sigma_Z\}$  are the representations of the Pauli matrices in the pseudospin basis  $\{|\pm\rangle\}$ , we can set  $\theta \hat{\mathbf{n}}/2 = t \mathbf{b}$  in Eq. (A.13), which gives

$$V(t) = e^{it \mathbf{b} \cdot \boldsymbol{\Sigma}} \quad (\text{A.14})$$

$$= \cos\left(\frac{\sqrt{\Delta^2 + \omega^2} t}{2}\right) \mathbf{1} + i \sin\left(\frac{\sqrt{\Delta^2 + \omega^2} t}{2}\right) \left( -\frac{\Delta}{\sqrt{\Delta^2 + \omega^2}} \Sigma_X \right. \quad (\text{A.15})$$

$$\left. + \frac{\omega}{\sqrt{\Delta^2 + \omega^2}} \Sigma_Z \right). \quad (\text{A.16})$$

From this expression, we find

$$\begin{aligned} v_{++}(t) &= \cos\left(\frac{\sqrt{\Delta^2 + \omega^2}}{2}t\right) + i\frac{\omega}{\sqrt{\Delta^2 + \omega^2}}\sin\left(\frac{\sqrt{\Delta^2 + \omega^2}}{2}t\right), \\ v_{--}(t) &= -i\frac{\Delta}{\sqrt{\Delta^2 + \omega^2}}\sin\left(\frac{\sqrt{\Delta^2 + \omega^2}}{2}t\right). \end{aligned} \quad (\text{A.17})$$

The matrix elements  $u_{++}(t)$  and  $u_{--}(t)$  can then be obtained from these expressions by inverting Eq. (A.10). The above analysis can be repeated to find the remaining matrix elements  $u_{+-}(t)$  and  $u_{-+}(t)$  in order to obtain the full solution for  $U^1(t)$ .

Having obtained the general solution  $U^1(t)$ , we now set  $t = 2T = 4\pi/\omega$  and diagonalize the matrix  $U_{4\pi/\omega} \equiv U^1(2T)$  corresponding to two revolutions of the domain wall in order to obtain the Floquet states and quasienergies, each of which can be associated with an eigenstate of  $H_3^1(\Delta, \varphi)$  for a particular initial value of  $\varphi$ . Based on the analysis in Sec. 2.3, we choose  $\varphi = 0$ , so that the domain wall is located at site  $k = 3$  within the three-spin ring. In this case, the ground state is  $|\varphi = 0\rangle = \frac{1}{\sqrt{2}}(|+\rangle - |-\rangle) = |SS0\rangle$ , the pseudospin lies along the positive axis associated with  $\Sigma_X$  (see Fig. 2.4), and the associated Floquet state is found to be

$$|\phi_g(\Delta, \omega)\rangle = \frac{1}{N_0} \left\{ \left[ \frac{\omega}{\Delta} + \sqrt{1 + \left(\frac{\omega}{\Delta}\right)^2} \right] |+\rangle - |-\rangle \right\}, \quad (\text{A.18})$$

where

$$N_0 = \left\{ 2 \left[ \left(\frac{\omega}{\Delta}\right)^2 + \frac{\omega}{\Delta} \sqrt{1 + \left(\frac{\omega}{\Delta}\right)^2} + 1 \right] \right\}^{1/2}$$

is a normalization constant. The quasienergy corresponding to this Floquet state is

$$\epsilon_g = -\frac{\omega + \sqrt{\omega^2 + \Delta^2}}{2}.$$

The correspondence between  $|\phi_g(\Delta, \omega)\rangle$  and the initial ground state  $|SS0\rangle$  can be seen by taking the limit  $\omega \rightarrow 0$ . Re-expressing Eq. (A.18) in terms of  $|SS0\rangle$  and neglecting normalization constants leads to the state  $|X+; \omega\rangle$  in Eq. (2.5). Assuming  $\omega > 0$  and diagonalizing  $U_{-4\pi/\omega}$  gives the Floquet state  $|X+; -\omega\rangle$ .

### A.3 SPATIAL FORMULATION OF SPIN RESONANCE

In this section, we map the standard formalism used to describe spin resonance via the TDSE [200] to a description in terms of *spatial* evolution, which form the basis of the continuum analytical model for spin spatial resonance discussed in Sec. 5.3. This mapping is based on a spatial analogue of the TDSE, which is given in Eq. (5.2):

$$i\partial_y \tilde{U}(y) = K(y) \tilde{U}(y).$$

In Sec. 5.3, the quasimomentum operator [Eq. (5.15)]

$$K(y) = \frac{k_0}{2} \sigma_x - k_1 \cos(ky) \sigma_z$$

is chosen to have a form analogous to that of a time-dependent Hamiltonian which is known to give rise to spin resonance. In the expression for  $K(y)$ , the spatial coordinate  $y$  plays the role of time. The wavevectors  $k_0$ ,  $k_1$ , and  $k$  represent spatial analogues of temporal frequencies. In what follows, the Pauli matrices are represented with respect to the basis  $\{|\uparrow\rangle_x, |\downarrow\rangle_x\}$  used in Ch. 5:

$$\sigma_x = \begin{pmatrix} 1 & 0 \\ 0 & -1 \end{pmatrix}, \sigma_y = \begin{pmatrix} 0 & i \\ -i & 0 \end{pmatrix}, \sigma_z = \begin{pmatrix} 0 & 1 \\ 1 & 0 \end{pmatrix}. \quad (\text{A.19})$$

We denote the matrix elements of  $\tilde{U}(y)$  by  $u_{ab}(y) = \langle a | \tilde{U}(y) | b \rangle$ , where  $a, b = 1, 2$  with  $|1\rangle \equiv |\uparrow\rangle_x$  and  $|2\rangle \equiv |\downarrow\rangle_x$ . Substituting Eq. (5.15) into Eq. (5.2) yields the coupled equations

$$\begin{aligned} i \frac{du_{11}(y)}{dy} &= \frac{k_0}{2} u_{11}(y) - k_1 \cos(ky) u_{21}, \\ i \frac{du_{21}(y)}{dy} &= -k_1 \cos(ky) u_{11} - \frac{k_0}{2} u_{21}(y). \end{aligned} \quad (\text{A.20})$$

as well as the two equations obtained via the replacements  $u_{11} \rightarrow u_{12}$  and  $u_{21} \rightarrow u_{22}$ . In analogy to the method discussed in Sec. A.2, a transformation to a “rotating” frame can be defined via

$$\begin{aligned} v_{11} &\equiv e^{iky/2} u_{11}, \\ v_{21} &\equiv e^{-iky/2} u_{21}. \end{aligned} \quad (\text{A.21})$$

After some simplification, this leads to the equations

$$\begin{aligned}
i\frac{dv_{11}}{dy} &= -\frac{\Delta k}{2}v_{11} - \frac{k_1}{2}\left(1 + e^{2iky}\right)v_{21}, \\
i\frac{dv_{21}}{dy} &= -\frac{k_1}{2}\left(1 + e^{-2iky}\right)v_{11} + \frac{\Delta k}{2}v_{21},
\end{aligned} \tag{A.22}$$

where we have defined  $\Delta k \equiv k - k_0$ .

We now use a spatial counterpart of the rotating wave approximation to eliminate the exponential terms in Eq. (A.22), since they have the spatial frequency  $2k$  and therefore oscillate rapidly in space compared to the other terms in these equations when  $\Delta k \ll k$ . This is true near resonance, which occurs for  $k = k_0$ . The remaining terms can be written in the form

$$i\frac{d}{dy}\begin{pmatrix} v_{11} \\ v_{21} \end{pmatrix} = \tilde{K}\begin{pmatrix} v_{11} \\ v_{21} \end{pmatrix}, \tag{A.23}$$

with the space-independent quasimomentum operator

$$\tilde{K} = -\frac{1}{2}\begin{pmatrix} \Delta k & k_1 \\ k_1 & -\Delta k \end{pmatrix} = -\frac{1}{2}(\Delta k \sigma_x + k_1 \sigma_z). \tag{A.24}$$

Since the matrix elements  $v_{12}$  and  $v_{22}$  also satisfy Eq. (A.23), we can write

$$i\partial_y V(y) = \tilde{K}V(y). \tag{A.25}$$

The spatial evolution operator is then given by  $V(y) = e^{-i\tilde{K}y}$ . Using the method based on the identity in Eq. (A.13) given in Sec. A.2 to determine  $V(y)$  gives

$$V(y) = \cos\left(\frac{\sqrt{\Delta k^2 + k_1^2}}{2}y\right)\mathbf{1} + i\sin\left(\frac{\sqrt{\Delta k^2 + k_1^2}}{2}y\right)\left(\frac{\Delta k}{\sqrt{\Delta k^2 + k_1^2}}\sigma_x \tag{A.26}$$

$$+ \frac{k_1}{\sqrt{\Delta k^2 + k_1^2}}\sigma_z\right), \tag{A.27}$$

from which

$$\begin{aligned}
v_{11}(y) &= \cos\left(\frac{\sqrt{\Delta k^2 + k_1^2}}{2}y\right) + i\frac{\Delta k}{\sqrt{\Delta k^2 + k_1^2}}\sin\left(\frac{\sqrt{\Delta k^2 + k_1^2}}{2}y\right), \\
v_{21}(y) &= i\frac{k_1}{\sqrt{\Delta k^2 + k_1^2}}\sin\left(\frac{\sqrt{\Delta k^2 + k_1^2}}{2}y\right).
\end{aligned} \tag{A.28}$$

These expressions can be used to find  $u_{11}(y)$  and  $u_{21}(y)$  by inverting Eq. (A.21). In the same way,  $v_{12}(y)$  and  $v_{22}(y)$  can be used to determine  $u_{12}(y)$  and  $u_{22}(y)$ , and the full matrix for  $\tilde{U}(y)$  can be constructed.

The matrix elements of  $\tilde{U}(y)$  can be used to write expressions for the spin polarization components  $\langle S_{n\tau} \rangle$ , where  $\tau = x, y, z$ . For the spin polarization shown in Fig. 5.2(d), the spin is in the state  $|\uparrow\rangle_x$  at  $n = 1$  ( $y = 0$ ). In this case, the spin polarization components can be written in terms of the matrix elements  $u_{11}$  and  $u_{21}$  as

$$\begin{aligned}
\langle S_{nx} \rangle &= \frac{1}{2}(|u_{11}|^2 - |u_{21}|^2) \\
\langle S_{ny} \rangle &= \frac{i}{2}(u_{11}^*u_{21} - u_{21}^*u_{11}) \\
\langle S_{nz} \rangle &= \frac{1}{2}(u_{11}^*u_{21} + u_{21}^*u_{11})
\end{aligned} \tag{A.29}$$

At resonance, which corresponds to the condition  $\Delta k = k - k_0 = 0$ , the expressions for the spin polarization components simplify to

$$\begin{aligned}
\langle S_{nx} \rangle &= \frac{1}{2}\cos k_1 y, \\
\langle S_{ny} \rangle &= -\frac{1}{2}\cos ky \sin k_1 y, \\
\langle S_{nz} \rangle &= \frac{1}{2}\sin ky \sin k_1 y,
\end{aligned} \tag{A.30}$$

which are used to obtain Fig. 5.2(d).

## APPENDIX B

### SPIN-ORBIT SUPERLATTICE QUANTUM WIRE HAMILTONIAN

Here, we show how we obtain the expressions (5.12)-(5.14) given in Ch. 5 for the terms in the Hamiltonian describing a spin-orbit superlattice quantum wire [Eq. (5.3)]. From Eqs. (5.4)-(5.6), the tight-binding expressions for the terms in the Hamiltonian are

$$H_0 = -t_0 \sum_{n,\sigma} \left( c_{n+1,\sigma}^\dagger c_{n,\sigma} + \text{H.c.} \right), \quad (\text{B.1})$$

$$H_{\text{so}}^{\text{unif}} = -t_{\text{so}}^{\text{unif}} \sum_{n,\sigma,\sigma'} \left[ c_{n+1,\sigma'}^\dagger (i\sigma_x)_{\sigma'\sigma} c_{n,\sigma} + \text{H.c.} \right], \quad (\text{B.2})$$

$$H_{\text{so}}^{\text{osc}} = -t_{\text{so}}^{\text{osc}} \sum_{n,\sigma,\sigma'} \left[ \varphi_n c_{n+1,\sigma'}^\dagger (i\sigma_z)_{\sigma'\sigma} c_{n,\sigma} + \text{H.c.} \right], \quad (\text{B.3})$$

with  $\varphi_n = \cos(2\pi n/m)$ . The full Hamiltonian  $H = H_0 + H_{\text{so}}^{\text{unif}} + H_{\text{so}}^{\text{osc}}$  has a periodicity of  $m$  lattice sites that matches that of the spatially-oscillating spin-orbit hopping amplitude in Eq. (B.3). Since full translational invariance does not exist when  $t_{\text{so}}^{\text{osc}} \neq 0$ , the direct application of a Fourier transform such as that given in Eq. (4.30) is not possible. Instead, the lattice of  $N$  sites can be regarded as a smaller effective lattice of  $N' = N/m$  sites with  $m$  sublattices. The site index can then be re-expressed as  $n = mn' + l$ , where  $n' = 0, 1, \dots, N' - 1$  labels the site with respect to the effective lattice, and  $l = 1, 2, \dots, m$  labels the sublattice. In terms of these indices,  $\varphi_n$  is given by

$$\varphi_{mn'+l} = \cos \left[ \frac{2\pi}{m} (mn' + l) \right] = \cos \left( 2\pi n' + \frac{2\pi l}{m} \right) = \cos \left( \frac{2\pi l}{m} \right) \equiv \varphi_l, \quad (\text{B.4})$$

which shows that the spatially-oscillating spin-orbit hopping amplitude only depends on the sublattice index  $l$ .

The allowed dimensionless quasimomenta for the effective  $N'$ -site lattice can be written as  $q_j \equiv 2\pi j/N'$ , where  $j$  is an integer such that  $-N'/2 \leq j < N'/2$ . We also define reciprocal lattice vectors associated with the  $m$ -site periodicity as  $Q_p \equiv 2\pi p/m$ , with  $p$  an integer such that  $-m/2 \leq p < m/2$ . The effective lattice description then allows a Fourier transform of the operators  $c_{mn'+l,\sigma}$  and  $c_{mn'+l,\sigma}^\dagger$  to be defined for each sublattice  $l$  separately, which we carry out via Eq. (5.10):

$$\tilde{c}_{j,l,\sigma} = \frac{1}{\sqrt{N'}} \sum_{n'=0}^{N'-1} e^{-iq_j(mn'+l)} c_{mn'+l,\sigma}. \quad (\text{B.5})$$

Inverting this transformation gives

$$c_{mn'+l,\sigma} = \frac{1}{\sqrt{N'}} \sum_j e^{iq_j(mn'+l)} \tilde{c}_{j,l,\sigma}. \quad (\text{B.6})$$

We can rewrite Eqs. (B.1)-(B.3) in terms of the operators  $c_{mn'+l,\sigma}$  and  $c_{mn'+l,\sigma}^\dagger$ . Substituting the relation (B.6) for these operators then leads to

$$\begin{aligned} H_0 &= -\frac{t_0}{N'} \sum_{l,\sigma} \sum_{j,j'} \left\{ \left[ \sum_{n'} e^{i(q_j - q_{j'}) mn'} \right] e^{i(q_j - q_{j'}) l} e^{-iq_{j'} l} \tilde{c}_{j',l+1,\sigma}^\dagger \tilde{c}_{j,l,\sigma} + \text{H.c.} \right\}, \\ H_{\text{so}}^{\text{unif}} &= -\frac{t_{\text{so}}^{\text{unif}}}{N'} \sum_{l,\sigma,\sigma'} \sum_{j,j'} \left\{ \left[ \sum_{n'} e^{i(q_j - q_{j'}) mn'} \right] e^{i(q_j - q_{j'}) l} e^{-iq_{j'} l} \tilde{c}_{j',l+1,\sigma'}^\dagger (i\sigma_x)_{\sigma'\sigma} \tilde{c}_{j,l,\sigma} + \text{H.c.} \right\}, \\ H_{\text{so}}^{\text{osc}} &= -\frac{t_{\text{so}}^{\text{osc}}}{N'} \sum_{l,\sigma,\sigma'} \sum_{j,j'} \left\{ \left[ \sum_{n'} e^{i(q_j - q_{j'}) mn'} \right] \varphi_l e^{i(q_j - q_{j'}) l} e^{-iq_{j'} l} \tilde{c}_{j',l+1,\sigma'}^\dagger (i\sigma_z)_{\sigma'\sigma} \tilde{c}_{j,l,\sigma} \right. \\ &\quad \left. + \text{H.c.} \right\}, \end{aligned} \quad (\text{B.7})$$

where we have used Eq. (B.4) to replace  $\varphi_n$  by  $\varphi_l$ . To simplify these expressions, we apply the lattice-sum identity [23]

$$\sum_{n'=0}^{N'-1} e^{-i(q_j - q_{j'}) mn'} = N' \delta_{q_{j'}, q_j - Q_p}. \quad (\text{B.8})$$

By using Eq. (B.5) and noting that

$$q_{j'} = q_j - Q_p = \frac{2\pi j}{N'} - \frac{2\pi p}{m} = \frac{2\pi}{N'} \left( j - \frac{N' p}{m} \right) = q_{j - N' p/m},$$

we can also obtain the relation

$$\tilde{c}_{j - N' p/m, l+1, \sigma} = e^{iQ_p(l+1)} \tilde{c}_{j, l+1, \sigma}.$$

The expressions ( B.7) then reduce to

$$\begin{aligned}
H_0 &= -t_0 \sum_{j,l,\sigma} \left( e^{-iq_j} \tilde{c}_{j,l+1,\sigma}^\dagger \tilde{c}_{j,l,\sigma} + \text{H.c.} \right), \\
H_{\text{so}}^{\text{unif}} &= -t_{\text{so}}^{\text{unif}} \sum_{j,l,\sigma,\sigma'} \left[ e^{-iq_j} \tilde{c}_{j,l+1,\sigma'}^\dagger (i\sigma_x)_{\sigma'\sigma} \tilde{c}_{j,l,\sigma} + \text{H.c.} \right], \\
H_{\text{so}}^{\text{osc}} &= -t_{\text{so}}^{\text{osc}} \sum_{j,l,\sigma,\sigma'} \varphi_l \left[ e^{-iq_j} \tilde{c}_{j,l+1,\sigma'}^\dagger (i\sigma_z)_{\sigma'\sigma} \tilde{c}_{j,l,\sigma} + \text{H.c.} \right].
\end{aligned} \tag{B.9}$$

From Eq. ( B.9), we see that the transformation ( B.5) is not sufficient to bring the Hamiltonian to diagonal form.

In order to proceed, we apply a second transformation, defined in Eq. (5.11) by

$$d_{j,p,\sigma} \equiv \frac{1}{\sqrt{m}} \sum_{l=1}^m e^{-iQ_p l} \tilde{c}_{j,l,\sigma}, \tag{B.10}$$

for which the inverse transformation is

$$\tilde{c}_{j,l,\sigma} = \frac{1}{\sqrt{m}} \sum_p e^{iQ_p l} d_{j,p,\sigma}.$$

We then obtain

$$H_0 = -\frac{t_0}{m} \sum_{j,\sigma} \sum_{p,p'} \left\{ \left[ \sum_l e^{i(Q_p - Q_{p'})l} \right] e^{-i(q_j + Q_{p'})} d_{j,p',\sigma}^\dagger d_{j,p,\sigma} + \text{H.c.} \right\}, \tag{B.11}$$

$$H_{\text{so}}^{\text{unif}} = -\frac{t_{\text{so}}^{\text{unif}}}{m} \sum_{j,\sigma,\sigma'} \sum_{p,p'} \left\{ \left[ \sum_l e^{i(Q_p - Q_{p'})l} \right] e^{-i(q_j + Q_{p'})} d_{j,p',\sigma'}^\dagger (i\sigma_x)_{\sigma'\sigma} d_{j,p,\sigma} \right. \tag{B.12}$$

$$\left. + \text{H.c.} \right\}, \tag{B.13}$$

$$H_{\text{so}}^{\text{osc}} = -\frac{t_{\text{so}}^{\text{osc}}}{m} \sum_{j,\sigma,\sigma'} \sum_{p,p'} \left\{ \left[ \sum_l \varphi_l e^{i(Q_p - Q_{p'})l} \right] e^{-i(q_j + Q_{p'})} d_{j,p',\sigma'}^\dagger (i\sigma_z)_{\sigma'\sigma} d_{j,p,\sigma} \right. \tag{B.14}$$

$$\left. + \text{H.c.} \right\}. \tag{B.15}$$

Applying the identity

$$\sum_{l=1}^m e^{i(Q_p - Q_{p'})l} = m\delta_{p,p'} \tag{B.16}$$

to  $H_0$  and  $H_{\text{so}}^{\text{unif}}$  gives, after some manipulation of the indices in order to combine like terms,

$$H_0 = -2t_0 \sum_{j,p,\sigma} \cos(q_j + Q_p) d_{j,p,\sigma}^\dagger d_{j,p,\sigma}, \tag{B.17}$$

$$H_{\text{so}}^{\text{unif}} = -2t_{\text{so}}^{\text{unif}} \sum_{j,p,\sigma,\sigma'} (\sigma_x)_{\sigma'\sigma} \sin(q_j + Q_p) d_{j,p,\sigma}^\dagger d_{j,p,\sigma}. \tag{B.18}$$

Eq. ( B.17) is identical to Eq. (5.12) in Ch. 5 and shows that  $H_0$  is diagonal in the basis associated with the operators  $d_{j,p,\sigma}$  and  $d_{j,p,\sigma}^\dagger$ . To see that  $H_{\text{so}}^{\text{unif}}$  is also diagonal in this basis, we use  $(\sigma_x)_{\sigma'\sigma} = \sigma\delta_{\sigma'\sigma}$ , where  $\sigma, \sigma' = \pm$  refer to the  $x$  components of spin. This relation follows directly from the Pauli matrix representation given in Eq. ( A.19). Eq. ( B.18) then takes the diagonal form

$$H_{\text{so}}^{\text{unif}} = -2t_{\text{so}}^{\text{unif}} \sum_{j,p,\sigma} \sigma \sin(q_j + Q_p) d_{j,p,\sigma}^\dagger d_{j,p,\sigma}, \quad (\text{B.19})$$

which agrees with Eq. (5.13).

To obtain the expression in Eq. (5.14) for  $H_{\text{so}}^{\text{osc}}$ , we evaluate the sum in Eq. ( B.14) using the identity given in Eq. ( B.16):

$$\begin{aligned} \sum_{l=1}^m \varphi_l e^{i(Q_p - Q_{p'})l} &= \sum_l \cos\left(\frac{2\pi l}{m}\right) e^{i2\pi(p-p')l/m} \\ &= \frac{1}{2} \sum_l \left( e^{i2\pi l/m} + e^{-i2\pi l/m} \right) e^{i2\pi(p-p')l/m} \\ &= \frac{1}{2} \left[ \sum_l e^{i2\pi(p-p'+1)l/m} + \sum_l e^{i2\pi(p-p'-1)l/m} \right] \\ &= \frac{m}{2} (\delta_{p',p+1} + \delta_{p',p-1}), \end{aligned} \quad (\text{B.20})$$

which is simply the result for the discrete Fourier transform of the site-dependent hopping factor  $\varphi_l = \cos(2\pi l/m)$ . Substituting Eq. ( B.20) into Eq. ( B.14) and again performing some manipulation of indices in order to regroup terms yields

$$H_{\text{so}}^{\text{osc}} = -t_{\text{so}}^{\text{osc}} \sum_{j,p,\sigma,\sigma'} (\sigma_z)_{\sigma'\sigma} \sin\left(q_j + Q_p + \frac{\pi}{m}\right) \left( e^{-i\pi/m} d_{j,p+1,\sigma}^\dagger d_{j,p,\sigma} + \text{H.c.} \right).$$

With  $(\sigma_z)_{\sigma'\sigma} = 1 - \delta_{\sigma'\sigma}$  (see Eq. ( A.19)), this becomes

$$H_{\text{so}}^{\text{osc}} = -t_{\text{so}}^{\text{osc}} \sum_{j,p,\sigma,\sigma'} (1 - \delta_{\sigma'\sigma}) \sin\left(q_j + Q_p + \frac{\pi}{m}\right) \left( e^{-i\pi/m} d_{j,p+1,\sigma'}^\dagger d_{j,p,\sigma} + \text{H.c.} \right), \quad (\text{B.21})$$

which is identical to Eq. (5.14) in Ch. 5.

As is evident from Eq. ( B.21), the basis associated with the operators  $d_{j,p,\sigma}$  and  $d_{j,p,\sigma}^\dagger$  does not diagonalize the full Hamiltonian. However, writing  $H_{\text{so}}^{\text{osc}}$  in this basis reveals that the oscillating spin-orbit interaction couples neighboring bands  $p$  and  $p \pm 1$  of opposite spin ( $\sigma' \neq \sigma$ ). This coupling allows the full  $2m$ -dimensional representations of the Hamiltonian defined by the set of all possible states  $\{|j, p, \sigma\rangle\}$  for a fixed value of  $j$  to be reduced to two  $m$ -dimensional ones. For

the specific case  $N = 20$ ,  $m = 4$  considered in Ch. 5, the possible values of the band index are  $p = -2, -1, 0, 1$  so that there are  $2m = 8$  states for each value of  $j$ . The coupling of these states due to  $H_{s_0}^{\text{osc}}$  results in a division into two spaces of dimension  $m = 4$ ,

$$R_+ \equiv \{|j, -2, \uparrow\rangle, |j, -1, \downarrow\rangle, |j, 0, \uparrow\rangle, |j, 1, \downarrow\rangle\},$$

$$R_- \equiv \{|j, -2, \downarrow\rangle, |j, -1, \uparrow\rangle, |j, 0, \downarrow\rangle, |j, 1, \uparrow\rangle\}.$$

For this case, it is possible to obtain exact analytical expressions for the operators which diagonalize the  $4 \times 4$  matrix representations of the full Hamiltonian defined by the spaces  $R_+$  and  $R_-$ . Since these expressions are complicated, we use mainly numerical diagonalization to obtain the spectrum and spin polarization for the tight-binding Hamiltonian in Ch. 5.

## BIBLIOGRAPHY

- [1] G. E. Uhlenbeck and S. Goudsmit, *Naturwissenschaften* **13**, 953 (1925).
- [2] M. Tinkham, *Group Theory and Quantum Mechanics*, International Series in Pure and Applied Physics (McGraw-Hill, New York, 1964).
- [3] R. I. Nepomechie, *Int. J. Mod. Phys. B* **13**, 2973 (1999).
- [4] A. Einstein, B. Podolsky, and N. Rosen, *Phys. Rev.* **47**, 777 (1935).
- [5] E. Schrödinger, *Math. Proc. Cambridge Philos. Soc.* **31**, 555 (1935).
- [6] J. Stolze and D. Suter, *Quantum Computing: A Short Course from Theory to Experiment*, 2nd ed. (Wiley-VCH, Weinheim, 2008).
- [7] W. Heitler and F. London, *Z. Phys. A* **44**, 455 (1927).
- [8] J. D. Patterson, *Introduction to the Theory of Solid State Physics*, Addison-Wesley Series in Solid State Sciences (Addison-Wesley, Reading, 1971).
- [9] J. Stöhr and H. C. Siegmann, *Magnetism: From Fundamentals to Nanoscale Dynamics*, Springer Series in Solid-State Sciences, Vol. 152 (Springer, Berlin, 2006).
- [10] W. Heisenberg, *Z. Phys. A* **49**, 619 (1928).
- [11] E. Lieb and D. Mattis, *J. Math. Phys.* **3**, 749 (1962).
- [12] B. Nachtergaele and S. Starr, *Phys. Rev. Lett.* **94**, 057206 (2005).
- [13] F. D. M. Haldane, *Phys. Lett. A* **93**, 464 (1983).
- [14] F. D. M. Haldane, *Phys. Rev. Lett.* **50**, 1153 (1983).
- [15] H. Bethe, *Z. Phys.* **71**, 205 (1931).
- [16] K. V. Kavokin, *Phys. Rev. B* **64**, 075305 (2001).
- [17] K. V. Kavokin, *Phys. Rev. B* **69**, 075302 (2004).

- [18] P. Jordan and E. P. Wigner, *Z. Phys.* **47**, 631 (1928).
- [19] E. Fradkin, *Phys. Rev. Lett.* **63**, 322 (1989).
- [20] C. D. Batista and G. Ortiz, *Phys. Rev. Lett.* **86**, 1082 (2001).
- [21] F. Essler, *The One-Dimensional Hubbard model* (Cambridge University Press, Cambridge, 2005).
- [22] R. J. Elliott, *Phys. Rev.* **96**, 266 (1954).
- [23] N. Ashcroft and N. Mermin, *Solid State Physics* (Saunders College, Philadelphia, 1976).
- [24] R. Winkler, *Spin-Orbit Coupling Effects in Two-Dimensional Electron and Hole Systems*, Springer Tracts in Modern Physics, Vol. 191 (Springer, Berlin, 2003).
- [25] L. H. Thomas, *Nature* **117**, 514 (1926).
- [26] C. Kittel, *Quantum Theory of Solids* (Wiley, New York, 1963).
- [27] G. Dresselhaus, *Phys. Rev.* **100**, 580 (1955).
- [28] E. I. Rashba, *Sov. Phys. Solid State* **2**, 1109 (1960).
- [29] Y. A. Bychkov and E. I. Rashba, *J. Phys. C* **17**, 6039 (1984).
- [30] J. Nitta, T. Akazaki, H. Takayanagi, and T. Enoki, *Phys. Rev. Lett.* **78**, 1335 (1997).
- [31] D. P. DiVincenzo and D. Loss, *Superlattice Microst.* **23**, 419 (1998).
- [32] D. Deutsch, *Proc. R. Soc. Lond. A* **400**, 97 (1985).
- [33] R. Feynman, *Int. J. Theor. Phys.* **21**, 467 (1982).
- [34] R. Feynman, *Found. Phys.* **16**, 507 (1986).
- [35] D. P. DiVincenzo, *Fortschr. Phys.* **48**, 771 (2000).
- [36] D. P. DiVincenzo, *Phys. Rev. A* **51**, 1015 (1995).
- [37] A. Barenco, C. H. Bennett, R. Cleve, D. P. DiVincenzo, N. Margolus, P. Shor, T. Sleator, J. A. Smolin, and H. Weinfurter, *Phys. Rev. A* **52**, 3457 (1995).
- [38] T. D. Ladd, F. Jelezko, R. Laflamme, Y. Nakamura, C. Monroe, and J. L. O'Brien, *Nature* **464**, 45 (2010).
- [39] J. I. Cirac and P. Zoller, *Phys. Rev. Lett.* **74**, 4091 (1995).
- [40] D. J. Wineland, C. Monroe, W. M. Itano, D. Leibfried, B. E. King, and D. M. Meekhof, *J. Res. Natl. Inst. Stand. Technol.* **103**, 259 (1998).

- [41] G. K. Brennen, C. M. Caves, P. S. Jessen, and I. H. Deutsch, *Phys. Rev. Lett.* **82**, 1060 (1999).
- [42] D. Jaksch, H. J. Briegel, J. I. Cirac, C. W. Gardiner, and P. Zoller, *Phys. Rev. Lett.* **82**, 1975 (1999).
- [43] N. A. Gershenfeld and I. L. Chuang, *Science* **275**, 350 (1997).
- [44] D. G. Cory, A. F. Fahmy, and T. F. Havel, *Proc. Nat. Acad. Sci. USA* **94**, 1634 (1997).
- [45] E. Knill, R. Laflamme, and G. J. Milburn, *Nature* **409**, 46 (2001).
- [46] G. J. Milburn, *Phys. Scr.* **2009**, 014003 (2009).
- [47] D. Loss and D. P. DiVincenzo, *Phys. Rev. A* **57**, 120 (1998).
- [48] T. Tanamoto, *Phys. Rev. A* **61**, 022305 (2000).
- [49] B. E. Kane, *Nature* **393**, 133 (1998).
- [50] L. Childress, M. V. Gurudev Dutt, J. M. Taylor, A. S. Zibrov, F. Jelezko, J. Wrachtrup, P. R. Hemmer, and M. D. Lukin, *Science* **314**, 281 (2006).
- [51] M. V. G. Dutt, L. Childress, L. Jiang, E. Togan, J. Maze, F. Jelezko, A. S. Zibrov, P. R. Hemmer, and M. D. Lukin, *Science* **316**, 1312 (2007).
- [52] A. Shnirman, G. Schön, and Z. Hermon, *Phys. Rev. Lett.* **79**, 2371 (1997).
- [53] D. V. Averin, *Solid State Commun.* **105**, 659 (1998).
- [54] J. E. Mooij, T. P. Orlando, L. Levitov, L. Tian, C. H. van der Wal, and S. Lloyd, *Science* **285**, 1036 (1999).
- [55] T. Monz, P. Schindler, J. T. Barreiro, M. Chwalla, D. Nigg, W. A. Coish, M. Harlander, W. Hänsel, M. Hennrich, and R. Blatt, *Phys. Rev. Lett.* **106**, 130506 (2011).
- [56] R. Raussendorf and H. J. Briegel, *Phys. Rev. Lett.* **86**, 5188 (2001).
- [57] R. Raussendorf, D. E. Browne, and H. J. Briegel, *Phys. Rev. A* **68**, 022312 (2003).
- [58] Y. S. Weinstein, C. S. Hellberg, and J. Levy, *Phys. Rev. A* **72**, 020304 (2005).
- [59] C. Nayak, S. H. Simon, A. Stern, M. Freedman, and S. Das Sarma, *Rev. Mod. Phys.* **80**, 1083 (2008).
- [60] V. Privman, I. D. Vagner, and G. Kventsel, *Phys. Lett. A* **239**, 141 (1998).
- [61] A. Imamoglu, D. D. Awschalom, G. Burkard, D. P. DiVincenzo, D. Loss, M. Sherwin, and A. Small, *Phys. Rev. Lett.* **83**, 4204 (1999).

- [62] R. Vrijen, E. Yablonovitch, K. Wang, H. W. Jiang, A. Balandin, V. Roychowdhury, T. Mor, and D. DiVincenzo, *Phys. Rev. A* **62**, 012306 (2000).
- [63] J. Levy, *Phys. Rev. A* **64**, 052306 (2001).
- [64] T. D. Ladd, J. R. Goldman, F. Yamaguchi, Y. Yamamoto, E. Abe, and K. M. Itoh, *Phys. Rev. Lett.* **89**, 017901 (2002).
- [65] J. Wrachtrup and F. Jelezko, *J. Phys. Condens. Matter* **18**, S807 (2006).
- [66] R. Hanson, L. P. Kouwenhoven, J. R. Petta, S. Tarucha, and L. M. K. Vandersypen, *Rev. Mod. Phys.* **79**, 1217 (2007).
- [67] R. Hanson and D. D. Awschalom, *Nature* **453**, 1043 (2008).
- [68] C. H. Bennett, G. Brassard, C. Crepeau, R. Jozsa, A. Peres, and W. K. Wootters, *Phys. Rev. Lett.* **70**, 1895 (1993).
- [69] Y.-F. Huang, X.-F. Ren, Y.-S. Zhang, L.-M. Duan, and G.-C. Guo, *Phys. Rev. Lett.* **93**, 240501 (2004).
- [70] R. Ursin, F. Tiefenbacher, T. Schmitt-Manderbach, H. Weier, T. Scheidl, M. Lindenthal, B. Blauensteiner, T. Jennewein, J. Perdigues, P. Trojek, B. Omer, M. Furst, M. Meyenburg, J. Rarity, Z. Sodnik, C. Barbieri, H. Weinfurter, and A. Zeilinger, *Nature Phys.* **3**, 481 (2007).
- [71] S. Bose, *Contemp. Phys.* **48**, 13 (2007).
- [72] G. Burkard, D. Loss, and D. P. DiVincenzo, *Phys. Rev. B* **59**, 2070 (1999).
- [73] R. C. Ashoori, *Nature* **379**, 413 (1996).
- [74] M. Nielsen and I. Chuang, *Quantum Computation and Quantum Information* (Cambridge University Press, Cambridge, 2000).
- [75] J. R. Petta, A. C. Johnson, J. M. Taylor, E. A. Laird, A. Yacoby, M. D. Lukin, C. M. Marcus, M. P. Hanson, and A. C. Gossard, *Science* **309**, 2180 (2005).
- [76] P. W. Shor, *Phys. Rev. A* **52**, R2493 (1995).
- [77] P. Zanardi and M. Rasetti, *Phys. Rev. Lett.* **79**, 3306 (1997).
- [78] D. A. Lidar, I. L. Chuang, and K. B. Whaley, *Phys. Rev. Lett.* **81**, 2594 (1998).
- [79] D. Bacon, K. R. Brown, and K. B. Whaley, *Phys. Rev. Lett.* **87**, 247902 (2001).
- [80] Y. S. Weinstein and C. S. Hellberg, *Phys. Rev. Lett.* **98**, 110501 (2007).
- [81] J. Levy, *Phys. Rev. Lett.* **89**, 147902 (2002).

- [82] J. M. Taylor, H. A. Engel, W. Dur, A. Yacoby, C. M. Marcus, P. Zoller, and M. D. Lukin, *Nature Phys.* **1**, 177 (2005).
- [83] R. Hanson and G. Burkard, *Phys. Rev. Lett.* **98**, 050502 (2007).
- [84] J. M. Taylor, J. R. Petta, A. C. Johnson, A. Yacoby, C. M. Marcus, and M. D. Lukin, *Phys. Rev. B* **76** (2007).
- [85] I. van Weperen, B. D. Armstrong, E. A. Laird, J. Medford, C. M. Marcus, M. P. Hanson, and A. C. Gossard, *Phys. Rev. Lett.* **107**, 030506 (2011).
- [86] J. Kempe, D. Bacon, D. A. Lidar, and K. B. Whaley, *Phys. Rev. A* **63**, 042307 (2001).
- [87] D. P. DiVincenzo, D. Bacon, J. Kempe, G. Burkard, and K. B. Whaley, *Nature* **408**, 339 (2000).
- [88] Y. S. Weinstein and C. S. Hellberg, *Phys. Rev. A* **72**, 022319 (2005).
- [89] E. A. Laird, J. M. Taylor, D. P. DiVincenzo, C. M. Marcus, M. P. Hanson, and A. C. Gossard, *Phys. Rev. B* **82**, 075403 (2010).
- [90] L. Gaudreau, G. Granger, A. Kam, G. C. Aers, S. A. Studenikin, P. Zawadzki, M. Pioro-Ladriere, Z. R. Wasilewski, and A. S. Sachrajda, *Nature Phys.* **8**, 54 (2012).
- [91] F. Meier, J. Levy, and D. Loss, *Phys. Rev. Lett.* **90**, 047901 (2003).
- [92] F. Meier, J. Levy, and D. Loss, *Phys. Rev. B* **68**, 134417 (2003).
- [93] H.-A. Engel and D. Loss, *Phys. Rev. Lett.* **86**, 4648 (2001).
- [94] F. H. L. Koppens, C. Buizert, K. J. Tielrooij, I. T. Vink, K. C. Nowack, T. Meunier, L. P. Kouwenhoven, and L. M. K. Vandersypen, *Nature* **442**, 766 (2006).
- [95] S. Datta and B. Das, *Appl. Phys. Lett.* **56**, 665 (1990).
- [96] Y. Kato, R. C. Myers, D. C. Driscoll, A. C. Gossard, J. Levy, and D. D. Awschalom, *Science* **299**, 1201 (2003).
- [97] E. I. Rashba and A. L. Efros, *Phys. Rev. Lett.* **91**, 126405 (2003).
- [98] Y. Kato, R. C. Myers, A. C. Gossard, and D. D. Awschalom, *Nature* **427**, 50 (2004).
- [99] J.-M. Tang, J. Levy, and M. E. Flatté, *Phys. Rev. Lett.* **97**, 106803 (2006).
- [100] K. C. Nowack, F. H. L. Koppens, Y. V. Nazarov, and L. M. K. Vandersypen, *Science* **318**, 1430 (2007).
- [101] E. A. Laird, C. Barthel, E. I. Rashba, C. M. Marcus, M. P. Hanson, and A. C. Gossard, *Phys. Rev. Lett.* **99**, 246601 (2007).

- [102] M. Pioro-Ladriere, T. Obata, Y. Tokura, Y. S. Shin, T. Kubo, K. Yoshida, T. Taniyama, and S. Tarucha, *Nature Phys.* **4**, 776 (2008).
- [103] A. V. Moroz and C. H. W. Barnes, *Phys. Rev. B* **60**, 14272 (1999).
- [104] F. Mireles and G. Kirczenow, *Phys. Rev. B* **64**, 024426 (2001).
- [105] M. Governale and U. Zülicke, *Phys. Rev. B* **66**, 073311 (2002).
- [106] Y. V. Pershin, J. A. Nesteroff, and V. Privman, *Phys. Rev. B* **69**, 121306(R) (2004).
- [107] M. Governale and U. Zülicke, *Solid State Commun.* **131**, 581 (2004).
- [108] J. Knobbe and T. Schapers, *Phys. Rev. B* **71**, 035311 (2005).
- [109] S. Debald and B. Kramer, *Phys. Rev. B* **71**, 115322 (2005).
- [110] V. Y. Demikhovskii and D. V. Khomitsky, *JETP Lett.* **83**, 340 (2006).
- [111] S. Smirnov, D. Bercioux, and M. Grifoni, *Europhys. Lett.* **80**, 27003 (2007).
- [112] J. E. Birkholz and V. Meden, *J. Phys. Condens. Matter* **20** (2008).
- [113] C. H. L. Quay, T. L. Hughes, J. A. Sulpizio, L. N. Pfeiffer, K. W. Baldwin, K. W. West, D. Goldhaber-Gordon, and R. de Picciotto, *Nature Phys.* **6**, 336 (2010).
- [114] A. Bringer and T. Schäpers, *Phys. Rev. B* **83**, 115305 (2011).
- [115] X. F. Wang, *Phys. Rev. B* **69**, 035302 (2004).
- [116] M.-H. Liu and C.-R. Chang, *Phys. Rev. B* **74**, 195314 (2006).
- [117] G. I. Japaridze, H. Johannesson, and A. Ferraz, *Phys. Rev. B* **80**, 041308 (2009).
- [118] M. Malard, I. Grusha, G. I. Japaridze, and H. Johannesson, *Phys. Rev. B* **84**, 075466 (2011).
- [119] M. Duckheim and D. Loss, *Nature Phys.* **2**, 195 (2006).
- [120] V. N. Golovach, M. Borhani, and D. Loss, *Phys. Rev. B* **74**, 165319 (2006).
- [121] S. M. Frolov, S. Luscher, W. Yu, Y. Ren, J. A. Folk, and W. Wegscheider, *Nature* **458**, 868 (2009).
- [122] A. E. Popescu and R. Ionicioiu, *Phys. Rev. B* **69**, 245422 (2004).
- [123] D. Stepanenko and N. E. Bonesteel, *Phys. Rev. Lett.* **93**, 140501 (2004).
- [124] C. Flindt, A. S. Sorensen, and K. Flensberg, *Phys. Rev. Lett.* **97**, 240501 (2006).
- [125] S. J. Gong and Z. Q. Yang, *Phys. Lett. A* **367**, 369 (2007).

- [126] V. N. Golovach, M. Borhani, and D. Loss, *Phys. Rev. A* **81**, 022315 (2010).
- [127] S. Nadj-Perge, S. M. Frolov, E. P. A. M. Bakkers, and L. P. Kouwenhoven, *Nature* **468**, 1084 (2010).
- [128] M. I. D'yakonov and V. I. Perel', *Sov. Phys. Solid State* **13**, 3023 (1972).
- [129] M. M. Glazov and E. Y. Sherman, *Phys. Rev. Lett.* **107**, 156602 (2011).
- [130] V. Srinivasa, J. Levy, and C. S. Hellberg, *Phys. Rev. B* **76**, 094411 (2007).
- [131] A. M. Steane, *Quantum Inf. Comput.* **2**, 297 (2002).
- [132] T. Szkopek, P. O. Boykin, H. Fan, V. P. Roychowdhury, E. Yablonovitch, G. Simms, M. Gyure, and B. Fong, *IEEE Trans. Nanotechnol.* **5**, 42 (2006).
- [133] S. Bose, *Phys. Rev. Lett.* **91**, 207901 (2003).
- [134] G. M. Nikolopoulos, D. Petrosyan, and P. Lambropoulos, *J. Phys. Condens. Matter* **16**, 4991 (2004).
- [135] M. Christandl, N. Datta, A. Ekert, and A. J. Landahl, *Phys. Rev. Lett.* **92**, 187902 (2004).
- [136] T. J. Osborne and N. Linden, *Phys. Rev. A* **69**, 052315 (2004).
- [137] D. Burgarth and S. Bose, *Phys. Rev. A* **71**, 052315 (2005).
- [138] P. Karbach and J. Stolze, *Phys. Rev. A* **72**, 030301 (2005).
- [139] M.-H. Yung, *Phys. Rev. A* **74**, 030303 (2006).
- [140] M. Wieśniak, *Phys. Rev. A* **78**, 052334 (2008).
- [141] G. De Chiara, D. Rossini, S. Montangero, and R. Fazio, *Phys. Rev. A* **72**, 012323 (2005).
- [142] D. Petrosyan, G. M. Nikolopoulos, and P. Lambropoulos, *Phys. Rev. A* **81**, 042307 (2010).
- [143] V. Balachandran and J. Gong, *Phys. Rev. A* **77**, 012303 (2008).
- [144] G. Giavaras, J. H. Jefferson, M. Fearn, and C. J. Lambert, *Phys. Rev. B* **76**, 245328 (2007).
- [145] S. Hermelin, S. Takada, M. Yamamoto, S. Tarucha, A. D. Wieck, L. Saminadayar, C. Bauerle, and T. Meunier, *Nature* **477**, 435 (2011).
- [146] R. P. G. McNeil, M. Kataoka, C. J. B. Ford, C. H. W. Barnes, D. Anderson, G. A. C. Jones, I. Farrer, and D. A. Ritchie, *Nature* **477**, 439 (2011).
- [147] W. P. Su, J. R. Schrieffer, and A. J. Heeger, *Phys. Rev. Lett.* **42**, 1698 (1979).
- [148] W. P. Su, J. R. Schrieffer, and A. J. Heeger, *Phys. Rev. B* **22**, 2099 (1980).

- [149] A. J. Heeger, S. Kivelson, J. R. Schrieffer, and W. P. Su, *Rev. Mod. Phys.* **60**, 781 (1988).
- [150] J. Cullum and R. A. Willoughby, *Lanczos Algorithms for Large Symmetric Eigenvalue Computations* (Birkhauser, Boston, 1985).
- [151] A. Auerbach, *Interacting Electrons and Quantum Magnetism* (Springer-Verlag, New York, 1994).
- [152] R. Peierls, *Quantum Theory of Solids* (Clarendon, Oxford, 1955).
- [153] T. Nakano and H. Fukuyama, *J. Phys. Soc. Japan* **49**, 1679 (1980).
- [154] M. Born and V. Fock, *Z. Phys. A* **51**, 165 (1928).
- [155] A. Messiah, *Quantum Mechanics* (North-Holland, Amsterdam, 1961).
- [156] E. Farhi, J. Goldstone, S. Gutmann, and M. Sipser, arXiv:quant-ph/0001106v1 .
- [157] J. H. Shirley, *Phys. Rev.* **138**, B979 (1965).
- [158] T. Barnes, J. Riera, and D. A. Tennant, *Phys. Rev. B* **59**, 11384 (1999).
- [159] M. Friesen, R. Joynt, and M. A. Eriksson, *Appl. Phys. Lett.* **81**, 4619 (2002).
- [160] O. Guise, J. Ahner, J. John T. Yates, V. Vaithyanathan, D. G. Schlom, and J. Levy, *Appl. Phys. Lett.* **87**, 171902 (2005).
- [161] C. Pryor and M. E. Flatté, (unpublished).
- [162] V. Srinivasa and J. Levy, *Phys. Rev. B* **80**, 024414 (2009).
- [163] F. Troiani, M. Affronte, S. Carretta, P. Santini, and G. Amoretti, *Phys. Rev. Lett.* **94**, 190501 (2005).
- [164] M. Affronte, F. Troiani, A. Ghirri, S. Carretta, P. Santini, V. Corradini, R. Schuecker, C. Muryn, G. Timco, and R. E. Winpenny, *Dalton Trans.* **2006**, 2810.
- [165] S. Carretta, P. Santini, G. Amoretti, F. Troiani, and M. Affronte, *Phys. Rev. B* **76**, 024408 (2007).
- [166] G. A. Timco, S. Carretta, F. Troiani, F. Tuna, R. J. Pritchard, C. A. Muryn, E. J. L. McInnes, A. Ghirri, A. Candini, P. Santini, G. Amoretti, M. Affronte, and R. E. P. Winpenny, *Nature Nanotech.* **4**, 173 (2009).
- [167] M. Friesen, A. Biswas, X. Hu, and D. Lidar, *Phys. Rev. Lett.* **98**, 230503 (2007).
- [168] V. Subrahmanyam, *Phys. Rev. B* **52**, 1133 (1995).
- [169] C. Raghu, I. Rudra, S. Ramasesha, and D. Sen, *Phys. Rev. B* **62**, 9484 (2000).

- [170] M. E. Zhitomirsky, Phys. Rev. B **71**, 214413 (2005).
- [171] H. M. McConnell, J. Chem. Phys. **39**, 1910 (1963).
- [172] K. Yoshizawa and R. Hoffmann, J. Am. Chem. Soc. **117**, 6921 (1995).
- [173] K. Hida, Phys. Rev. B **45**, 2207 (1992).
- [174] M. Trif, F. Troiani, D. Stepanenko, and D. Loss, Phys. Rev. Lett. **101**, 217201 (2008).
- [175] S. Datta, *Electronic Transport in Mesoscopic Systems* (Cambridge University Press, Cambridge, 1995).
- [176] C. W. J. Beenakker and H. van Houten, Solid State Phys. **44**, 1 (1991).
- [177] C. Cen, S. Thiel, G. Hammerl, C. W. Schneider, K. E. Andersen, C. S. Hellberg, J. Mannhart, and J. Levy, Nature Mater. **7**, 298 (2008).
- [178] C. Cen, S. Thiel, J. Mannhart, and J. Levy, Science **323**, 1026 (2009).
- [179] A. Ohtomo and H. Y. Hwang, Nature **427**, 423 (2004).
- [180] S. Thiel, G. Hammerl, A. Schmehl, C. W. Schneider, and J. Mannhart, Science **313**, 1942 (2006).
- [181] C. Cen, D. Bogorin, V. Srinivasa, and J. Levy, arXiv:1103.3036v1 .
- [182] R. Landauer, IBM J. Res. Dev. **1**, 223 (1957).
- [183] M. Ben Shalom, M. Sachs, D. Rakhmilevitch, A. Palevski, and Y. Dagan, Phys. Rev. Lett. **104**, 126802 (2010).
- [184] A. D. Caviglia, M. Gabay, S. Gariglio, N. Reyren, C. Cancellieri, and J. M. Triscone, Phys. Rev. Lett. **104**, 126803 (2010).
- [185] A. Joshua, S. Pecker, J. Ruhman, E. Altman, and S. Ilani, arXiv:1110.2184v1 .
- [186] R. Bistritzer, G. Khalsa, and A. H. MacDonald, Phys. Rev. B **83**, 115114 (2011).
- [187] V. Y. Demikhovskii, D. V. Khomitsky, and A. A. Perov, Low Temp. Phys. **33**, 115 (2007).
- [188] L. Chirolli, D. Venturelli, F. Taddei, R. Fazio, and V. Giovannetti, arXiv:1111.0675v2 .
- [189] G. Metalidis, Ph.D. thesis, Martin Luther University of Halle-Wittenberg (2007).
- [190] V. Srinivasa and J. Levy, arXiv:1111.5311v1 .
- [191] R. P. Feynman, Rev. Mod. Phys. **20**, 367 (1948).
- [192] D. R. Nelson, Phys. Rev. Lett. **60**, 1973 (1988).

- [193] A. M. Tsvetik, *Quantum Field Theory in Condensed Matter Physics* (Cambridge University Press, Cambridge, 1995).
- [194] L. Susskind, *J. Math. Phys.* **36**, 6377 (1995).
- [195] G. Burkard, H. A. Engel, and D. Loss, *Fortschr. Phys.* **48**, 965 (2000).
- [196] D. F. Bogorin, C. W. Bark, H. W. Jang, C. Cen, C. M. Folkman, C. Eom, and J. Levy, *Appl. Phys. Lett.* **97**, 013102 (2010).
- [197] L. M. K. Vandersypen and I. L. Chuang, *Rev. Mod. Phys.* **76**, 1037 (2005).
- [198] S. Balasubramanian, *Am. J. Phys.* **69**, 508 (2001).
- [199] J. J. Sakurai, *Modern Quantum Mechanics* (Addison-Wesley, Reading, 1994).
- [200] C. Cohen-Tannoudji, B. Diu, and F. Laloë, *Quantum Mechanics* (Wiley-VCH, New York, 1977).